CMOS co-design of a haptic drill press feed controller

Final Report

S. Harischandre

23843528

Submitted as partial fulfilment of the requirements of Project EPR400 in the Department of Electrical, Electronic and Computer Engineering, University of Pretoria

November 2026

Study leader: Dr. D. J. De Beer

Part 1. Preamble

This report describes work that I have completed in my final year project, developing a single-axis bilateral haptic feed interface for a bench drill press, in which a motor-driven lever commands the quill feed and renders the measured drilling thrust, with the three-phase motor driver designed both at transistor level in a 0.18 µm high-voltage CMOS process and as a discrete printed circuit board.

1. Project Proposal and technical documentation

This main report contains an unaltered copy of the approved Project Proposal (as Part 2 of the report).

All the code that I developed appears as a separate submission on the AMS.

2. Project history

This project is new and does not extend any previous EPR project. It was derived from concept note DJDB8 ("CMOS co-design of a universal haptic input controller"). After feedback from my study leader and the course coordinator, the application was narrowed from a general-purpose haptic knob to a drill-press feed controller. The proposal was revised twice (Rev1 and Rev2) and approved on 22 July 2026.

I designed, built, programmed and tested everything described in Part 3 myself, except the following. The DF4015 brushless motor with its AS5600 encoder, the FIT0185 (GB37, 131:1) gearmotor with its quadrature encoder, the BTS7960 H-bridge module, four 50 kg half-bridge load cells with an HX711 converter board, the ESP32 and STM32F405 development boards and the MAC AFRIC 13 mm bench drill were bought as finished products. JLCPCB fabricated the printed circuit board from my Gerber files. The herringbone gear profiles (and the pulleys of the earlier belt drive) were generated with online generators and printed by me. The CMOS design uses the device models of the X-FAB XH018 process design kit. A SimpleFOC Mini (DRV8313) board was used only as an early test platform for open-loop commutation before my own board arrived, and no SimpleFOC library code was used.

3. Language editing

This document has been language edited by a knowledgeable person. By submitting this document in its present form, I declare that this is the written material that I wish to be examined on.

My language editor was ..... Ms. Sunayna Balgobind.....

Editor's signature:  Date: ....26/10/2026.....

4. Plagiarism declaration

I, Shoalin Harischandre, understand what plagiarism is and have carefully studied the plagiarism policy of the University. I hereby declare that all the work described in this report

is my own, except where explicitly indicated otherwise. Although I may have discussed the design with my study leader, fellow students or consulted various books, articles or the internet, the design work is my own. I have mastered the design and I have made all the required calculations in my lab book (and/or they are reflected in this report) to authenticate this. I am not presenting a complete solution of someone else or that I found somewhere.

Wherever I have used information from other sources, I have given credit by proper and complete referencing of the source material so that it can be clearly discerned what is my own work and what was quoted from other sources. I acknowledge that failure to comply with the instructions regarding referencing will be regarded as plagiarism. If there is any doubt about the authenticity of my work, I understand that I may have to attend an oral ancillary examination/evaluation about the work.

5. AI usage declaration

The author confirms that artificial intelligence tools were used only as described in the next paragraph.

AI was used to assist with literature and datasheet searches, and the browser test console. All design decisions, testing, firmware and validation on the hardware are my own. AI was also used to explain certain concepts with illustrations to better technical understanding.

6. Software library usage declaration

Unless explicitly stated otherwise in the next paragraph, the author confirms that no software library functions, packages, or toolboxes were used in the design, implementation, or analysis presented in this report.

The only exception is that the following libraries were used, only for interfacing with hardware peripherals: the STM32 HAL and the STMicroelectronics USB device (CDC) middleware on the STM32F405, the Arduino-ESP32 core and ESP-IDF drivers (PWM, GPIO, UART and NVS Preferences) on the ESP32, the ESP32Encoder library (madhephaestus) for the pulse-counter peripheral, no HX711 library (the converter is read by a short bit-banged routine), and the Web Serial API of the browser for the console. No motor-control library was used. The coordinate transforms, modulation, observer, servo and haptic laws, force rendering, bilateral coupling, drill-side controllers and safety logic were written from first principles.

7. Unaltered Project Proposal

I certify that the Project Proposal appearing as the Introduction section of the report is an unaltered copy of the approved Project Proposal.

Signature

With my signature below, I hereby certify that all statements, declarations, and information presented above are complete.

Signature: ..... Date: 02 November 2026

Table of contents

1. Literature study..... 1
1.1 Background and context of the problem..... 1
1.1.1 Haptic interfaces and transparency..... 1
1.1.2 Bilateral teleoperation and force reflection..... 1
1.1.3 Drilling thrust force and its measurement..... 2
1.1.4 Torque control of permanent-magnet motors..... 2
1.1.5 Position sensing, velocity estimation and friction..... 3
1.1.6 Half-bridge gate driving and dead time..... 3
1.1.7 CMOS realisation of the driver..... 4
1.1.8 Communication in the control loop..... 4
1.2 Application of the literature to this project..... 4
2. Approach..... 6
2.1 Concept..... 6
2.2 Alternatives and trade-offs..... 6
3. Design and implementation..... 8
3.1 Design summary..... 8
3.2 System block diagram..... 9
3.3 Theoretical analysis and design calculations..... 10
3.3.1 Drill feed mechanics..... 10
3.3.2 Lever force capability and transmission ratio..... 11
3.3.3 Motor model, voltage-mode FOC and the drive model..... 13
3.3.4 Bottom-clamped modulation with current-direction chopping..... 15
3.3.5 Angle processing, servo and haptic laws..... 16
3.3.6 Gate-drive analysis..... 18
3.3.7 CMOS dead-time generation..... 18
3.3.8 Drill-side control, thrust measurement and protection..... 19
3.3.9 Link timing budget..... 20
3.3.10 Force reflection and bilateral coupling..... 20
3.4 Simulation study..... 21
3.4.1 LTspice simulation of the discrete half-bridge..... 21
3.4.2 Cadence simulation of the CMOS driver..... 23
3.4.3 Numerical study of speed estimation..... 24
3.5 Hardware design: discrete three-phase inverter..... 24
3.5.1 Power stage..... 24
3.5.2 Input conditioning and dead-time block..... 25

3.5.3 Low-side gate driver....25
3.5.4 High-side gate driver, level shifter and bootstrap supply....25
3.5.5 Current sensing....25
3.5.6 Supplies....26
3.6 Hardware design: CMOS gate driver....26
3.6.1 Architecture....26
3.6.2 Delay channel and bias....26
3.6.3 BJT interlock stage....27
3.6.4 High-side driver....28
3.6.5 Low-side driver....29
3.6.6 Power FETs and off-chip components....29
3.6.7 Layout and verification....30
3.7 Hardware implementation....31
3.7.1 PCB fabrication and bring-up....31
3.7.2 User-side mechanism....32
3.7.3 Drill-side mechanism....32
3.8 Software design and implementation....33
3.8.1 User-side firmware (STM32F405)....33
3.8.2 Drill-side firmware....35
3.8.3 Communication link....36
3.8.4 Safety functions....36
3.8.5 Console....37
3.9 System integration....37
4. Results....38
4.1 Summary of results achieved....38
4.2 Qualification tests....39
Qualification test 1: Bilateral feed control and force replication (Requirement 1)....39
Qualification test 2: Switching, dead time and shoot-through (Requirement 2)....46
Qualification test 3: Drive model and torque ripple (Requirement 3)....47
Qualification test 4: Drill-side thrust and position measurement (Requirement 4)....49
Qualification test 5: Rotor position and speed estimation (Requirement 5)....50
Qualification test 6: Safety limits and fault response (Requirement 6)....52
Qualification test 7: Operation under laboratory conditions (field condition)....53
5. Discussion....55
5.1 Critical evaluation of the design....55
5.1.1 Interpretation of results....55
5.1.2 Critical evaluation....57

5.1.3 Unsolved problems....58
5.1.4 Strong points of the design....58
5.1.5 Expected failure conditions....59
5.1.6 Comparison with the literature....59
5.2 Considerations in the design....59
5.2.1 Ergonomics....59
5.2.2 Health and safety....60
5.2.3 Environmental impact....60
5.2.4 Social and legal impact....60
5.2.5 Ethics clearance....60
6. Conclusion....61
6.1 Summary of the work completed....61
6.2 Summary of observations and findings....61
6.3 Contribution....61
6.4 Suggestions for future work....62
7. References....63
Appendix A. Additional results....65
A.1 Thrust available from the drill (push test)....65
A.2 Further timing measurements....65
Appendix B. Supplementary design material....66
B.1 Development path and console commands....66
B.2 Firmware constants....66
B.3 Discrete inverter components and bring-up faults....67
B.4 Additional simulation results....68
Appendix C. Physical Hardware Photographs....71

List of abbreviations and notation

The abbreviations used in this report are listed in Table 1.

Abbreviation	Meaning	Abbreviation	Meaning
AC	Alternating current	LVS	Layout versus schematic
ADC	Analogue-to-digital converter	MCPWM	Motor-control PWM peripheral (ESP32)
AMS	Assessment management system	MCU	Microcontroller unit
BJT	Bipolar junction transistor	MOSFET	Metal-oxide-semiconductor field-effect transistor
BLDC	Brushless direct current (motor)	NMOS, PMOS	N-channel, P-channel MOS transistor
CCR	Capture/compare register	NVS	Non-volatile storage
CDC	Communications device class (USB)	PAV	Pool-adjacent-violators (algorithm)
CMOS	Complementary metal-oxide-semiconductor	PCB	Printed circuit board
CMRR	Common-mode rejection ratio	PCNT	Pulse counter peripheral (ESP32)
CPR	Counts per revolution	PD, PI	Proportional-derivative, proportional-integral
DC	Direct current	PDK	Process design kit
DPWM	Discontinuous pulse width modulation	PMSM	Permanent-magnet synchronous machine
DRC	Design rule check	PWM	Pulse width modulation
EMI	Electromagnetic interference	RPM	Revolutions per minute
CRC	Cyclic redundancy check	SELV	Safety extra-low voltage
FET	Field-effect transistor	SPWM	Sinusoidal PWM
FF	Feed-forward	SR	Set-reset (latch)
FOC	Field-oriented control	SVM	Space-vector modulation
GPIO	General-purpose input/output	UART	Universal asynchronous receiver-transmitter
HAL	Hardware abstraction layer	USB	Universal serial bus
HV	High voltage	VSW	Half-bridge switching (phase) node
I²C	Inter-integrated circuit bus	LEDC	LED-control PWM peripheral (ESP32)
IC	Integrated circuit	ISR	Interrupt service routine

Table 1. Abbreviations.

Notation. Scalars are printed in italics. θ_m and θ_e are the mechanical and electrical rotor angles, p is the number of pole pairs and θ_{off} is the electrical offset. i_d, i_q and v_d, v_q are stator currents and voltages in the rotor (d-q) frame, and v_α, v_β are voltages in the stationary frame. $\hat{\theta}$ and $\hat{\omega}$ are the observer estimates of angle and speed. K_t is a torque constant, N is a transmission ratio, η is a transmission efficiency, L is the lever length, r_g is the grip radius and r is the pinion radius. F is force, T is torque, D is duty cycle, t_{dt} is dead time and f_{sw} is switching frequency.

Part 2. Project definition: approved Project Proposal

This section contains the problem identification in the form of the complete, approved Project Proposal, unchanged from the final approved version that appears on the AMS.

For use by the Project lecturer	Approved ✓	Revision required	

Feedback

For use by the Project module lecturer only

APPROVED
Prof JJ Hanekom , 7/22/2026, 3:57:56 PM

To be completed by the student

PROJECT PROPOSAL 2026

Project no	DJDB8	Revision no	2

Title	Surname	Initials	Student no	Study leader (title, initials, surname)
Mr	**Harischandre**	**S**	23843528	Dr. D. J. De Beer

Project title (this is the title on the project concept note)

CMOS co-design of a haptic drill press feed controller

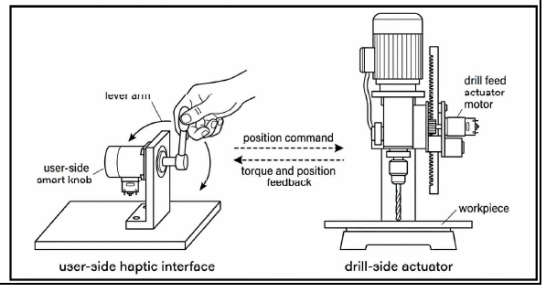
Language editor details	Language editor signature
Sunayna Balgobind	

Student declaration	**Study leader declaration**
I understand what plagiarism is and that I have to complete my project on my own.	This is a clear and unambiguous description of what is required in this project. Approved for submission (Yes/No) ✓
Student signature	Study leader signature and date
	DJdB 17/07/26

1. Project description. What is the problem to be solved with your project? Describe in non-technical language what your project is about. What does your system have to do? Refer explictly to Figure 1 that you inserted on the right.

Most rotary knobs and dials, like a volume control or a selector switch, have a fixed physical feel set by the springs and detents built into them at the time of manufacture. A single knob cannot feel like a smooth dial in one application and a precise clicking selector in another without physically swapping the hardware. This project develops a smart knob in which a small electric motor replaces all mechanical components, here applied to the remote operation of a drill press. By controlling the motor's force electronically in real time, the knob replicates drill feed resistance exactly as experienced at the workpiece, conveying the experience of drilling into materials such as soft wood, hard wood, aluminium, and plastic, including binding events, directly to the user via a lever. Feed resistance is continuously measured on the drill side and reproduced at the user side, giving the operator single-axis haptic control of the remote drill-press feed, as shown in Figure 1. A unique feature of this project is that the motor driver circuit is designed twice: once as a simulated microchip design using professional IC design software, and once built physically from real electronic components for live demonstration.

Figure 1. Insert an image below that captures the idea with your project. Explain in the text on the left.



2. Technical challenges in this project

Describe the technical challenges that are *beyond* those encountered up to the end of third year and in other final year modules.

2.1 Primary *design* challenges

What is the intended core technical challenge in the project? Which aspect or aspects of the design of the system do you expect to be the most challenging?

The primary design challenge is balancing Field-Oriented Control (FOC) current loop rate against haptic fidelity: higher loop rates improve torque smoothness and cogging rejection but demand faster sensing and greater computational load. A second challenge is deriving a cogging torque compensation model analytically from the motor's reluctance torque characteristics, requiring both theoretical derivation and empirical validation. A third challenge is achieving sufficient performance in the CMOS motor driver: the gate driver topology must balance drive strength against switching speed while maintaining shoot-through immunity, and the current sense amplifier must achieve adequate common-mode rejection in a PWM switching environment. A fourth challenge is bilateral haptic transparency.

2.2 Primary *implementation* challenges

Which aspect or aspects of the implementation do you expect to be the most challenging?

Fast PWM switching generates large common-mode transients that corrupt the small differential signals required by the FOC algorithm, demanding careful PCB layout to minimise noise coupling into the sensing path. Dead-time insertion introduces systematic torque errors most pronounced at low velocities, precisely the haptic operating regime, and must be compensated in firmware. Encoder resolution further limits haptic fidelity, as positional noise manifests as tactile roughness.

All processing will be done on an embedded platform, and not on a PC platform. Confirmed by having ticked this box. ☑

Library functions will be used for hardware interfacing only. Confirmed by having ticked this box. ☑

3. Functional analysis

3.1 Functional description

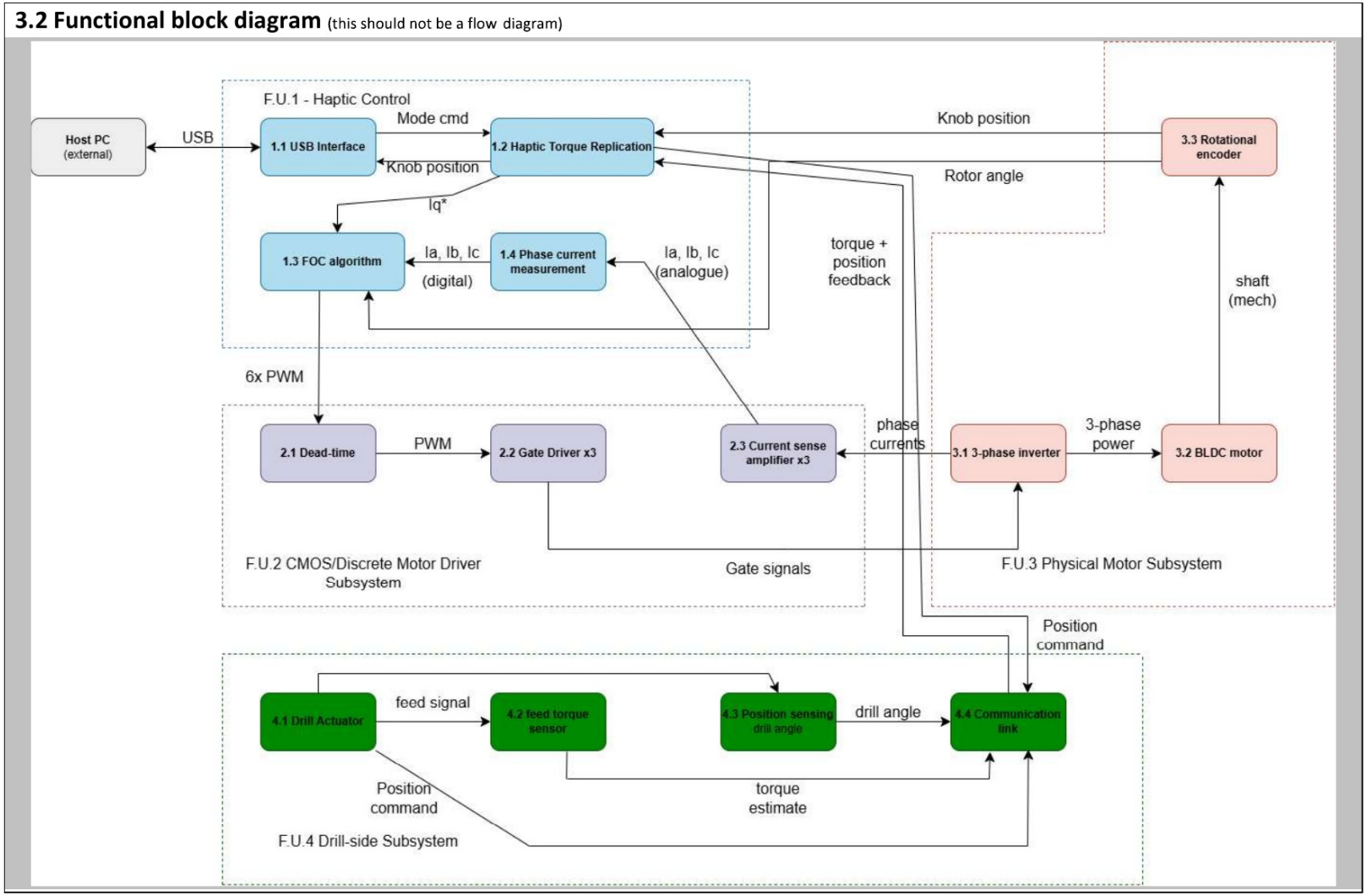
Describe the design in terms of system functions as shown on the functional block diagram in section 3.2. This description should be in *narrative format*. **DO NOT** use a bullet list.

The system operates as a bilateral haptic drill press control peripheral, comprising a user-side smart knob and a drill-side actuator subsystem linked via a deterministic communication interface (F.U.1, F.U.2, F.U.3, F.U.4). The user-side lever commands drill-side feed motion via the communication link, while drill-side feed resistance is continuously measured and transmitted back. The haptic torque replication logic (F.U.1, block 1.2) reads absolute rotor angle from the magnetic encoder and computes a torque command directly from the drill-side feed resistance, providing the operator with an exact haptic representation of drilling into soft wood, hard wood, aluminium, and plastic, including binding events, at the user-side lever in real time.

The torque command is realised by a field-oriented current control function (F.U.1, block 1.3), which regulates motor phase currents in a rotating reference frame synchronised to the rotor. This function continuously receives rotor angle and velocity from the position sensing function (F.U.3, block 3.3), and phase current measurements from the motor drive subsystem (F.U.2, block 2.3), closing a high-bandwidth current loop that produces smooth, accurate torque output. Cogging torque disturbances are rejected by a feedforward compensation function that applies a counter-torque derived from a characterised rotor angle lookup table on every control cycle.

The motor drive subsystem converts torque commands into physical three-phase voltages applied to the BLDC motor (F.U.3, block 3.2). A gate drive function (F.U.2, block 2.2) conditions PWM signals with precise dead-time insertion (F.U.2, block 2.1), preventing simultaneous conduction in any half-bridge. A current sensing function (F.U.2, block 2.3) measures phase currents across shunt resistors, providing the feedback signal necessary for closed-loop torque regulation. Both the CMOS simulation and the discrete physical realisation of this subsystem are designed at transistor level in Cadence Virtuoso, allowing direct comparison between simulated and measured circuit behaviour.

3.2 Functional block diagram (this should not be a flow diagram)



4. System requirements and specifications

These are the core requirements of the system or product (the mission-critical requirements) in table format **IN ORDER OF IMPORTANCE**. Requirement 1 is the most fundamental requirement.

	Requirement 1: the fundamental functional and performance requirement of your project	**Requirement 2** (Second in order of importance)	**Requirement 3** (Third in order of importance)
1. Core mission requirements of the system or product. Focus on requirements that are **core** to solving the engineering problem. These will reflect the solution to the problem.	The system shall control drill-press feed depth via a user-side lever and replicate drill-side feed resistance exactly at the lever, realising a single-axis bilateral haptic feed interface.	The system shall drive a three-phase BLDC motor via a discrete transistor-level inverter PCB with no shoot-through. The motor driver shall also be designed at transistor level in Cadence Virtuoso as a separate deliverable.	The system shall regulate motor phase currents in real time using Field-Oriented Control, maintaining stable closed-loop torque output across all lever positions and speeds during haptic drill press demonstration.
2. What is the target specification (this must be in *measurable* terms) to be met in order to achieve the requirement in 1. above?	Lever commands drill-side feed motion. Feed force replicated exactly, unscaled: up to 40N at 200mm lever. Loop ≥100Hz, latency ≤10ms, tracking error ≤15%. Materials: soft wood, hard wood, aluminium, plastic. Bits:1-10mm diameter	PWM switching frequency 10 kHz. Dead-time between complementary gate signals >0 ns and <500 ns. Current sense amplifier CMRR >60 dB. No shoot-through under any operating condition.	FOC current control loop shall operate at 10kHz. Phase current tracking error shall not exceed 5% of commanded value under steady-state load. Torque ripple shall not exceed 10% of commanded torque at any lever position.
3. Explain where this specification originated : i.e., **explain** the value that you selected. I.e., *how* will meeting the specification given in point 2 above *solve the problem*?	40N is required to drill aluminium . 200mm lever matches physical drill press feed wheel diameter. ≥100Hz and ≤10ms ensure bilateral loop stability and force transparency across all specified materials.	10 kHz limits current ripple for accurate FOC regulation [1]. Dead-time prevents shoot-through [2]. 60 dB CMRR prevents switching transients corrupting current measurement [3].	10 kHz gives 100 µs cycle sufficient to reject cogging disturbances [1]. An unstable current loop produces vibration felt as noise rather than intentional haptic feedback, making the device non-functional.
4. How will you demonstrate at the examination that this requirement and specification (points 1 and 2 above) have been met? Be explicit about how you will ***prove*** these were met.	Drill into each material with each bit size. Serial output confirms ≥100Hz loop rate and ≤10ms latency. Examiner operates actual drill press and user-side haptic lever consecutively, confirming equivalent resistance feel across materials.	Oscilloscope on switching node confirms PWM ≥ 10 kHz and visible dead-time gap. Sustained operation confirms no shoot-through. Cadence simulation waveforms confirm dead-time insertion and CMRR.	Phase current waveforms observed on oscilloscope via PCB test points. Commanded vs measured Iq displayed on serial terminal confirming ≤5% tracking error under steady-state load. Examiner confirms smooth torque by hand.
5. Your own design contribution: what are the aspects that *you will design and implement yourself* to meet the requirement in point 2? If none, *remove this requirement.*	Bilateral firmware: lever position measured and transmitted as feed command. Drill-side feed torque measured, transmitted, applied directly as torque command to FOC algorithm. Saturation logic implemented. No libraries.	Discrete inverter PCB: MOSFET selection, gate driver circuit, dead-time control block, bootstrap high-side supply, level shifter. Cadence Virtuoso: CMOS IC-level design of all equivalent subcircuits using 180nm PDK.	FOC entirely from scratch: Clarke and Park transforms, dual PI controllers with anti-windup, inverse transforms, SVM, cogging feedforward lookup table, dead-time distortion compensation. No motor control libraries used.
6. What are the aspects to be taken off the shelf to meet this requirement? If none, indicate "none". Clearly specify for what tasks **library functions** will be used (if relevant to the project).	BLDC motor. Rotational encoder. Hardware interfacing library functions permitted for peripheral communication only.	Power MOSFETs, bootstrap diodes, shunt resistors, gate resistors, decoupling capacitors. Cadence Virtuoso and CMOS PDK. No off-the-shelf gate driver ICs. PCB fabricated externally.	Embedded microcontroller platform. ADC peripheral. SPI, ADC, timer and PWM hardware interfacing library functions permitted for peripheral communication only.

System requirements and specifications page 2			
	Requirement 4 (Fourth in order of importance)	**Requirement 5**	**Requirement 6**
1. Core mission requirements of the system or product. Focus on requirements that are core to solving the engineering problem. These will reflect the solution to the problem.	The drill-side subsystem shall continuously measure feed torque and angular position, and transmit both to the user-side haptic interface in real time to close the bilateral haptic control loop.	The system shall continuously measure absolute rotor position and estimate angular velocity, providing the FOC algorithm and torque replication logic with accurate real-time angle and speed data at every control cycle.	The system shall enforce safe operating limits on both subsystems, including maximum force limits, emergency stop functionality, and defined safe-state behaviour on communication loss or sensor fault.
2. What is the target specification (this must be in *measurable* terms) to be met in order to achieve the requirement in 1. above?	The drill-side subsystem shall continuously measure feed torque and angular position, and transmit both to the user-side haptic interface in real time to close the bilateral haptic control loop.	Absolute rotor position and velocity estimate shall be updated at the FOC loop rate. Velocity estimation error shall not exceed ±5 RPM when the system executes a commanded rotation of one full revolution in one second.	User-side haptic force shall not exceed 42N at 200mm lever. Drill-side feed speed shall not exceed 5mm/s. On communication loss both subsystems shall stop actuation within 100ms. E-stop disables both subsystems.
3. Explain where this specification originated: i.e., explain the value that you selected. I.e., *how* will meeting the specification given in point 2 above solve the problem?	Accurate real-time feed torque and position measurement on the drill side is necessary to close the bilateral haptic loop. Without this, the user-side actuator has no signal to replicate and the system is non-functional.	Accurate rotor angle compensates for readout latency in the Park transform, preventing d/q axis cross-coupling [2]. Velocity is required for cogging feedforward timing and torque replication stability.	Uncontrolled haptic forces pose a risk to the user. 42N is the motor continuous force ceiling. 5mm/s is approximately twice the normal drilling feed rate, limiting quill motion. Safe-state on fault prevents runaway on either subsystem.
4. How will you demonstrate at the examination that this requirement and specification (points 1 and 2 above) have been met? Be explicit about how you will *prove* these were met.	Known mass suspended from feed lever. System-reported torque compared to expected value confirming ±5% accuracy. Serial output confirms ≥100Hz transmission. Examiner confirms lever responds to drill-side resistance.	System commands one full rotation in one second via FOC. Encoder velocity estimate displayed on screen shall read 60 ±5 RPM during rotation, confirming accurate velocity tracking against a self-generated reference.	Maximum torque commanded to user-side lever, force confirmed ≤42N via suspended mass. Communication loss simulated, confirming both subsystems cease actuation within 100ms. E-stop confirmed to disable both subsystems.
5. Your own design contribution: what are the aspects that *you will design and implement yourself* to meet the requirement in point 2? If none, *remove this requirement.*	Drill-side firmware: feed torque measurement, angular position measurement, and continuous transmission to user-side subsystem. No libraries.	Encoder polling firmware, electrical angle computation from mechanical angle and pole pairs, velocity estimation from successive readings, cogging profile characterisation and feedforward lookup table construction.	Firmware: user-side torque saturation at motor limit. Drill-side feed speed limiting. Watchdog timer triggering safe-state on communication timeout. Sensor fault detection disabling actuation. Emergency stop interrupt handler.
6. What are the aspects to be taken off the shelf to meet this requirement? If none, indicate "none". Clearly specify for what tasks **library functions** will be used (if relevant to the project).	Drill-side actuator. Feed torque sensor. Rotational encoder. Motor driver hardware. Hardware interfacing library functions permitted for peripheral communication only.	Rotational encoder. Shaft magnet mounted on motor shaft bottom end. Hardware interfacing library functions permitted.	None.

System requirements and specifications page 3			
	Requirement 7 (Seventh in the order of importance)	**Requirement 8**	**Requirement 9**
1. Core mission requirements of the system or product. Focus on requirements that are core to solving the engineering problem. These will reflect the solution to the problem.			
2. What is the target specification (this must be in *measurable* terms) to be met in order to achieve the requirement in 1. above?			
3. **Explain where this specification originated**: i.e., explain the value that you selected. I.e., *how* will meeting the specification given in point 2 above solve the problem?			
4. **How will you demonstrate at the examination** that this requirement and specification (points 1 and 2 above) have been met? Be explicit about how you will *prove* these were met.			
5. Your own design contribution: what are the aspects that *you will design and implement yourself* to meet the requirement in point 2? If none, *remove this requirement.*			
6. What are the aspects to be taken off the shelf to meet this requirement? If none, indicate "none". Clearly specify for what tasks **library functions** will be used (if relevant to the project).			

5. Real world field conditions

These are the ACTUAL, REAL WORLD CONDITIONS under which your project has to work *and will be demonstrated.*

	Real world field condition 1 (required to include)	**Real world field condition 2** (optional to include)	**Real world field condition 3** (optional to include)
Field condition requirement. In which real world conditions does the system have to operate?E.g., "lab conditions" or "outside in uncontrolled conditions". Describe the one, two or three most important field conditions.	The system shall operate under ambient indoor laboratory conditions, including ambient temperature variations between 15–35°C and background electromagnetic interference from co-located lab equipment.		

6. Student tasks

6.1 Design and implementation tasks of the student

List your primary design and implementation tasks in bullet list format (5-10 bullets). These are *NOT* product requirements, but *YOUR* tasks.

- The motor driver subsystem functional blocks will be designed at transistor level in Cadence Virtuoso and validated by simulation.
- A discrete three-phase inverter PCB will be designed and built, physically realising the motor driver subsystem functional blocks.
- The torque control functional block will be designed and implemented entirely in embedded firmware from first principles, using no motor control libraries.
- The position sensing functional block will be designed and implemented in firmware, providing rotor angle and velocity data to the torque control and closed-loop torque replication blocks.
- The drill-side instrumentation functional block will be designed and implemented in firmware, continuously measuring feed torque and angular position and transmitting both to the user-side subsystem.
- The bilateral haptic control loop will be designed and implemented in firmware, commanding drill-side feed motion from lever position and replicating drill-side feed torque exactly at the user-side lever.

6.2 New knowledge to be acquired by the student

Describe what the theoretical foundation to the project is, and which *new* knowledge you will acquire (*beyond* that covered in any other undergraduate modules).

Field-Oriented Control theory will be studied and implemented: Clarke and Park transforms, rotating reference frame current regulation, and space vector modulation extend beyond undergraduate coverage. CMOS analog IC design will be studied: transistor-level design of differential amplifiers, current mirrors, inverter buffer chains, and high-voltage level shifters in Cadence Virtuoso extends beyond undergraduate digital CMOS modules. Gate driver design for power electronics will be studied: bootstrap circuit operation, dead-time insertion effects on output voltage, and shoot-through prevention in half-bridge topologies are not covered in undergraduate coursework. Cogging torque compensation and dead-time distortion correction will be studied: the reluctance torque model, cogging profile characterisation, feed forward LUT compensation, and duty-cycle correction firmware are not addressed in the undergraduate curriculum. High-frequency PCB layout for power electronics will be studied: switching loop inductance management, decoupling strategies, and ground plane design to prevent noise coupling into current sensing paths are not covered in undergraduate coursework. Bilateral haptic teleoperation will be studied: force replication between decoupled subsystems.

7. References

Format your reference list either in IEEE reference format or in APA reference format. Check what your study leader prefers and use consistently.

[1] N. Mohan, T. M. Undeland, and W. P. Robbins, Power Electronics: Converters, Applications, and Design, 3rd ed. Hoboken, NJ: John Wiley & Sons, 2003.
[2] D. G. Holmes and T. A. Lipo, Pulse Width Modulation for Power Converters: Principles and Practice. Hoboken, NJ: IEEE Press/Wiley-Interscience, 2003.
[3] B. Razavi, Design of Analog CMOS Integrated Circuits, 2nd ed. New York, NY: McGraw-Hill, 2017.
[4] V. Hayward, O. R. Astley, M. Cruz-Hernandez, D. Grant, and G. Robles-De-La-Torre, "Haptic interfaces and devices," Sensor Review, vol. 24, no. 1, pp. 16–29, 2004.

Part 3. Main report

1. Literature study

This section reviews the literature behind the design. Section 1.1 sets out the background as one chain of argument: what a haptic feed interface must do, how bilateral teleoperation achieves it, how large drilling forces are, how a brushless motor produces controlled torque, and how the power stage and its CMOS counterpart are driven safely. Section 1.2 then states which of these results were applied, and where.

1.1 Background and context of the problem

1.1.1 Haptic interfaces and transparency

A haptic interface is an actuated mechanism that exchanges mechanical energy with a human hand, so that the user feels forces generated or measured by a computer rather than by a fixed mechanism [1]. Hayward et al. identify the properties that decide whether such a device feels convincing. They are low friction and low inertia, so that the device is "transparent" when no force is commanded, backdrivability, so that the user can move the device against the actuator, and a torque source whose output follows its command over the bandwidth that human touch perceives [1]. Conventional knobs and levers do not have these properties because their feel is set by springs, detents and friction at manufacture. A motor-driven lever can instead change its feel in software, which is the starting point of this project.

Achieving the required force with a small motor usually needs a transmission, and the transmission is where transparency is lost. Gosselin et al. compared transmission options for backdrivable haptic and collaborative-robot actuators [2]. Gear trains, including planetary gearboxes, introduce backlash and friction that reduce backdrivability. Cable capstan drives have almost no backlash but are limited in rotation range and need several wraps of cable. Belt-type transmissions sit between the two, with low backlash and unlimited rotation, but a toothed belt can skip teeth when the load reverses. Herringbone (double-helical) gears improve on plain spur gears: several teeth share the load at every instant, so the mesh is smooth, and the opposed helices cancel the axial thrust, although some backlash remains. Any reduction N also scales the friction felt at the output by N and the reflected rotor inertia by N^2, so the ratio is a compromise between force capability and transparency.

A second limit on haptic rendering is stability. Colgate and Brown showed that the range of impedances a sampled-data haptic display can render passively (its "Z-width") is bounded by the sample rate, the quantisation of the position sensor and the physical damping present in the device [3]. Stiff virtual springs and walls, which are exactly what a lever needs to feel the onset of cutting, are therefore limited by sensor resolution and loop rate. Physical damping in the mechanism, such as that of a hand gripping a lever, widens the range that can be rendered.

1.1.2 Bilateral teleoperation and force reflection

The drill-press feed interface is a bilateral teleoperator. A master device held by the operator commands a slave device that interacts with the environment, and the force measured at the slave is reflected to the master. Anderson and Spong placed this problem on a control-theoretic footing, and showed that communication delay between master and slave can make a force-reflecting loop unstable unless the communication channel is made passive [4]. Lawrence formalised the trade-off between stability and transparency, where transparency means that the impedance felt by the operator equals the impedance of the environment. He

showed that the architecture chosen, in particular which signals are sent forward and back, sets how transparent the loop can be for a given stability margin [5].

Hokayem and Spong surveyed four decades of such architectures [6]. The two most common are position-position coupling, in which each side tracks the position of the other, and position-force coupling (direct force reflection), in which the master position is sent to the slave and the measured slave force is sent back as a force command. Direct force reflection is attractive when a force measurement is available at the slave, because it reflects the true interaction force rather than a position error. Heck et al. showed that direct force reflection can be made passive in the presence of time delay by adding a separate passivity layer, without degrading the transparency of the underlying loop [7]. In the present application both nodes move slowly (a drill feed rarely exceeds a few millimetres per second), which reduces the effect of a few milliseconds of link delay. The literature nevertheless indicates that update rate and latency set the upper bound on transparency.

1.1.3 Drilling thrust force and its measurement

To replicate the feed resistance, the magnitude of the force must be known. The thrust force in twist drilling depends on the workpiece material, the drill diameter and the feed per revolution. Shaw and Oxford gave the classical empirical relations for thrust and torque, in which thrust grows approximately linearly with drill diameter and sub-linearly with feed [8]. For small bits and light hand feeds on a bench drill, the thrust in wood and plastics is of the order of tens of newtons, and in aluminium it reaches a few hundred newtons. Kishore Kumar et al. measured about 320 N for a 6 mm drill and about 410 N for an 8 mm drill in Al 6061-T6 at a feed of 0.2 mm per revolution [9]. Uddin et al. found that doubling the feed of an 8 mm drill in Al 6061 from 0.04 to 0.08 mm per revolution raised the axial force by only 29 to 45 % [10], so at low feeds the thrust varies roughly with the square root of the feed. Reflected through the pinion and grip radius of this design (Section 3.3.10), a thrust of 400 N corresponds to about 40 N at the lever, which is consistent with the proposal specification.

The thrust can be measured directly with a dynamometer or load cell under the workpiece, or it can be inferred from the drive. In a multi-sensor study of drilling, thrust force, torque and the electrical power drawn by the drive all correlated with the cutting condition [11], so inference from motor current is possible in principle. It is only valid in steady feed, however, because during acceleration, reversal and stiction breakaway the motor current also supplies inertia and friction torque, not cutting force [12]. A direct measurement with strain-gauge load cells avoids this, and is valid at every instant. Its bandwidth is set by the bridge converter: the common HX711 sigma-delta converter samples at 10 or 80 samples per second [13], which is adequate for the slowly varying thrust of a hand-fed drill but smooths sharp events such as break-through.

1.1.4 Torque control of permanent-magnet motors

Rendering a commanded force at the lever requires a motor whose torque follows a command smoothly at very low speed. Field-oriented control (FOC), introduced by Blaschke for induction machines [14], meets this need for permanent-magnet synchronous machines, of which the brushless DC motor with sinusoidal back-EMF is a practical example. FOC transforms the three phase quantities into a two-axis frame that rotates with the rotor (the Clarke and Park transforms). In that frame the torque-producing current iq and the flux-producing current id are DC quantities that can be regulated with PI controllers, and the inverse transforms produce the three phase voltage commands [15]. For a surface-mounted

magnet machine, torque is proportional to iq alone, so id is held at zero for maximum torque per ampere.

FOC does not need specialised hardware. Prayogo et al. implemented the complete current-controlled FOC loop with space-vector modulation on a low-cost STM32F103 microcontroller [16], which shows that a general-purpose MCU of the class used in this project is sufficient. An alternative variant, voltage-mode FOC, omits the current loop and commands vq directly. The torque then follows vq only as closely as the winding resistance is constant and the back-EMF is small compared with vq. This condition holds at the low speeds typical of a hand-operated haptic device, but it removes the ability to regulate current against disturbances.

The three voltage commands are converted into switching signals by a modulator. Holmes and Lipo [15] and Hava et al. [17] showed that any common-mode (zero-sequence) voltage can be added to the three references without changing the line-to-line voltages seen by the motor. Discontinuous PWM (DPWM) uses this freedom to clamp one phase to a DC rail for 120 electrical degrees at a time. The clamped phase does not switch, which reduces switching losses and the number of switching events by about one third [17].

1.1.5 Position sensing, velocity estimation and friction

FOC needs the electrical rotor angle at every update, obtained from a mechanical angle sensor as $\theta e = p\theta m + \theta off$. An angle error $\Delta\theta e$ reduces the torque by a factor $\cos(\Delta\theta e)$ and couples the d and q axes [15]. Haptic control also needs velocity, for damping and friction compensation. Lorenz and Van Patten showed that differentiating a quantised position signal produces velocity noise inversely proportional to the sample interval. They recommended an observer, which models the rotor as an integrator chain and corrects its estimate with the measured position, as a way to obtain a velocity estimate that is both smooth and fast [18].

Friction is the other obstacle to smooth low-speed motion. Armstrong-Hélouvry et al. reviewed friction models and compensation methods [12]. Their review identifies stiction (static friction greater than kinetic friction) as the cause of stick-slip motion and of limit cycles in position loops with integral action. It also identifies Coulomb friction feed-forward and the limiting of integral action near rest as standard remedies. These results apply both to the haptic lever and to the drill-press quill, which is loaded by a return spring and has considerable static friction.

The motor itself adds a position-dependent disturbance, the cogging torque, which comes from the interaction between the rotor magnets and the stator slots. Bianchi and Bolognani described its origin and design-level reduction [19], and Jahns and Soong reviewed control-side techniques for suppressing pulsating torque, including feed-forward compensation from a table indexed by rotor angle [20]. In a geared haptic device the cogging period is divided by the reduction ratio at the handle, which moves it into the frequency range where the skin is most sensitive.

1.1.6 Half-bridge gate driving and dead time

Each motor phase is driven by a half-bridge of two MOSFETs. If both conduct at once, the DC link is shorted ("shoot-through"). A dead time, during which both switches are held off, is inserted at each transition to prevent this [21]. The dead time must exceed the difference between the turn-off and turn-on delays of the switches and their drivers. However, each

dead-time interval makes the output voltage depend on the current direction, and Murai et al. showed that this distortion is most severe at low current and low output voltage [22]. That is precisely the operating region of a haptic motor. Grezaud et al. showed that the dead time can be generated inside the gate driver and adapted to the switching conditions [23].

The high-side switch needs a gate voltage referenced to the switching node, which moves between the rails. The usual low-cost solution is a bootstrap supply, in which a capacitor charged through a diode while the low-side switch conducts. The capacitor must hold enough charge for the high-side on-time, and the low side must conduct often enough to recharge it [21]. A level shifter carries the ground-referenced command into the floating domain, and it must stay correct while the switching node slews rapidly.

1.1.7 CMOS realisation of the driver

Gate drivers with integrated timing are routinely built in high-voltage CMOS processes of the same class as the 0.18 µm process used here. Ly et al. reported a reconfigurable half-bridge gate driver in 0.18 µm HV SOI CMOS with on-chip dead-time generation in the nanosecond range [24]. The basic timing element in such circuits is the current-starved inverter. A current source limits the current available to charge a capacitive node, so the delay is set by the ratio of capacitance and voltage swing to bias current [25], [26]. Nasre and Asutkar used the same principle, with a stabilised bias reference, to build a current-starved oscillator in 0.18 µm CMOS [27]. A design of this kind is verified by transient simulation, then by physical layout checked with design-rule (DRC) and layout-versus-schematic (LVS) checks [26].

1.1.8 Communication in the control loop

In a bilateral system the communication channel is part of the control loop. Anderson and Spong showed that delay in the channel can destabilise force reflection [4], and Heck et al. showed how the loop can be kept passive in the presence of delay [7]. Two practical consequences follow. First, the channel should have a fixed, short and measurable delay, which favours a dedicated wired serial link over a shared wireless one when the two nodes are close together. Second, any force that depends only on the operator's own position, such as a virtual spring or a modelled workpiece, should be computed locally at the master rather than sent across the channel, because a delayed position-dependent force behaves like a spring with a time lag and can drive the loop into oscillation [3], [7]. Frames on the link need integrity checks (a CRC) and sequence numbers so that corrupted or stale data are discarded, and a timeout must place both nodes in a safe state when frames stop arriving.

1.2 Application of the literature to this project

The literature was applied to the design as follows.

- Transparency and transmission [1], [2]: a backdrivable BLDC motor with a two-stage herringbone gear reduction was chosen for the lever, after a timing-belt reduction skipped teeth when the lever back-drove the motor as well as inflicted heavy frictional forces which hindered haptic transparency. The 16:1 ratio was set by balancing the force requirement against friction (×N) and reflected inertia (×N²) (Section 3.3.2).
- Bilateral architecture [5], [6], [7]: a position-force (direct force reflection) structure was adopted, with lever position sent forward as the quill target and the measured thrust returned and rendered as lever force. The update-rate and latency specifications of the proposal follow from this literature (Sections 3.2 and 3.8.3).

- Drilling force [8], [11], [13]: the feed thrust is measured directly by four load cells under the work platform rather than inferred from motor current, which is not valid during transients. (Sections 3.3.8 and 3.8.2).
- Delay in the loop [4], [7], [3]: the two nodes are joined by a wired UART with CRC-checked, sequence-numbered frames, and the position-dependent forces (return spring, virtual workpiece and walls) are computed on the lever node so that link delay does not enter them (Sections 3.3.9 and 3.8.3).
- FOC and modulation [14], [15], [17], [16]: the Clarke, Park and inverse transforms were implemented from first principles on a general-purpose MCU. Bottom-clamped DPWM was used so that within each phase the two switches are never switched complementarily (Sections 3.3.3 and 3.8.1).
- Velocity estimation and friction [18], [12], [3]: an α-β observer replaced finite differencing of the 12-bit encoder signal. Friction feed-forward was taken from the reference trajectory rather than the measurement, and integral action was limited near rest (Sections 3.3.4 and 3.4.3).
- Dead time and CMOS timing [21], [22], [23], [24], [25], [27]: a current-starved delay channel followed by a BJT interlock stage was designed in the XH018 process to provide non-overlapping outputs. The discrete board was designed with an RC and Schmitt-trigger dead-time block, which was later found to be incompatible with PWM operation (Sections 3.5 and 3.6).

The reviewed literature treats force-reflecting control, transparent transmissions, motor control and gate-driver design as separate problems. No comparable system was found in which a transistor-level CMOS driver and a discrete driver of the same topology are co-designed to power a bilateral drill-feed haptic interface. The contribution of the project is this integration, not new control theory.

2. Approach

This section explains, at concept level, how the problem in the approved proposal was approached, which alternatives were considered and why the preferred solution was chosen. The detailed design follows in Section 3.

2.1 Concept

The proposal defines four functional units: haptic control (F.U.1), the motor driver (F.U.2), the physical motor and lever (F.U.3) and the drill-side subsystem (F.U.4). The approach keeps this split and builds the system as two nodes joined by a cable. The user-side node holds a lever driven by a brushless motor through a two-stage gear reduction. Its angle is sent to the drill-side node as a feed target, and the thrust measured at the drill is returned and rendered at the lever as force. The drill-side node moves the quill of an unmodified bench drill with a geared DC motor mounted directly on the feed shaft, measures quill position with the motor encoder, and measures the axial thrust on the workpiece with four load cells under the work platform. The motor driver of the user-side node was designed twice: as a discrete board that drives the real motor, and at transistor level in CMOS as a simulation deliverable.

2.2 Alternatives and trade-offs

The main design decisions are summarised in Table 2. Three choices shaped the final system most. First, the feed thrust is measured directly with load cells instead of being inferred from motor current, because the inference is valid only in steady feed and proved too inaccurate in practice. Second, the lever motor runs voltage-mode FOC, and its phase current is estimated from a measured model of the drive rather than measured, a deliberate choice that gives smoother torque than a current loop on this motor (Section 3.3.3). Third, the nodes are joined by a wired UART rather than a radio link, which gives a fixed, short and checkable delay. Forces that depend only on the lever position are computed on the lever node so that this delay does not enter them.

Decision	Alternatives considered	Chosen	Main reason
Lever actuator	Brushed DC, stepper, BLDC	DF4015 BLDC, 11 pole pairs	Backdrivable, brushless, suits FOC
Lever transmission	Direct drive, capstan, planetary gear, timing belt, herringbone gears	Two-stage 3D-printed herringbone gearbox 16:1 (18:72 per stage), 150 mm angled handle (95 mm grip radius)	Belts skipped teeth when back-driven, smooth mesh, no axial thrust, backlash comparable to the press's rack and pinion
Modulation	Six-step, complementary SPWM, bottom-clamp DPWM	Bottom-clamp DPWM, and each phase chops the one FET that matches its current direction	A leg is never switched as a complementary pair, correct phase voltage for both current directions
Torque control	Current-mode FOC, voltage-mode FOC	Voltage-mode FOC with a measured drive model	Current predictable from Vq, and no current sensors needed
Discrete dead time	RC + Schmitt + SR latch, software, none needed	Latch removed, modulation avoids complementary switching but RC deadtime is present,	SR latch locks under PWM
User-side MCU	ESP32, STM32F405	STM32F405 (168 MHz)	Timer PWM, interrupt-driven timing, USB CDC
Drill actuator	BLDC, brushed gearmotor, lead screw	FIT0185 131:1 gearmotor on the feed shaft	High torque, built-in encoder, no change to the drill
Feed-force sensing	Motor current, load cells	Four load cells in a full bridge, HX711	Direct, valid in transients, current inference too inaccurate

Decision	Alternatives considered	Chosen	Main reason
Link	ESP-NOW radio, wired UART	Wired UART, 460.8 kbaud, CRC-8	Fixed delay, no packet loss at short range (enabling function only)
CMOS scope	Driver only, driver with power stage	Gate driver on chip, power FETs and bootstrap capacitor external	A 100 nF capacitor needs about 43 mm² of silicon, commercial gate-driver ICs drive external power FETs

Table 2. Design alternatives and the preferred solution.

The ESP32 used on the drill side is a general-purpose device. It was chosen for specific peripherals the design depends on and acts more as a dummy extension of the STM32 for more hardware interfacing: the pulse-counter (PCNT) unit, which decodes the quadrature encoder in hardware, the hardware PWM units and a spare UART. The serial link is an enabling subsystem and is not claimed as a design contribution.

3. Design and implementation

This section describes the design and implementation of the system in detail. It opens with the compulsory design summary and system block diagram, derives the governing relations and design values, reports the simulation studies, and then describes the discrete hardware, the CMOS driver, the mechanical build and the firmware of both nodes.

3.1 Design summary

This section summarises the project design tasks and how they were implemented (see Table 3).

Deliverable or task	**Implementation**	**Completion of deliverable or task, and section in the report**
6.1: The motor driver subsystem functional blocks will be designed at transistor level in Cadence Virtuoso and validated by simulation. Req 2 (row 5): Cadence Virtuoso: CMOS IC-level design of all equivalent subcircuits using 180nm PDK.	XH018 0.18 µm HV process: current-starved delay channels, BJT interlock stage, high-side and low-side drivers and power FETs, simulated in Spectre, one-phase cell laid out, power FETs and bootstrap capacitor external, no current-sense amplifier, because the design does not measure current.	Complete. One phase simulated, DRC and LVS clean. Sections 3.4.2, 3.6
6.1: A discrete three-phase inverter PCB will be designed and built, physically realising the motor driver subsystem functional blocks. Req 2 (row 5): Discrete inverter PCB: MOSFET selection, gate driver circuit, dead-time control block, bootstrap high-side supply, level shifter.	Logic-level IRLZ44N MOSFETs, BJT low-side drivers, bootstrap high-side drivers with ground-referenced level shifters, RC turn-on delay in every gate channel (SR latch removed), one 5 V gate supply, fabricated and reworked.	Completed. Sections 3.4.1, 3.5, 3.7.1
6.1: The torque control functional block will be designed and implemented entirely in embedded firmware from first principles, using no motor control libraries. Req 3 (row 5): FOC entirely from scratch: Clarke and Park transforms, dual PI controllers with anti-windup, inverse transforms, SVM, cogging feedforward lookup table, dead-time distortion compensation. No motor control libraries used.	Transforms, electrical-angle alignment and inverse transforms from first principles, voltage-mode control (vd = 0) with the current estimated from a measured drive model, which replaces the PI current controllers, bottom-clamp DPWM in place of SVM, current-direction chopping corrects the switching-induced voltage distortion, cogging table built but disabled. No motor control libraries.	Completed in voltage mode: the phase current is set through the measured drive model in place of PI current loops, because the current is predictable from the commanded voltage at haptic speeds. Sections 3.3.3, 3.3.4, 3.8.1
6.1: The position sensing functional block will be designed and implemented in firmware, providing rotor angle and velocity data to the torque control and closed-loop torque replication blocks. Req 5 (row 5): Encoder polling firmware, electrical angle computation from mechanical angle and pole pairs, velocity estimation from successive readings, cogging profile characterisation and feedforward lookup table construction.	AS5600 read at 1 kHz by interrupt-driven I²C, multi-turn unwrap, electrical angle from 11 pole pairs, α-β observer for angle and speed, cogging profile measured and stored as a lookup table, which is disabled because it did not reduce the ripple.	Completed. Sections 3.3.5, 3.8.1

Deliverable or task	Implementation	Completion of deliverable or task, and section in the report
6.1: The drill-side instrumentation functional block will be designed and implemented in firmware, continuously measuring feed torque and angular position and transmitting both to the user-side subsystem. Req 4 (row 5): Drill-side firmware: feed torque measurement, angular position measurement, and continuous transmission to user-side subsystem. No libraries.	Feed force measured as thrust by a four-cell load platform and HX711 (read without a library), position by the PCNT encoder, and both sent in every 200 Hz drill frame.	Completed. Sections 3.3.8, 3.8.2
6.1: The bilateral haptic control loop will be designed and implemented in firmware, commanding drill-side feed motion from lever position and replicating drill-side feed torque exactly at the user-side lever. Req 1 (row 5): Bilateral firmware: lever position measured and transmitted as feed command. Drill-side feed torque measured, transmitted, applied directly as torque command to FOC algorithm. Saturation logic implemented. No libraries.	Lever target sent at 1 kHz, thrust returned at 200 Hz and rendered unscaled at the grip, leash and wall coupling, force and current saturation, virtual workpiece and return spring rendered locally.	Completed. Sections 3.3.10, 3.8.3
Req 6 (row 5): Firmware: user-side torque saturation at motor limit. Drill-side feed speed limiting. Watchdog timer triggering safe-state on communication timeout. Sensor fault detection disabling actuation. Emergency stop interrupt handler.	Lever force capped at 40 N and phase current at 3.4 A, feed-speed cap available but left off (Section 5.1.1), 30 mm/s limit and end-of-stroke slow-down, 60 ms link timeout on both nodes, latched E-stop carried in every link frame, 32 kg thrust cap, maximum drill duty and heat budget.	Completed. Section 3.8.4

Table 3. Design summary. Column 1 quotes the tasks of section 6.1 and row 5 of the requirements in the approved Project Proposal.

3.2 System block diagram

The final system is shown in Figure 1. On the user side the STM32F405 reads the AS5600 encoder on the motor shaft and runs the FOC, haptic and force-rendering logic. It drives the six gate inputs of the discrete three-phase inverter, which powers the DF4015 motor, and the motor turns a 150 mm lever handle through a 16:1 herringbone gearbox. A browser console on USB selects modes and displays telemetry. The STM32 sends the lever target to the drill node over a wired UART at 1 kHz. On the drill side an ESP32 moves the quill through a BTS7960 H-bridge and the FIT0185 gearmotor, reads the quill position from the motor encoder and the thrust from four load cells through an HX711, and returns position, thrust and status at 200 Hz. The lever node converts the thrust into a lever force and renders it.

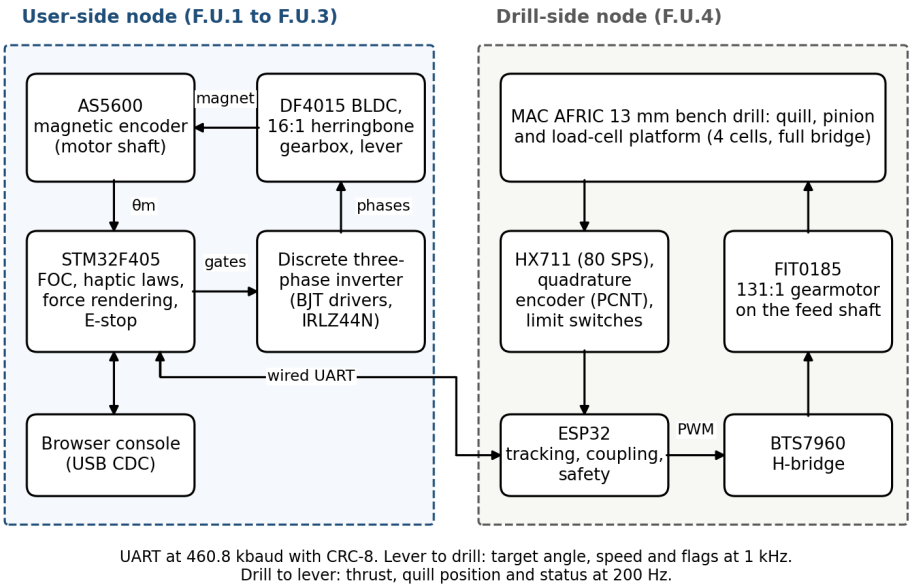


Figure 1. Final system block diagram.

Compared with the functional block diagram of the proposal, three blocks changed. Phase-current measurement in the user-side path (block 1.4) was replaced by a current estimate from a measured drive model, the drill-side feed-torque sensor became a load-cell platform, and the host-PC impedance programming over USB became a console that selects modes and sends virtual-workpiece profiles. A cogging-compensation table was built for the position-sensing block, but it is disabled in the final system because the ripple it measured came mainly from the modulation (Section 3.8.1).

3.3 Theoretical analysis and design calculations

This section derives the relations used to size the system and to set its firmware constants.

3.3.1 Drill feed mechanics

The quill of the MAC AFRIC drill travels s = 50 mm over its full stroke. The feed gearmotor sits directly in the feed-shaft hub where the hand levers were, so the feed pinion turns with the motor output shaft. The calibration run measured about 7100 encoder counts over the stroke, which corresponds to about 305° of shaft rotation, so the effective pinion radius is given by Eq. 1, where θs is the shaft rotation over the stroke in radians.

$$r = s / \theta s = 50\ mm / (305° \times \pi/180) \approx 9.4\ mm \quad (1)$$

The radius is smaller than the 7.96 mm that one full turn per stroke would give, and the difference matters: a force conversion based on 7.96 mm rendered forces about 15 % too weak. The firmware therefore takes the radius from the stroke measured in each calibration run, and the drill sends it to the lever node in every frame, so the force and depth conversions on both nodes follow the mechanism. An axial thrust Fax at the quill corresponds to a pinion torque Tp (Eq. 2).

$$Tp = Fax \cdot r \quad (2)$$

The FIT0185 gearmotor has a stall torque of 48 kg·cm (4.71 N·m), so the largest thrust it can produce at stall is about 4.71/0.0094 ≈ 500 N, or 51 kg. Near stall the motor draws about 7 A and heats rapidly, so it can approach this value only for seconds. The firmware caps the thrust at 32 kg (314 N), a pinion torque of 2.95 N·m or 63 % of the stall torque, to protect the motor, its gearbox and the shaft coupling. Aluminium is the hardest material of Requirement 1. In Al 6061-T6 an 8 mm drill needs about 410 N at 0.2 mm per revolution [9], and at low feeds the thrust varies roughly with the square root of the feed [10], which gives about 410 × (0.05/0.2)^0.5 ≈ 205 N (21 kg) at 0.05 mm per revolution. Thrust scales roughly with the drill diameter [8], so a 3 mm drill needs about 80 N, and wood and plastics need less. In teleoperation at the 60 % duty limit the drill pressed about 15 kg (147 N) on the scale, enough for wood and plastic at any bit size up to 10 mm, while an 8 mm hole in aluminium needs a slow feed or a 3 mm pilot hole, which removes most of the thrust of the larger bit.

A feed-speed cap for the 5 mm/s of Requirement 6 is available as a drill setting. It is converted to encoder counts per second with the calibrated counts-per-millimetre ratio kx = (counts over the stroke)/50 mm, so that the limit stays correct if the mechanism is re-calibrated. In the final system the cap is left off, for the reasons given in Section 5.1.1, and the drill never exceeds 30 mm/s and slows down near both ends of the stroke.

3.3.2 Lever force capability and transmission ratio

The lever copies the feed handle of the drill press: it is 150 mm long and, like the press handle, leans 30° out of its plane of rotation, so that the three press handles form a shallow cone. A hand does not hold such a handle at its tip. It closes around the grip, and the centre of the hand sits about 110 mm along the handle from the hub, so this is where the operator's force acts. Only the component of the hand's position perpendicular to the shaft axis makes torque, and because the handle leans 30° out of the plane in which it turns, that distance, the grip radius, is shorter than the 110 mm measured along the handle (Figure 2, Eq. 3).

$$rg = 110\ mm \times \cos 30° \approx 95\ mm \tag{3}$$

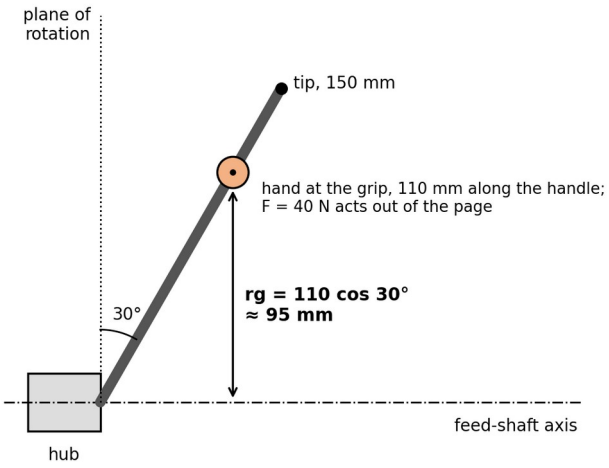


Figure 2. Side view of the angled handle: the hand acts 110 mm along the 150 mm handle, and the 30° lean puts it 95 mm from the shaft axis.

A force F at the grip therefore produces a shaft torque T = F·rg. For 40 N this is 3.8 N·m, against 4.4 N·m if the 110 mm were taken along the handle, 6.0 N·m at the 150 mm tip and 8.0 N·m at the 200 mm lever assumed in the proposal. The grip radius does not reduce the

requirement: it is the torque a person applies to the real press handle, which the lever reproduces. Every lever force in this report, the limit included, is quoted at the grip (rg = 95 mm by default). The force at the grip follows from the motor torque Kt·I, the gear ratio N and the gearbox efficiency η (Eq. 4).

$$F = Kt \cdot I \cdot N \cdot \eta / rg \tag{4}$$

With the datasheet value Kt ≈ 0.25 N·m/A, N = 16, an assumed efficiency of 0.9 per greased printed stage (η ≈ 0.81) and rg = 0.095 m, Eq. 4 gives 34 N per ampere, or 48 N at the 1.4 A continuous rating, so 40 N would need about 1.17 A (Figure 3). The measured effective constant of Eq. 14 is lower, and with it 40 N needs 1.95 A and about 7.0 V, as the load-cell measurements in Figure 3 confirm: inside the 3.4 A firmware limit, but above the continuous rating, so the full force can be held only briefly. In drill-press mode the reflected force and the walls are capped at 40 N at the grip, below the 42 N of Requirement 6. The proposal states both forces at a 200 mm lever, at the 95 mm grip radius, 40 N is a pivot torque of 3.8 N·m rather than 8.0 N·m, and this difference is reported in Section 4.

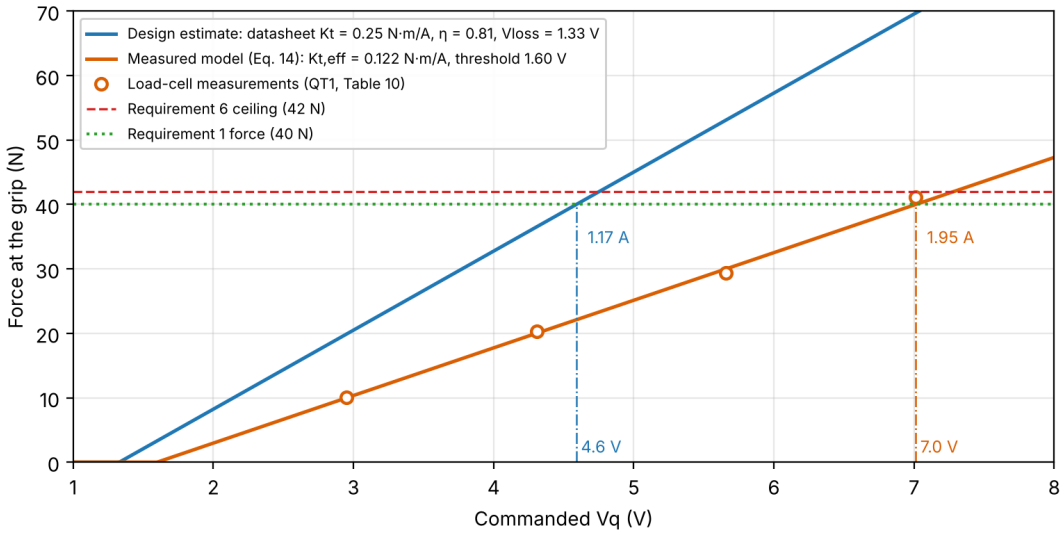


Figure 3. Force at the grip against commanded voltage at the 95 mm grip radius (N = 16): the design estimate from the datasheet torque constant, and the measured model of Eq. 14 with the load-cell measurements of QT1. 40 N needs about 4.6 V (1.17 A) by the estimate and 7.0 V (1.95 A) on the hardware.

The ratio was reduced from an initial 24:1, through about 18:1, to 16:1, because transparency favours a low ratio and 16:1 still leaves force margin. At N = 16 the rotor inertia appears 256 times larger at the handle and the motor and gear friction 16 times larger [2]. The torque ripple as a fraction of the commanded torque is not changed by the reduction, but its spatial period at the handle becomes 16 times shorter: one electrical period of 32.7° at the motor becomes 2.0° at the handle. With the encoder on the motor shaft, the angular resolution at the handle is 4096 × 16 = 65 536 counts per revolution (0.0055°).

The reduction was first built as two timing-belt stages (20:80 teeth on HTD-3M belt). The belts skipped teeth whenever the operator back-drove the motor through the lever, and the printed pulley shaft broke repeatedly, so the belt drive was replaced by a gearbox. The final reduction is two identical 4:1 stages of 3D-printed herringbone gears, an 18-tooth pinion driving a 72-tooth gear in each stage, with module m = 1.5, helix angle β = 25° and a face width b = 15 mm. The middle shaft carries a compound gear, the 72-tooth gear of stage 1 and

the 18-tooth pinion of stage 2 printed as one piece, and the lever is bolted to the face of the output gear so that its shaft carries no lever torque. The centre distance of each stage follows from Eq. 5.

$$a = m\,(z1 + z2) / (2 \cos \beta) = 1.5 \times (18 + 72) / (2 \cos 25°) \approx 74.5 \text{ mm} \quad (5)$$

The pitch diameters are 29.8 mm and 119.2 mm, and the shafts are set 74.6 mm apart, 0.1 mm more than Eq. 5, to allow for printing tolerance. The two gears of each pair are mirror images, so that their V-shaped teeth interlock. Herringbone teeth centre themselves axially, so only the motor pinion is fixed along its shaft and the other two gears float by about 0.5 mm, fixing all three would make them bind. Stage 2 carries the full lever torque and sets the strength. Its tooth-root stress is estimated with the Lewis equation (Eq. 6), where Ft is the tangential tooth load and Y ≈ 0.31 is the Lewis form factor of an 18-tooth pinion.

$$\sigma = Ft / (b \cdot m \cdot Y) \quad (6)$$

At 40 N on the grip the lever torque is 3.8 N·m, the tooth load on the 59.6 mm pitch radius of the output gear is Ft ≈ 64 N, and Eq. 6 gives σ ≈ 9 MPa, several times below the strength of printed PLA or PETG. The equation ignores the helix, which spreads the load along a longer contact line and adds margin. The gears also cannot be overloaded through the lever: the BLDC motor is not locked, so a hand force above what the motor resists simply turns it, and the motor's peak torque of about 0.3 N·m limits the lever torque to about 4 to 5 N·m. Printed gears have about 0.1 to 0.2 mm of play per mesh, about 0.3° at the lever or 0.5 mm at the grip, which is comparable with the backlash of the press's own rack and pinion, and the study leader accepted this. In drill-press mode the artificial return spring always loads the teeth in one direction, which hides the play.

3.3.3 Motor model, voltage-mode FOC and the drive model

The DF4015 has p = 11 pole pairs, so one electrical revolution corresponds to 32.7° of mechanical rotation. The electrical angle is obtained from the mechanical encoder angle by Eq. 7, where θoff is the offset found by the alignment procedure of Section 3.8.1.

$$\theta e = p \cdot \theta m + \theta off \quad (7)$$

The Clarke and Park transforms map the phase currents to the rotor frame (Eqs. 8 and 9), and for a surface-magnet machine the electromagnetic torque depends on iq only (Eq. 10), where ψm is the magnet flux linkage [15].

$$i\alpha = ia, \quad i\beta = (ia + 2ib) / \sqrt{3} \quad (8)$$

$$id = i\alpha \cos\theta e + i\beta \sin\theta e, \quad iq = -i\alpha \sin\theta e + i\beta \cos\theta e \quad (9)$$

$$Te = (3/2) \cdot p \cdot \psi m \cdot iq \quad (10)$$

In voltage mode no current is measured. The firmware sets vd = 0 and commands vq, then applies the inverse Park and inverse Clarke transforms (Eqs. 11 and 12) to obtain the three phase-voltage references.

$$v\alpha = vd \cos\theta e - vq \sin\theta e, \quad v\beta = vd \sin\theta e + vq \cos\theta e \quad (11)$$

$$va = v\alpha, \quad vb = -\tfrac{1}{2}v\alpha + (\sqrt{3}/2)v\beta, \quad vc = -\tfrac{1}{2}v\alpha - (\sqrt{3}/2)v\beta \tag{12}$$

The phase current that a given vq produces was characterised instead of measured in operation. With the rotor held still (no back-EMF) and a 24 V supply, the supply current was measured at vq = 4, 6 and 8 V (Table 4). For a star-equivalent motor with amplitude-invariant transforms, the power delivered is $1.5 \cdot Veff^2/R$, so the supply current is $Isup = Veff^2/(16R)$ at 24 V, where Veff = vq - Vloss is the voltage that actually reaches the winding. A plot of √Isup against vq is therefore a straight line, whose intercept gives Vloss and whose slope gives R (Figure 4).

Commanded vq (V)	Measured supply current (A)	Model supply current (A)	Estimated peak phase current (A)
4	≈ 0.16	0.16	0.96
6	≈ 0.50	0.49	1.68
8	1.00	1.00	2.40

Table 4. Drive characterisation with the rotor held still at 24 V.

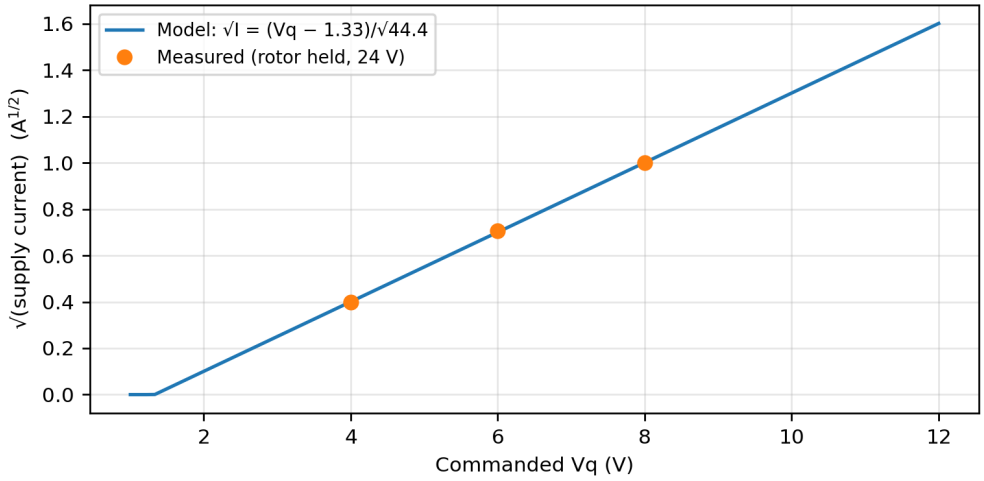


Figure 4. Square root of the supply current against commanded voltage: measured points and the fitted drive model.

The fit gives Vloss ≈ 1.33 V and R ≈ 2.78 Ω per phase (star equivalent). The resistance includes the 2.4 Ω winding (4.8 Ω measured terminal to terminal) plus wiring, connectors and FET on-resistance. The voltage loss collects the switching delay of the discrete high side and the voltage error of the original, high-side-only chopping scheme (Section 3.3.4), with which the characterisation was made. The force calibration of Section 4 was made with the final modulation. The phase current is then estimated by Eq. 13.

$$\hat{I} = (vq - Vloss) / R = (vq - 1.33\ V) / 2.78\ \Omega \tag{13}$$

This estimate matches the three measurements to within the reading accuracy of the supply. It is the worst case, because back-EMF reduces the current once the rotor moves: at a lever speed of 30°/s the motor turns at 8.4 rad/s and the back-EMF is about 2.1 V. Two practical consequences follow. A 2 A phase-current limit corresponds to vq ≈ 6.9 V, and below about 1.3 V the drive produces almost no torque, which is why small restoring forces need the loss to be added back.

The proposal targeted FOC with closed current loops. While the drive was being built and programmed, a closer study of what current control needs on this hardware showed that it

would make the haptic feel worse, not better. The phase currents of a haptic lever are small and change slowly, so at the low speeds where the lever spends most of its time the sensed signal is small, while the fast switching edges of the bridge (high dv/dt) couple noise into it. A current loop acting on that signal feeds the noise back into the torque, which the hand feels as grit. The DF4015 is a gimbal motor with a high phase resistance (2.4 Ω, 2.78 Ω with the drive), and at the speeds of a hand-moved lever its back-EMF stays small compared with the drive voltage, so the phase current is set almost entirely by the applied voltage divided by the resistance, as Eq. 13 and Table 4 confirm. Voltage-mode FOC uses this directly: it applies clean sinusoidal voltage vectors computed from the rotor angle, with no measured current in the loop, so no sensor noise reaches the torque, and the measured drive model keeps the torque accurate (the force at the grip was within 1.3 % of the command in the closest run at each level and within 6.4 % across all five runs from 10 to 40 N, Section 4). Voltage mode was therefore chosen because it suits this motor and this application better than a current loop, and the reasoning was discussed with the study leader.

For force rendering the model was refined against the load cells (QT1, Section 4). With the lever tip on the load-cell platform, the force appears only above about 1.60 V rather than the 1.33 V of the held-rotor fit, because the static friction of the gearbox must be overcome before the lever pushes. The firmware therefore computes the drive voltage for a force F at the grip by Eq. 14, where the threshold enters through a smooth tanh term so that small forces do not switch it on and off abruptly. The effective torque constant Kt,eff = 0.122 N·m/A at the motor shaft includes the losses of the gearbox, and is lower than the datasheet value with the assumed efficiency (about 0.20 N·m/A).

$$vq = 1.60\ V \cdot \tanh(I / 0.03\ A) + 2.78\ \Omega \cdot I, \quad I = F \cdot rg / (N \cdot Kt,eff) \tag{14}$$

3.3.4 Bottom-clamped modulation with current-direction chopping

The three references va, vb and vc are converted into high-side duty cycles by subtracting the most negative reference (Eq. 15), where VDC is the DC-link voltage.

$$Dx = (vx - \min(va, vb, vc)) / VDC, \quad x \in \{a, b, c\} \tag{15}$$

The line-to-line voltages are unchanged by this common-mode shift [17]. In every 120° electrical sector the lowest phase has zero duty and is clamped to the negative rail by holding its low-side FET on continuously. Each of the other two phases chops one FET only, chosen by the direction of its current. While the current flows out of the leg into the motor, the high-side FET switches with duty Dx and the current freewheels through the low-side body diode during the off-time, so the node sits at 0 V and the average phase voltage is Dx·VDC. While the current flows back into the leg, the low-side FET switches with duty 1 - Dx and the current freewheels through the high-side body diode during its off-time, which holds the node at VDC, so the average is again Dx·VDC. Figure 5 shows the reference voltages and the resulting duties over one electrical cycle.

The first version chopped only the high-side FETs. For current flowing back into the leg the node then stays at the positive rail for the whole off-time, whatever the duty, so the phase voltage is wrong for part of every electrical cycle. A switching model of the bridge (8 Ω, 2 mH, 24 V, 20 kHz) showed about 26 % peak-to-peak torque ripple from this effect alone, and 1 to 5 % with current-direction chopping. The direction is estimated from the commanded phase voltage less the back-EMF, with 0.15 V of hysteresis so that it does not chatter near a

zero crossing. When a leg changes FET, or enters or leaves the clamp, the FET in use is switched off first and both are held off for 3 µs, and a phase whose duty is below 1 % is treated as clamped to avoid pulses shorter than the driver can reproduce.

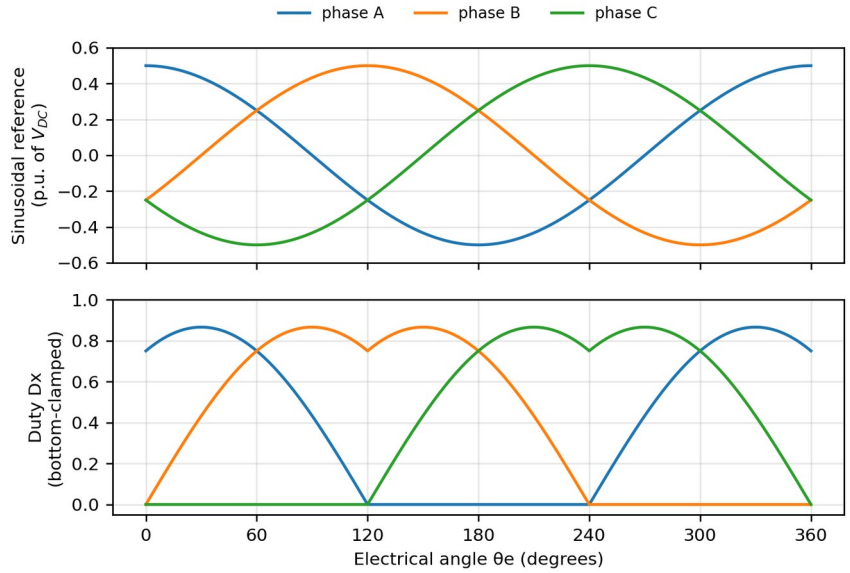


Figure 5. Sinusoidal references (top) and bottom-clamped duties (bottom) over one electrical cycle, for a modulation amplitude of 0.5.

The PWM period is 50 µs (20 kHz). No single STM32F405 timer reaches all three high-side pins of the board, so each phase has its own timer (TIM3, TIM4 and TIM12). All three run from the same 84 MHz timer clock with a period of 4200 counts and are started together, so they stay in step. They count edge-aligned, because TIM12 cannot count up and down, with only one FET of a leg switching at a time this has no effect on the motor.

3.3.5 Angle processing, servo and haptic laws

The AS5600 returns a 12-bit angle that wraps at 4096 counts. A continuous multi-turn count c is maintained by accumulating the shortest signed difference between successive readings (Eq. 16). This is unambiguous while the shaft turns less than half a revolution per 1 ms sample, that is, below 30 000 RPM.

$$\Delta k = ((rk - rk\text{-}1 + 2048) \bmod 4096) - 2048, \quad ck = ck\text{-}1 + \Delta k \tag{16}$$

The accumulator is initialised with the first absolute reading r0 and not with zero, so that the electrical angle of Eq. 7 is correct from the first sample after power-up. The alignment routine estimates θoff from K pairs of commanded electrical angles φk and measured mechanical angles θm,k taken during forward and reverse sweeps, and averages the estimates on the unit circle (Eq. 17) so that values near -π and +π do not cancel. Averaging the two sweep directions also cancels the lag caused by friction.

$$\theta off = atan2(\Sigma k \sin(\varphi k - p\theta m,k), \Sigma k \cos(\varphi k - p\theta m,k)) \tag{17}$$

The lever feel is produced by a position servo whose target and stiffness depend on the selected mode. The plant seen by the servo, including back-EMF damping, is given by Eq. 18, where J is the inertia at the motor shaft, u = vq - Vloss is the effective control voltage and b = Kt^2/R is the electrical damping.

$$J \cdot d^2\theta/dt^2 = (Kt/R) \cdot u - b \cdot d\theta/dt \quad (18)$$

A step change of target would demand unbounded acceleration and cause overshoot, so the target θ* is passed through a critically damped second-order reference generator with bandwidth ωr (Eq. 19), which produces a smooth reference position θr, velocity ωr' and acceleration αr.

$$\alpha r = \omega r^2(\theta^* - \theta r) - 2\omega r \cdot \omega r' \quad (19)$$

The speed is estimated with an α-β observer [18], which predicts the angle from the previous estimate and corrects it with the measured angle θm (Eq. 20). The gains l1 = 2ωobs and l2 = ωobs² place both observer poles at -ωobs, Δt is the 1 ms control period.

$$e = \theta m - (\theta\hat{} + \omega\hat{}\Delta t), \quad \theta\hat{} \leftarrow \theta\hat{} + \omega\hat{}\Delta t + l1\Delta t \cdot e, \quad \omega\hat{} \leftarrow \omega\hat{} + l2\Delta t \cdot e \quad (20)$$

The control voltage is formed by Eq. 21. It combines PD action on the tracking error, Coulomb-friction feed-forward Vf driven by the sign of the reference velocity (smoothed over a band ε), inertia feed-forward kJαr and a slow integral term I that is clamped and active only near rest. The friction feed-forward is taken from the reference rather than from the measured speed so that it does not chatter at zero crossings [12]. The drive loss Vloss is added to the magnitude of the result before it is applied, so that small restoring voltages still produce torque.

$$u = Kp(\theta r - \theta\hat{}) + Kd(\omega r' - \omega\hat{}) + Vf \cdot sat(\omega r'/\varepsilon) + kJ\alpha r + I \quad (21)$$

With the measured R = 2.78 Ω, Kt/R ≈ 0.090 N·m/V and the electrical damping b ≈ 0.022 N·m·s/rad is already substantial. The gains were therefore set experimentally, starting from small values and raising Kp only once the damping was adequate: Kd = 0.5 V·s/rad caused chatter from residual noise on the speed estimate, Kd = 0.05 V·s/rad left the loop oscillatory, and the final values were Kp = 20 V/rad, Kd = 0.25 V·s/rad and Ki = 0, with ωobs = 100 rad/s. The integral term was disabled because integral action through stiction produced a limit cycle at the set-point.

The stiffness that the servo can render stably is bounded by the sample period T and the physical damping b, in the form K < 2b/T given by Colgate and Brown [3]. With b ≈ 0.022 N·m·s/rad and T = 1 ms, the bound at the motor shaft is about 45 N·m/rad, whereas the servo stiffness Kp·Kt/R is about 1.8 N·m/rad, a factor of 25 lower. Stiffness is therefore limited by the available force, not by sampled-data stability.

The haptic modes use this servo as their core. In spring mode the restoring voltage rises linearly with displacement from the centre to a maximum (3 V at 30° of lever travel, about 25 N at the grip), with a separate damping term that stops ringing on release. In detent mode the lever is pulled towards the nearest of Nd equally spaced centres by u = Vj·tanh(e/w), where e is the error to the centre, Vj the strength (1.8 V, about 7 N) and w the width (1.5° of lever angle), so the pull is nearly full within one width of the centre and holds firmly. The lever snaps to the next detent only at 52 % of the spacing, which stops it buzzing on the boundary. All user-facing angles are in lever degrees and are multiplied by N = 16 to obtain motor angle. Drill-press mode is described in Section 3.3.10.

3.3.6 Gate-drive analysis

The high-side totem pole of each phase is biased by a pull-up resistor R12 from the bootstrap rail. The base current available to the totem-pole NPN is IB ≈ (Vboot - VBE)/R12, which with a 5 V rail is 0.43 mA for R12 = 10 kΩ and 4.3 mA for R12 = 1 kΩ, giving peak gate currents of about 43 mA and 430 mA at a current gain of about 100. The IRLZ44N has a total gate charge of up to 48 nC [28], so the gate charge time of Eq. 22 falls from about 1.1 µs to about 0.11 µs when R12 is reduced to 1 kΩ.

$$tg \approx Qg / Ig \approx Qg \cdot R12 / (\beta\,(Vboot - VBE)) \tag{22}$$

The switching loss of one FET is estimated by Eq. 23, where tsw is the sum of the rise and fall times.

$$Psw \approx \tfrac{1}{2} \cdot VDC \cdot I \cdot tsw \cdot fsw \tag{23}$$

At VDC = 24 V, I = 2 A and fsw = 20 kHz, transitions of 0.11 µs each give about 0.1 W per switching FET, whereas transitions of 1.1 µs each give about 1.1 W. In a TO-220 package without a heat sink (junction-to-ambient about 62 K/W) [28], the higher figure causes a temperature rise of about 65 K, which is consistent with the heating observed on phase A before R12 was reduced. The cost of the lower value is a drain of about 5 mA from the bootstrap capacitor C7 = 10 µF whenever the level shifter holds the node low, a droop of 0.5 V/ms. The capacitor is recharged through D1 while the phase is clamped, and during each off-interval of an active phase while that phase's current freewheels through the low-side body diode.

The peak gate currents are about 0.43 A on the low side (5 V through R7 = 10 Ω) and on the high side, where they are limited by the base drive from R12, and both are below the 0.6 A rating of the 2N2907 output transistor, with little margin. A 1N4148 diode across the emitter-base junction of each totem-pole PNP protects it from reverse avalanche, which had progressively reduced the gain of the phase B transistor. The board was designed around the IRFZ44N, specified at VGS = 10 V [29], which would have needed a 12 V gate supply. It was replaced by the pin-compatible logic-level IRLZ44N, specified at 4 V and 5 V (RDS(on) at most 35 mΩ and 25 mΩ) [28], which the roughly 4.3 V from the 5 V bootstrap rail enhances fully, so a single 5 V supply serves the drivers and logic besides the 24 V link.

3.3.7 CMOS dead-time generation

In a current-starved delay stage a bias current Ib charges or discharges a timing capacitance C through the switching threshold, and the delay per edge is approximately that of Eq. 24 [25], where ΔV is the voltage swing to the threshold of the next stage.

$$td \approx C \cdot \Delta V / Ib \tag{24}$$

Both reference branches carry about 4 µA (Section 3.6.2). With C = 200 fF and ΔV = VDD/2 = 1.65 V, Eq. 24 gives about 200 fF x 1.65 V / 4 µA ≈ 80 ns per edge when the charging and discharging currents are equal. Equal currents delay both edges by the same amount and leave no gap, so the two mirrors are made unequal: the PMOS source M4 is set to the minimum width of its device generator and the NMOS source M2 to the maximum. The timing capacitor then charges more slowly than it discharges, so the rising edge of each channel is

delayed more than the falling edge. The BJT interlock stage that follows (Section 3.6.3) turns this edge difference into a non-overlap of about 10 ns between the outputs (Section 3.4.2).

3.3.8 Drill-side control, thrust measurement and protection

The quill has high static friction, and its return spring cannot back-drive the 131:1 gearbox, so the motor must drive the quill in both directions. The drill follows the lever target with a cascaded position and velocity controller. The speed is estimated from the change in encoder count over each control period and smoothed by an exponential moving average (Eq. 25), where λ is the smoothing factor.

$$vk = \lambda \cdot vk\text{-}1 + (1 - \lambda) \cdot (ck - ck\text{-}1)/\Delta t \tag{25}$$

The velocity controller forms Eq. 26, where bdir is a breakaway bias learned separately for extension and retraction and a is the filtered acceleration. The integral is updated only while the output is not saturated (conditional integration). Near the target, control passes to a hold law (Eq. 27): a learned breakaway bias b, proportional action capped at 100 duty counts, an integral term active only at rest and clamped to ±150, and derivative action on the filtered speed.

$$utravel = bdir + Kp{,}v(v^* - v) + Ki{,}v\,\Sigma(v^* - v)\Delta t - Kd{,}v \cdot a \tag{26}$$

$$uhold = b + Kp{,}h \cdot e + I - Kd{,}h \cdot v \tag{27}$$

The axial thrust is measured by four 50 kg half-bridge load cells under the work platform, wired as one full Wheatstone bridge and read by an HX711 [13]. The breakout board tied the HX711 rate pin to ground, which fixes the rate at 10 samples per second. The trace was cut and the pin tied to the supply, which selects the fast setting of 80 samples per second (85.6 measured). The calibration factor is found once with a known mass and stored, and the zero can be re-taken at any time to remove the platform and workpiece. A three-sample median filter rejects spikes and a first-order smoother (weight 0.5) follows, with the converter's own settling (50 ms at 80 samples per second [13]) and the sampling interval, a thrust step reaches 90 % at the lever 80 to 130 ms later (QT1). At the original 10 samples per second this delay was about 0.59 s. The bridge's 200 kg rating leaves a factor of six above the 32 kg thrust cap.

The force the drill can exert is bounded in two ways. A maximum PWM duty limits how hard the motor can push when the quill meets resistance, and the thrust cap stops it pushing harder once the load cells read 32 kg, whatever the duty. To check the actuator against its datasheet, a stalled-motor model predicts the thrust at a duty D: the winding current D·Vs/Rm sets the output torque by linear interpolation between the no-load and stall points of the datasheet, the torque is divided by the pinion radius, and the force of the return spring at the present quill position is subtracted. The push test of Section 3.8.2 logs the measured thrust beside this prediction.

Two protective mechanisms replace the motor-current trip of earlier versions. The heat budget H integrates the square of the duty D while the motor is stalled (Eq. 28), where Hmax corresponds to 6 s at full duty. When H reaches Hmax, the duty is limited to 25 % until the budget refills, which takes about 20 s at rest. An oscillation guard caps the duty at 30 % for 1 s if the drill reverses hard six or more times within 0.3 s.

$$H \leftarrow H + D^2 \cdot \Delta t \;\; (\text{while stalled}), \quad D \le 0.25 \text{ while } H \ge Hmax \tag{28}$$

3.3.9 Link timing

Requirement 1 specifies a loop rate of at least 100 Hz and a latency of at most 10 ms. Each frame carries two synchronisation bytes, a type, a length, the payload and a CRC-8. A knob frame (11-byte payload, 16 bytes) takes 0.35 ms at 460.8 kbaud and, sent at 1 kHz, uses 35 % of the link, and a drill frame (42-byte payload, 47 bytes) takes 1.02 ms and, at 200 Hz, uses 20 %. The forward latency is the frame time plus the wait for the next drill control tick, about 1 ms, and the return latency is set mainly by the 5 ms drill-frame interval. Each drill frame echoes the number and age of the last knob frame, so the lever node measures the latency continuously (1.00 ms one-way, QT1). The thrust itself is sampled at about 85.6 Hz (Section 3.3.8), so a new value arrives only every 11 ms although it is sent at 200 Hz.

3.3.10 Force reflection and bilateral coupling

The lever force that represents a measured thrust follows from equal work through the rack and pinion and the angle mapping between the two sides. If the drill turns G degrees for every degree of lever rotation, a lever rotation $\Delta\theta l$ moves the quill by $G \cdot r \cdot \Delta\theta l$, and equating the work done at the two ends gives Eq. 29.

$$Flever = Fthrust \cdot G \cdot r / rg \tag{29}$$

With G = 1 the lever turns exactly as the pinion does, so it behaves as the press's own feed handle on a separate stand. With r = 9.4 mm and rg = 95 mm, 1 kg of thrust produces 0.97 N at the grip, and the 32 kg thrust cap corresponds to 31 N. At the grip, 40 N would need 41 kg of thrust, 81 % of the drill motor's stall torque, and at the tip of the handle more than the stall torque, so the drill side replicates the thrust exactly up to its cap, while the lever alone can render 40 N (Section 3.3.2). The firmware takes r from the calibrated stroke and converts the force to a drive voltage by Eq. 14. Because the thrust arrives with the link and filter delay, it is smoothed (about 30 ms), limited in rate of rise to 400 N/s and damped before it is rendered, so that it cannot excite the lever. In voltage mode the back-EMF of the moving motor changes the current for a given vq, so a force feels heavier while the lever pushes against it and lighter while it gives way. A back-EMF feed-forward of 0.06 V per rad/s of motor speed, about half the estimated back-EMF constant, cancels part of this effect, and a larger value made the walls bounce.

Forces that depend only on the lever position are computed on the lever node at 1 kHz, so no link delay enters them. Drill-press mode adds an artificial return spring, because the real press spring cannot back-drive the feed gearbox: a target point moves back towards the top at 5 mm/s, never more than 10° from the lever, and pulls the lever with an effort capped at 1.6 V (about 4 N at the grip), so that the released lever walks home and the drill follows. Stiff walls act beyond both ends of the stroke. While the bit is in contact with the work, an optional press-feel spring adds the force of the real quill return spring, rising linearly with depth, so that the lever feels like the handle it replaces. A virtual workpiece of up to eight depth and force points renders material resistance without drilling. An earlier version computed this force on the drill node, because the quill trails the lever, the force arrived late and the loop oscillated violently, which moving the computation to the lever node removed.

Coupling rules keep the two sides consistent when the quill cannot follow. The target sent to the drill is clamped to ±3 mm of the quill (the leash), so the drill cannot wind up. The drill

declares itself stuck when, for 150 ms, it pushes at 40 % duty or more while the quill moves slower than 0.5 mm/s with an error above 0.3 mm and no load-cell contact, and it then drops to 20 % duty and reports it, and the lever responds with a wall latched 0.3 mm beyond the quill. When the operator pushes harder than the drill can follow, the lever meets a second wall 3 mm past the still quill, so the excess is felt as a firm stop. Walls act only against a still quill, since a wall against a moving quill behaves as a delayed spring, which buzzed in simulation. In contact, the lever renders the larger of the load-cell and wall forces, not their sum.

3.4 Simulation study

Three simulation studies supported the design: circuit simulation of one discrete half-bridge in LTspice, transistor-level simulation of the CMOS driver in Cadence Spectre, and a numerical study of speed estimation from the quantised encoder signal.

3.4.1 LTspice simulation of the discrete half-bridge

One phase of the discrete driver was simulated in LTspice at its real supply voltages: 3.3 V logic, 5 V and 12 V gate-drive rails and a 24 V DC link. The simulated circuit is the design-stage version of the board, with IRFZ44N FETs and a 12 V rail to enhance them. The board was later fitted with the logic-level IRLZ44N, which runs from a single 5 V gate supply (Section 3.5.1), and the switching waveforms did not change. The other changes made during bring-up are described in Sections 3.5 and 3.7.1.

The dead-time generator is shown in Figure 6. Two complementary 20 kHz pulse sources (V1 and V2) stand in for the MCU outputs. In each channel a Schmitt inverter (A1, A2) squares the input, and an RC network (R6 or R5 = 1 kΩ, C2 or C1 = 220 pF) delays the rising edge only, since the diode across the resistor (D2, D3) discharges the capacitor immediately on the falling edge. A second Schmitt inverter (A3, A4) restores sharp edges, and a cross-coupled NOR pair (A5, A7) forms the SR interlock that produces Out_H and Out_L. Turn-off is therefore immediate and turn-on is delayed, which creates a gap at every transition. The delay is the time the capacitor takes to charge to the upper threshold VT+ of the following Schmitt trigger (Eq. 30).

$$tdt = R \cdot C \cdot \ln(VDD / (VDD - VT+)) \tag{30}$$

With R = 1 kΩ, C = 220 pF, VDD = 3.3 V and VT+ ≈ 1.75 V, Eq. 30 gives tdt ≈ 220 ns × 0.76 ≈ 166 ns.

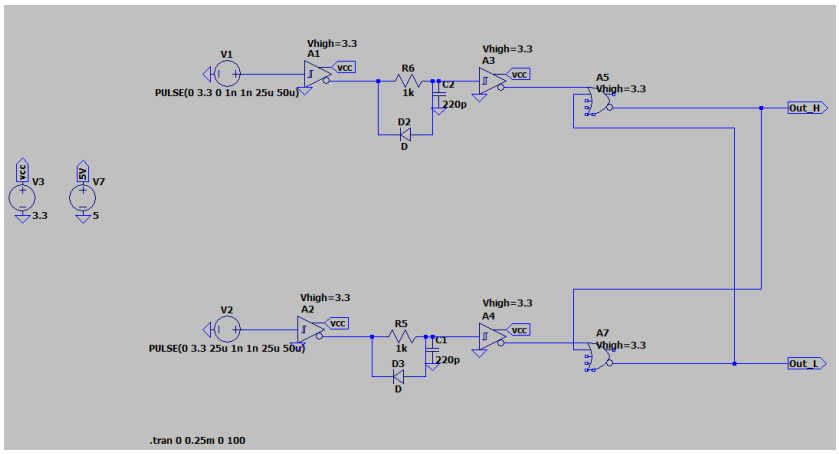


Figure 6. LTspice dead-time generator: Schmitt inverters, RC delay with diode bypass and NOR interlock.

The low-side driver and output stage (Figure 35, Appendix B) consist of the NPN inverter Q7 (R8 = 4.7 kΩ with the 220 pF speed-up capacitor C6), the push-pull pair Q5/Q6 from the 5 V rail through R9 = 1 kΩ, and R7 = 10 Ω to the gate, with a 10 Ω resistor to 24 V standing in for the motor winding. The high-side driver (Figure 36, Appendix B) charges the bootstrap capacitor C7 from the 12 V rail through D1, drives the level shifter Q8 from Out_H through R10 = 470 Ω, and biases the totem pole Q9/Q10 with R12 to drive the IRFZ44N through R11 = 4.7 Ω.

The simulated waveforms are shown in Figure 7, and in Figure 37 and Figure 38 (Appendix B). The two Schmitt outputs are clean complementary 3.3 V square waves with a period of 50 µs. At a transition, Out_H falls at 50.001 µs and Out_L rises at 50.164 µs, a dead time of 164 ns measured with the cursors, in close agreement with the 166 ns of Eq. 30 and inside the 0 to 500 ns range of Requirement 2. On the board C1 and C2 were later raised to 470 pF (Section 3.5.2), for which Eq. 30 gives tdt ≈ 470 ns × 0.76 ≈ 360 ns. The switching node VSW toggles between about 0.2 V and 24 V at 20 kHz with sharp edges, and the 0.2 V on-state level is the drop across the low-side FET carrying about 2.4 A into the 10 Ω load.

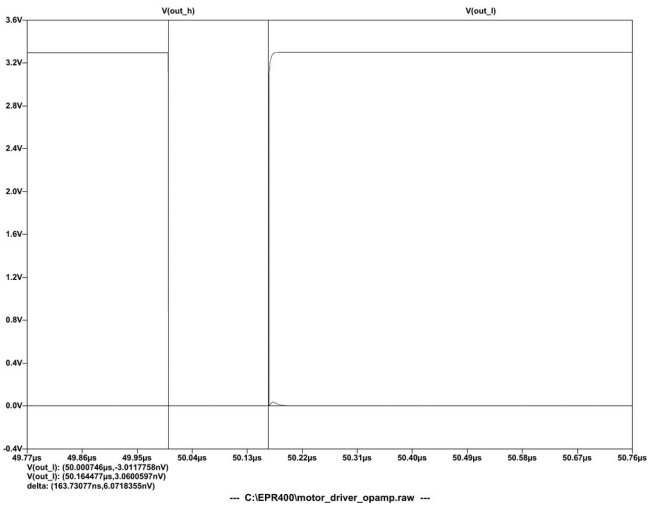


Figure 7. Detail of Out_H and Out_L at one transition: a dead time of 164 ns between the falling and rising edges.

The simulation verified the timing and the low-side path, but two faults that later appeared on the board were outside what this test circuit exercised. The SR interlock passes a single

complementary pulse train correctly, but on the board it locked under the rapidly changing duty of motor PWM (Section 3.5.2). In the test circuit the switching node is pulled up by the load resistor and held down by the low-side FET, with the high-side FET connected through 100 Ω, so the case in which the high-side FET itself carries the node up to the rail was never simulated. In that case the emitter of Q8, connected to the switching node, rises far above the 3.3 V available at its base, so Q8 can no longer conduct and the high-side FET cannot be turned off. This fault was found and corrected during bring-up (Section 3.5.4).

3.4.2 Cadence simulation of the CMOS driver

The CMOS driver was simulated in Spectre with complementary 10 kHz PWM inputs, one per channel, and the same 3.3 V, 5 V and 24 V supplies as the discrete board. Figure 8 shows the two channel outputs over five periods. They are exact complements at the 3.3 V logic level, with a 50 µs half-period and no glitches at the transitions. At the scale of Figure 39 (Appendix B), which spans 1 µs around one transition, the two edges coincide, so the outputs themselves carry no visible gap.

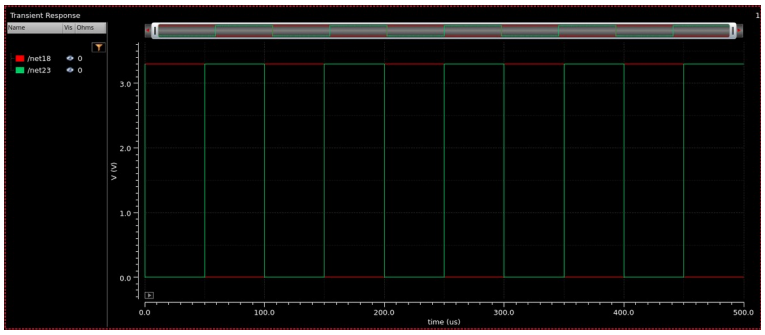


Figure 8. Simulated channel outputs (net18, net23) for complementary 10 kHz inputs.

The non-overlap is created in the BJT interlock stage that follows (Section 3.6.3). Figure 9 shows two of its internal nodes across a transition. The node that is switching off (net15) falls first, and the node that is switching on (net11) begins to rise only after it, reaching its final level of about 0.9 V within about 20 ns. The two waveforms cross near 0.2 V, below the turn-on threshold of the following stage, which is the property a dead-time circuit must provide. The separation at this point is about 10 ns. This lies inside the 0 to 500 ns range of Requirement 2, and it can be lengthened by enlarging the timing capacitors of the delay stage.

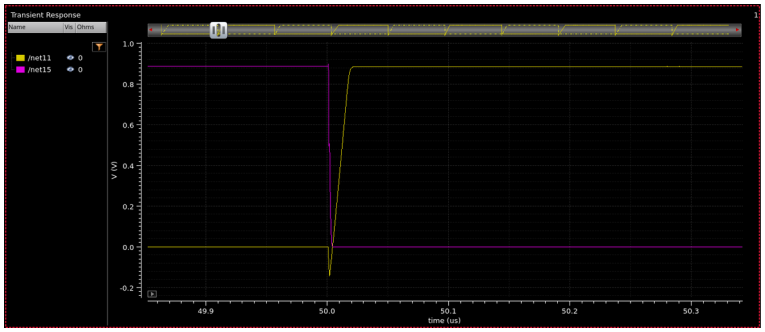


Figure 9. Interlock-stage nodes (net11, net15) across one transition, showing the non-overlap.

Figure 40 (Appendix B) shows the drain of the low-side power FET, simulated with the FET and a resistive load to the 24 V rail drawn in the schematic. The node switches cleanly between about 23 V and about 3 V at 10 kHz, following the gate command with sharp edges

and a short settling tail after each transition. The 3 V on-state level is the voltage across the power FET at this test load.

3.4.3 Numerical study of speed estimation

Requirement 5 allows a speed error of ±5 RPM at 60 RPM, which is ±0.52 rad/s. The AS5600 resolves 4096 counts per revolution, a quantum of 1.53 mrad, and is read at 1 kHz, so a one-count change between samples reads as 1.53 rad/s (14.6 RPM) when the angle is differentiated directly. To compare estimators, a rotation at 60 RPM with a ±2 % ripple at 1.5 Hz was simulated in Python, quantised to 12 bits with half-count noise and sampled at 1 kHz. The finite-difference estimate, the α-β observer of Eq. 20 with ωobs = 100 rad/s, and the same observer with the second gain multiplied by an extra Δt were each applied to the samples (Figure 10). The last case reproduces a firmware fault found during development.

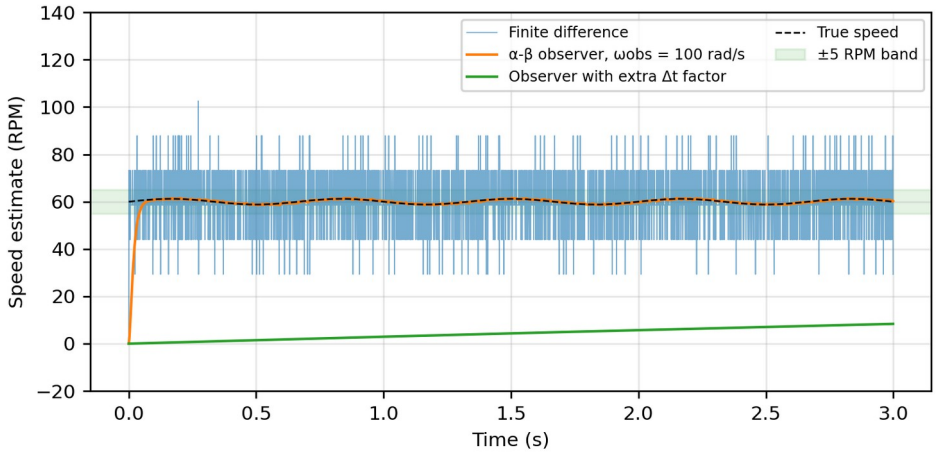


Figure 10. Simulated speed estimates at 60 RPM from a 12-bit encoder sampled at 1 kHz.

After the first 0.5 s the finite-difference estimate had an RMS error of 11.8 RPM and a peak error of 32 RPM, far outside the specification. The observer had an RMS error of 0.21 RPM and a peak error of 0.69 RPM, well inside ±5 RPM. With the extra Δt factor the observer speed gain was 1000 times too small, and the estimate crept towards the true speed so slowly that its mean over the run was only 5.0 RPM. On hardware this fault removed all damping from the servo, because the Kd term then acted on a speed estimate close to zero. The simulation assumes ideal quantisation, so the hardware result of Section 4 was still needed.

3.5 Hardware design: discrete three-phase inverter

The discrete inverter realises the motor driver of F.U.2 from individual transistors, without gate-driver ICs, as the proposal requires. Each of the three identical phases has an input conditioning stage, a low-side driver, a high-side driver with level shifter and bootstrap supply, and two power MOSFETs. Table 21 (Appendix B) lists the components of one phase and the basis of each value.

3.5.1 Power stage

The IRLZ44N (55 V, 47 A, at most 25 mΩ at VGS = 5 V [28]) gives ample margin at the 24 V link and phase currents below 2 A, where its conduction loss of 0.1 W needs no heat sink, and it is fully enhanced from the 5 V gate supply (Section 3.3.6). A 470 µF, 50 V bulk capacitor with local decoupling supports the link. A 10 kΩ gate-source resistor on every FET,

added during bring-up, holds each gate off when its driver is idle and removed a shoot-through fault at six-step transitions.

3.5.2 Input conditioning and dead-time block

Each gate command from the MCU passes through a 74LS14 Schmitt-trigger inverter, which squares the edges and translates the 3.3 V logic. The original design followed this with an RC delay with diode bypass (1 kΩ, 220 pF, 164 ns in simulation) and a cross-coupled 74HC02 NOR SR latch (Section 3.4.1). During bring-up the latch locked under rapid toggling, so no duty below 100 % reached the drivers, and it was removed on all three phases, and a high GPIO level now turns the corresponding FET off. The RC delay remains in every gate channel and still delays each turn-on edge, which sets the hardware dead time between the gate signals of a leg. With 220 pF the gap between the gate signals on the board was only about 65 ns, shorter than the time the FET gates take to discharge at turn-off, so a leg could still conduct briefly at each transition. C1 and C2 were therefore raised to 470 pF, for which Eq. 30 gives tdt ≈ 470 ns × 0.76 ≈ 360 ns. The faster high-side bias (R12 = 1 kΩ, Section 3.3.6) shortens the turn-off itself. Without the latch the two channels of a leg are no longer interlocked, so the firmware never commands both FETs on and holds both off for 3 µs at every change-over (Section 3.3.4).

3.5.3 Low-side gate driver

The low-side driver is an NPN inverter (Q7, 2N2222) with a 4.7 kΩ base resistor R8 and a 220 pF speed-up capacitor C6 in parallel, and a 1 kΩ collector pull-up R9 to the 5 V gate supply. It drives a complementary emitter-follower (Q5/Q6, 2N2222/2N2907), which charges and discharges the gate through R7 = 10 Ω. The base current into Q7 is (3.3 - 0.7)/4.7 kΩ = 0.55 mA, enough to saturate Q7 at its 4.3 mA collector current with a forced gain of 8. The speed-up capacitor supplies a charge pulse at each edge that removes stored base charge, with a time constant R8C6 = 1.0 µs. The 2N2222 has a storage time of at most about 225 ns, so the charge pulse lasts several times longer than the stored charge takes to clear.

3.5.4 High-side gate driver, level shifter and bootstrap supply

The high-side driver has the same totem-pole output (Q9/Q10, R11 = 4.7 Ω), supplied from a 10 µF bootstrap capacitor C7 charged through a 1N5817 Schottky diode D1 while the switching node is low. A level-shift transistor Q8 (2N2222, R10 = 470 Ω) pulls the totem-pole base low against R12 to turn the FET off. In the original layout the emitter of Q8 sat on the switching node, once the node rose to the rail, Q8 could no longer conduct and the FET could not be turned off (Section 3.4.1). The emitter was moved to ground on all three phases, R12 was reduced from 10 kΩ to 1 kΩ (Section 3.3.6) and the PNP clamp diode was added.

3.5.5 Current sensing

The board carries 10 mΩ shunts in the low-side source paths of phases A and B, but they are not used. A low-side shunt carries current only while its own low-side FET or body diode conducts, so with the original high-side-only modulation only the clamped phase could be measured, and samples near switching edges were corrupted. Voltage-mode FOC (Section 3.3.3) needs no measured current, so the shunts are left unused and the phase current is estimated from the drive model.

3.5.6 Supplies

The board takes 24 V for the DC link and a single 5 V supply for the gate drivers, the bootstrap rails and the logic. The 12 V rail of the original design, needed only to enhance the IRFZ44N, was removed when the logic-level IRLZ44N was fitted. Power-supply design earns no credit and is not described further.

3.6 Hardware design: CMOS gate driver

The same driver function was designed at transistor level in Cadence Virtuoso as a separate, simulation-only deliverable, in the X-FAB XH018 0.18 µm high-voltage process (library DJDB8_driverIC). The study leader required a physical layout that passes the design-rule check (DRC) and the layout-versus-schematic check (LVS), and the layout did not need to be compact or optimised for area. One phase of the driver forms a single cell, LayoutDriver, which was laid out and verified. A three-phase driver is three instances of this cell.

3.6.1 Architecture

Figure 11 shows the complete one-phase schematic. Each PWM input passes through its own current-starved delay channel (left), which sets the timing of its edges. The two channels then meet in a BJT interlock stage (centre), which guarantees that one output has turned off before the other turns on. The interlocked signals drive a high-side driver with a bootstrap supply (top right) and a low-side driver (bottom right), each of which ends in a complementary output pair that charges and discharges the gate of a power FET. The topology deliberately mirrors the discrete board, so that the two realisations of Requirement 2 can be compared stage by stage.

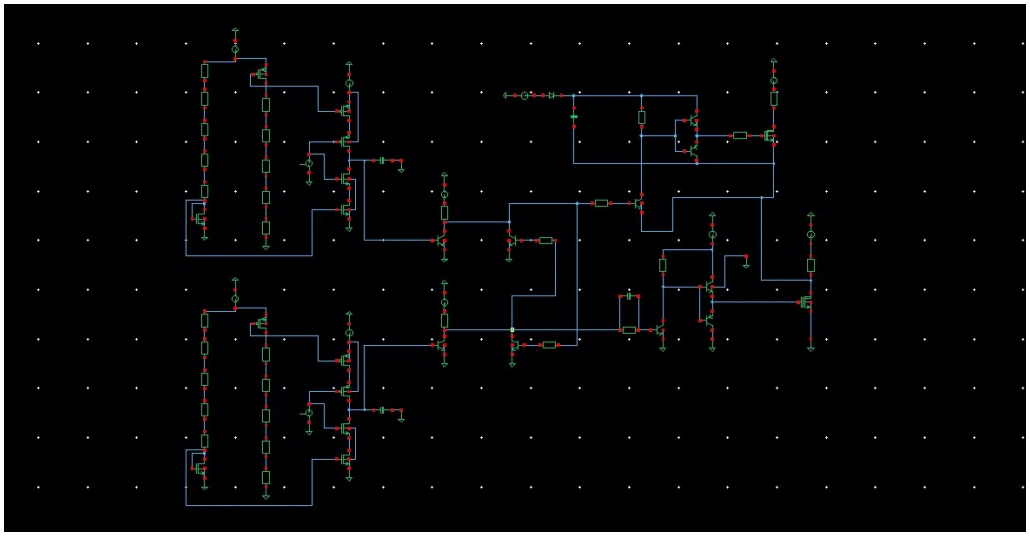


Figure 11. Overview of the one-phase gate-driver schematic: two delay channels, BJT interlock stage, high-side and low-side drivers.

3.6.2 Delay channel and bias

Each delay channel is a current-starved inverter (Figure 12). Two resistor-referenced branches set its bias currents. In the NMOS branch a chain of five rnp1 resistors (R0 to R4) feeds a diode-connected NMOS (M0), and in the PMOS branch a diode-connected PMOS (M1) feeds a second chain (R5 to R9). DC sweeps of the reference devices gave 4 µA at VGS = 0.57 V for M0 and at a gate voltage of 2.62 V (VSG = 0.68 V) for M1, so R0 to R4 = (3.3 V - 0.57

V)/4 µA = 682.5 kΩ (five of 136.5 kΩ) and R5 to R9 = 2.62 V/4 µA = 655 kΩ (five of 131 kΩ). Series chains were used because a single rnp1 instance cannot reach these values. Both reference devices are W = 2 µm, L = 0.54 µm, and each branch carries about 4 µA. The references are mirrored into the current sources M4 (PMOS) and M2 (NMOS), which limit the current available to the switching pair M6 and M3. The pulse input drives the gates of M6 and M3, and a cmm3 MIM capacitor on the output node is charged and discharged by the mirrored currents. Each edge is therefore delayed by the time the limited current takes to move the capacitor voltage through the threshold of the next stage (Eq. 24).

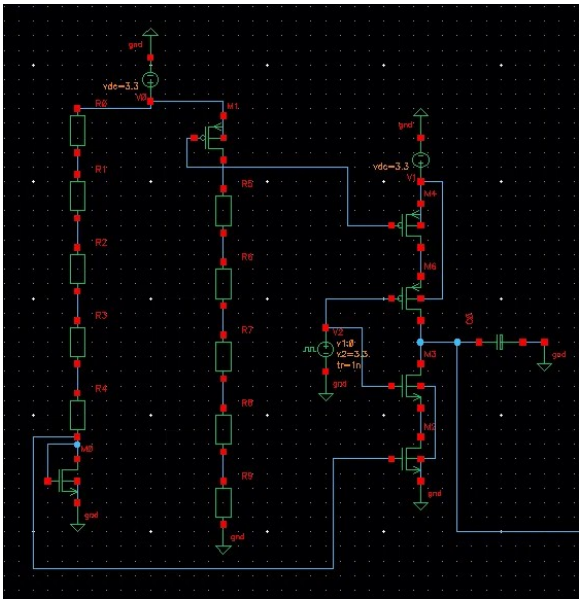


Figure 12. Current-starved delay channel with its two mirrored bias branches and timing capacitor.

3.6.3 BJT interlock stage

The interlock stage (Figure 13) uses vertical NPN transistors (qnva). In each channel, an input transistor (Q0, Q1) has a 1 kΩ collector pull-up (R20, R21) from the 3.3 V supply, and its collector drives the base of an output transistor (Q2, Q3). Each pull-up is formed from parallel rnp1 instances, since a single instance cannot go below about 1.7 kΩ. The cross-coupling resistors R22 and R23 tie each channel's output node to the other channel's control path, so that one output cannot turn on while the other is still on. The separation between the outputs comes from the saturation and storage-time behaviour of these transistors, which depends on the base drive set by the pull-ups, rather than from the delay channels alone. This is why the gap appears at the interlock nodes in Figure 9 and not at the channel outputs. A diode bypass across the delay stage was considered for this function and rejected, because at a bias of about 4 µA a junction never reaches its 0.6 to 0.7 V turn-on voltage.

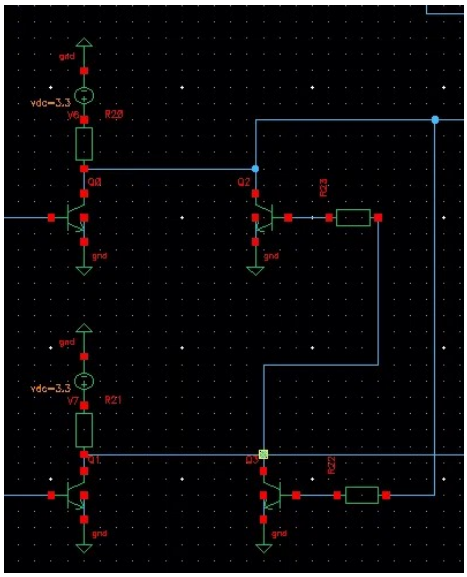


Figure 13. BJT interlock stage with cross-channel feedback.

3.6.4 High-side driver

The high-side driver (Figure 14) is supplied from a bootstrap node, charged from the 5 V rail through the diode D0 and held by the bootstrap capacitor C4. The level-shift NPN Q7, with its base resistor R30, is referenced to ground, the lesson carried over from the discrete board. It pulls the bias node of the output pair low against the pull-up R31 to turn the FET off. The complementary output pair Q8 and Q9 drives the gate of the power FET M17 through the gate resistor R32, and M17 switches the phase output between the 24 V rail and its load.

In XH018 the p-substrate is common to the whole chip, so the substrate terminal of each qnva NPN and the collector of each qpva PNP connect to ground in both the schematic and the layout.

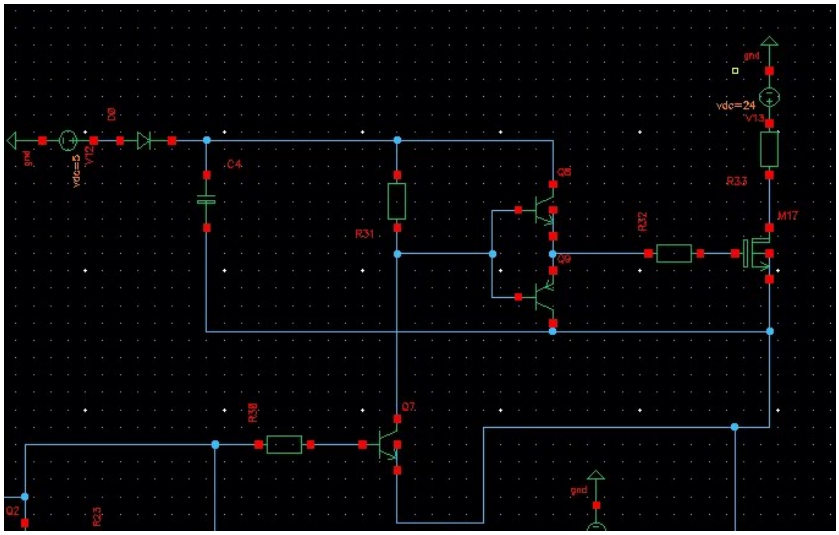


Figure 14. High-side driver: bootstrap supply, ground-referenced level shifter and complementary output stage.

3.6.5 Low-side driver

The low-side driver (Figure 15) matches the discrete design. An NPN inverter Q4, with base resistor R26 and speed-up capacitor C1 in parallel, drives the push-pull pair Q5 and Q6 from the 5 V rail through the pull-up R25. The pair drives the gate of the power FET M16, whose drain is loaded by R27 (4 Ω) from the 24 V rail in the test circuit. This is the stage whose output is shown in Figure 40.

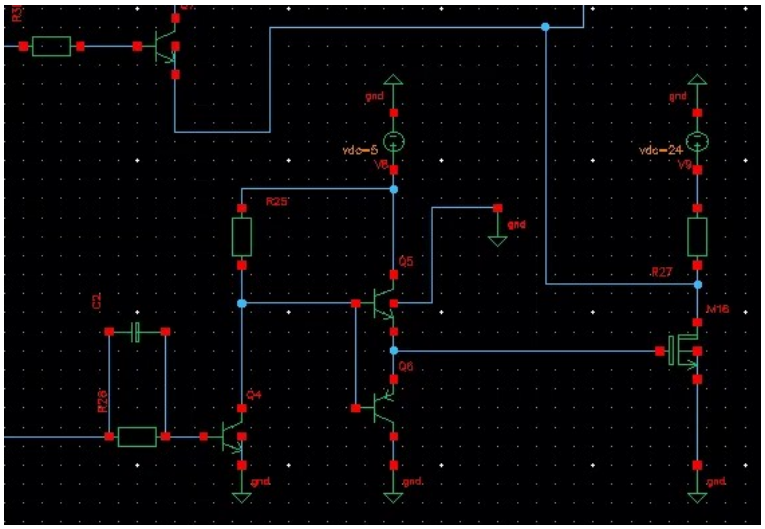


Figure 15. Low-side driver: inverter with speed-up capacitor and push-pull output stage.

3.6.6 Power FETs and off-chip components

The 100 nF bootstrap capacitor and the power FETs M16 and M17 are external to the layout. The capacitor connects between the BSTA and Aout pins, as in commercial bootstrap gate-driver ICs, on silicon it would need about 43 mm² even with the high-density MIM option (2.35 fF/µm²), many times the area of the rest of the driver. The power FETs remain in the schematic and the simulations, where they stand in for the IRLZ44N: the discrete board was designed around that FET, and the CMOS driver was designed to drive the same kind of device. Each is an nhv device (L = 3 µm) of 300 fingers of 4 µm with a multiplier of 100, about 120 mm wide in total, with properties similar to the IRLZ44N. Commercial gate-driver ICs likewise drive external power FETs, and the IRLZ44N is a vertical discrete device that this lateral process cannot reproduce. The study leader agreed that keeping the FETs external is justified. No current-sense amplifier was laid out, because the design does not measure current (Sections 3.3.3 and 3.5.5). The component values of the cell and the basis of each are listed in Table 5.

Block	Component	Value	Basis
Delay channel	R0 to R4 (rnp1)	5 x 136.5 kΩ	(3.3 V - 0.57 V)/4 µA = 682.5 kΩ
	R5 to R9 (rnp1)	5 x 131 kΩ	2.62 V/4 µA = 655 kΩ
	M0, M1 (bias diodes)	W = 2 µm, L = 0.54 µm	4 µA reference branches
	M2, M4 (sources)	Maximum, minimum width	Rising edge delayed more than falling (Section 3.3.7)
	M3, M6 (switches)	W = 2 µm, L = 0.18 µm	Minimum length for fast edges
	Timing capacitor (cmm3)	200 fF	Eq. 24: about 80 ns per edge at 4 µA
Interlock	Q0 to Q3 (qnva)	Emitter 3 µm x 1.02 µm	Process default
	R20, R21 (pull-ups)	1 kΩ (parallel rnp1)	Base drive of Q2, Q3 from 3.3 V
	R22, R23 (cross-coupling)	27 kΩ	As in the LTspice design of the stage

Block	Component	Value	Basis
Low side	R26, C1	4.7 kΩ, 220 pF	IB = (3.3 - 0.7)/4.7 kΩ = 0.55 mA, R26·C1 = 1.0 µs
	R25	1 kΩ	Pull-up to 5 V, as R9 of the discrete board
High side	R30	470 Ω	IB = (3.3 - 0.7)/470 Ω = 5.5 mA
	R31, R32	1 kΩ, 4.7 Ω	As R12 and R11 of the discrete board (Section 3.3.6)
	D0 (dnhpw)	2 µm x 2 µm	Rated 5.5 V, above the 5 V bootstrap supply
Off-chip	C4 (bootstrap)	100 nF	As the discrete design, about 42 mm² on die
	M16, M17 (nhv)	L = 3 µm, 300 x 4 µm, m = 100	Sized in simulation for the 4 Ω load at 24 V
Test circuit	R27	4 Ω	Load from the 24 V rail

Table 5. Component values of the one-phase CMOS driver and their basis.

3.6.7 Layout and verification

Figure 16 shows part of the LayoutDriver layout. The long horizontal strips on the left are the rnp1 resistor strings of the bias and pull-up networks, which dominate the area, and the labelled rectangles are metal-1 resistors (rm1) that LVS extracts from the routing. The transistors and the timing capacitors occupy the small region between them. The layout was placed for correctness rather than density.

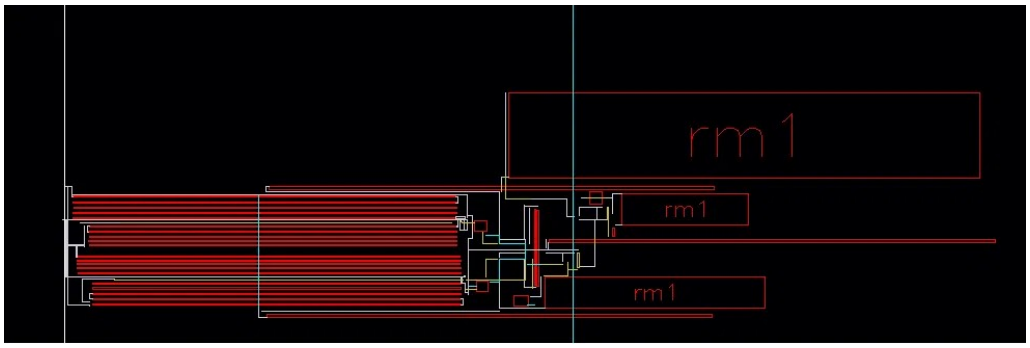


Figure 16. Partial view of the LayoutDriver layout: rnp1 resistor strings (left), active devices (centre) and rm1 metal resistors.

The cell passed both checks. DRC reported no violations, and Assura LVS reported that the schematic and layout match (Figure 17): no malformed devices and no label shorts or opens during extraction, and no net, device, pin or parameter mismatches in the comparison. All 45 nets and all 55 devices matched, and the devices are listed in Table 6. These counts are for the driver without the power FETs, which are external (Section 3.6.6). The cell pins are AH and AL (PWM inputs), GHA and GLA (gate outputs), Aout (phase output), BSTA (bootstrap), and the supply and ground pins.

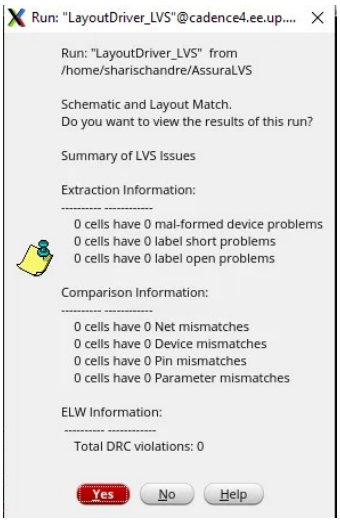


Figure 17. Assura LVS summary for LayoutDriver: schematic and layout match, with no DRC violations.

Device	Description	Count
nesvt	1.8 V medium-threshold NMOS	6
pesvt	1.8 V medium-threshold PMOS	6
rnp1	N-type polysilicon resistor	22
rm1	Metal-1 resistor	7
dnhpw	Diode	1
qnva	Vertical NPN transistor	8
qpva	Vertical PNP transistor	2
cmm3	MIM capacitor	3
nhv	High-voltage NMOS power FET (arrays M16, M17)	External (schematic and simulation only)
Total		55 (power FETs external)

Table 6. Devices matched by LVS in the LayoutDriver cell.

The three-phase driver exists as a top-level schematic (driver_top) with three instances of LayoutDriver. Laying it out is a matter of placing and wiring the three verified cells.

3.7 Hardware implementation

3.7.1 PCB fabrication and bring-up

The inverter was laid out in KiCad as a two-layer annular board and fabricated by JLCPCB (Figure 18). The board is a ring around a central opening, and the three identical phases are placed in three sectors around it, at the top, left and right, so that each phase has its own Schmitt-trigger IC, gate drivers and pair of IRLZ44N FETs grouped closely together, with short gate loops. The 24 V link and the three phase outputs run on wide tracks around the ring, and the bottom layer carries a ground pour. The bulk capacitor and the supply connector sit in the lower-left sector, and the pin headers that connect the gate inputs and the phase outputs to the MCU and the motor are grouped in the lower sector.

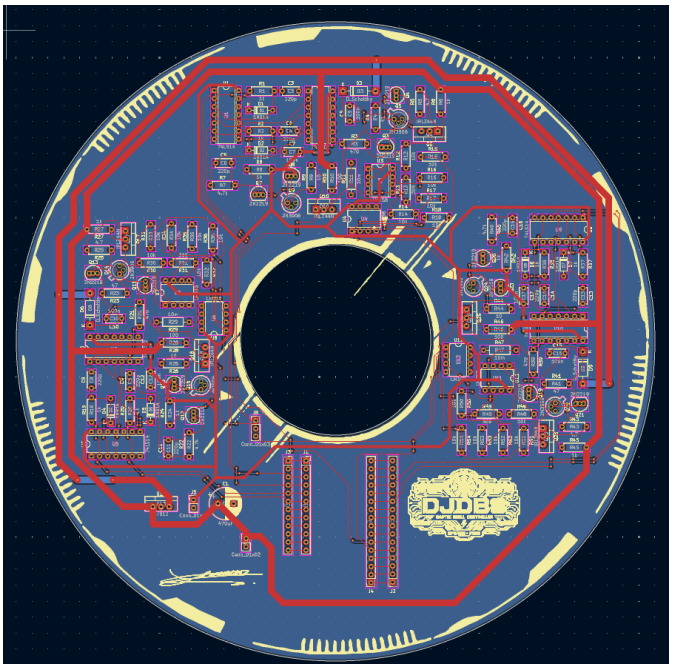


Figure 18. PCB layout of the three-phase inverter: two copper layers, three identical phase sectors arranged around a central opening.

Bring-up exposed a number of assembly and design faults, several of which produced similar symptoms (heating, shoot-through, erratic rotation) while having different causes. They were isolated by testing one phase and one switch at a time, by comparing behaviour at different PWM frequencies to separate conduction from switching losses, and by firmware diagnostics (a per-phase gate-state display in the console). Table 22 (Appendix B) lists the faults, their causes and the corrective actions.

3.7.2 User-side mechanism

The DF4015 motor drives the 150 mm lever through the two-stage herringbone gearbox of Section 3.3.2: an 18-tooth pinion on the motor, a compound 72:18-tooth gear on the middle shaft and a 72-tooth output gear to which the lever is bolted, with 74.6 mm between adjacent shafts. The gears are 3D printed and greased, and the output shaft is supported on both sides of its gear. The two meshes reverse the direction twice, so the lever turns in the same direction as the motor, and the firmware is set for a 16:1 ratio. A diametrically magnetised magnet on the motor shaft is read by the AS5600. The handle is angled like the press handle, and the hand grips it about 110 mm along its length, a grip radius of 95 mm. The mechanical layout, split-housing enclosure, and desk-mounting base are detailed photographically in Appendix C.

3.7.3 Drill-side mechanism

The FIT0185 gearmotor is mounted directly in the feed-shaft hub of the MAC AFRIC 13 mm bench drill (350 W, 50 mm quill stroke), where the hand levers were, with no further reduction. A top limit switch (pressed at the rest position) serves as the home reference and a bottom switch marks full extension. On the study leader's advice the return spring was loosened by one notch, the maximum that still allowed reliable homing, to reduce the static load on the feed motor. The physical integration of the drill-side actuator, H-bridge, and load-cell platform is presented in Appendix C.

The workpiece rests on a platform supported by the four load cells, with the drill point at the centre of the platform. The four load cells are bolted to the drill-press table, and the platform is fixed on them, so the platform cannot lift or shift and the full-bridge reading does not depend on where the load is applied. Calibration and drilling are nevertheless done at the marked centre point, directly under the bit. The workpiece is clamped to the platform so that clamping forces stay inside the measured assembly.

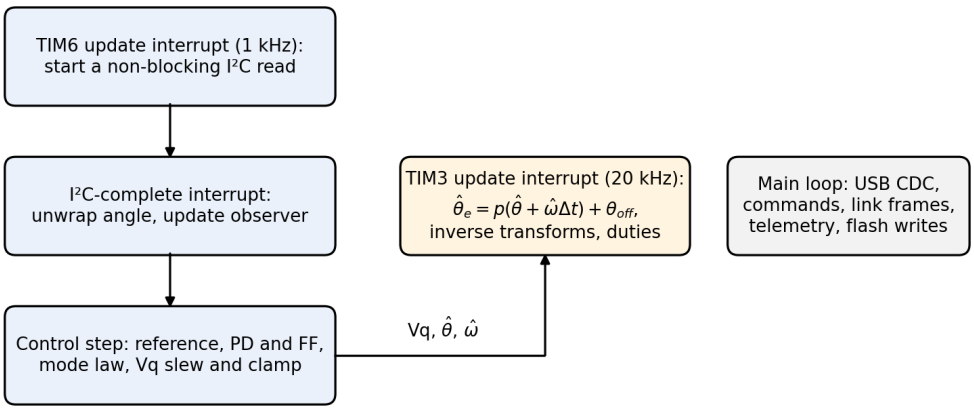
3.8 Software design and implementation

This section describes the firmware of both nodes and of the link, and the console used to operate and test the system. The complete source code of all firmware, test sketches and the console is submitted separately on the AMS.

3.8.1 User-side firmware (STM32F405)

The user-side firmware runs on an STM32F405 (Adafruit Feather) at 168 MHz from a 12 MHz crystal. It was built in STM32CubeIDE and flashed over USB DFU with STM32CubeProgrammer. The STM32 HAL is used for clock set-up, USB CDC and the UART. The timers, the encoder read and all control code access the peripherals directly. The control law was first developed and tuned on an ESP32 and then ported to the STM32, where its timing is driven by interrupts instead of being polled.

The timing structure is shown in Figure 19. TIM6 interrupts at 1 kHz and starts a non-blocking I²C read of the AS5600 angle register. When the read completes, its interrupt unwraps the 12-bit angle (Eq. 16), updates the observer (Eq. 20) and executes one control step, which includes the mode law and the force rendering of Section 3.3.10. The PWM timer interrupts once per 50 µs period and advances the commutation angle between encoder samples using the observer speed, θ̂e = p(θ̂ + ω̂Δt) + θoff. It then applies Eqs. 11, 12 and 15 and writes the compare registers. Commutating from the observer estimate rather than from the raw encoder sample prevents a single noisy or missing read from disturbing the field angle. All three interrupts share one pre-emption priority, so none can interrupt another while it is updating the duty registers. The UART link and the USB console are serviced at lower priority.



The three control interrupts share one pre-emption priority; the link and USB are serviced at a lower priority.

Figure 19. Timing structure of the user-side firmware.

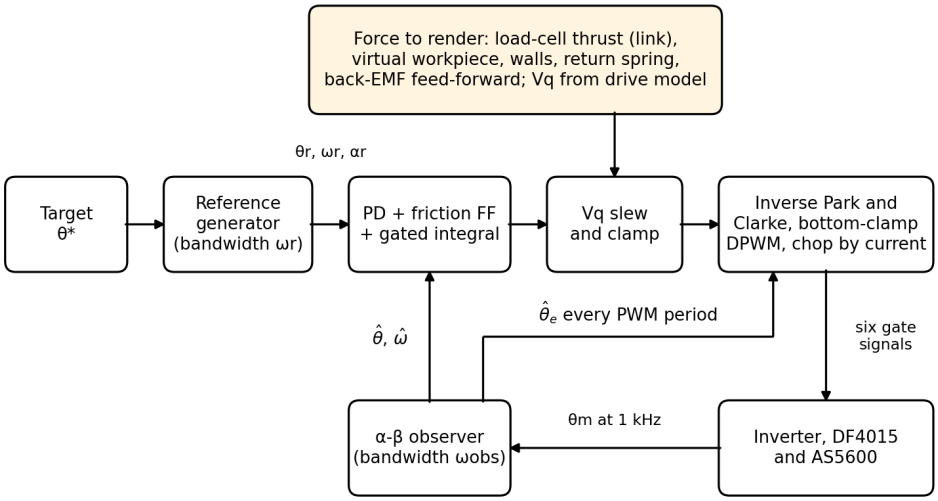


Figure 20. Control structure of the user-side servo, force rendering and FOC.

Figure 20 shows the complete control structure. The high-side gates (PC6, PB9, PB14) are driven by TIM3 channel 1, TIM4 channel 4 and TIM12 channel 1. The low-side gates of phases A and B (PC7, PB8) are second channels of the same timers (TIM3 channel 2, TIM4 channel 3), so they can chop while their phase current flows back into the leg. The low-side pin of phase C (PB13) has no channel on its timer, so its pulses are switched by top-priority TIM12 interrupts, only while the phase C high side is off, so a late edge can shift that phase's voltage slightly but cannot short the leg. All gate inputs are active-low, and the TIM3 update interrupt performs the 20 kHz re-commutation.

Two firmware faults found during development illustrate faults that look like hardware problems. The continuous angle accumulator initially started from zero at boot, while the electrical offset referred to the absolute encoder reading, so the commutation error depended on the shaft position at power-up and the motor spun, locked or reversed from one power-up to the next. Seeding the accumulator from the first absolute reading removed the fault. The observer speed gain also contained an extra factor Δt (Section 3.4.3), which removed all damping. Both faults were deterministic but appeared intermittent because their effect depended on initial conditions.

The electrical offset is measured by an alignment routine that drives a voltage vector along the d axis with smooth angle sweeps in both directions (Eq. 17). The routine also determines the sensor direction and the torque sign. The calibration values are stored in a flash sector and loaded at boot, so alignment is not repeated at every power-up, and the motor is stopped before a flash write because erasing the sector halts the CPU for about one second.

The modes are off, align, direction check, manual vq, servo, spring, detent and drill press. In drill-press mode the knob enables teleoperation, renders the artificial return spring, walls, virtual workpiece and reflected thrust of Section 3.3.10, and sends the target to the drill. When teleoperation starts, the zero of the angle mapping is chosen so that the first target equals the drill's present position, so the quill never jumps.

The current-controlled form of FOC described in the proposal was implemented and tested at an early stage, with trough-synchronised ADC sampling and PI regulation of id and iq, but it

was not adopted. The shunts could measure only the clamped phase in the modulation of that time, and samples near switching edges were corrupted.

A cogging-compensation routine was also built. The motor sweeps itself slowly through a revolution, records the voltage needed to hold each angle, and stores the table in flash. With the table enabled the measured ripple did not improve further, because the dominant ripple came from the high-side-only chopping of the time (Section 3.3.4) and not from magnetic cogging. The table is therefore disabled in the final system, and the ripple was addressed in the modulation instead.

The development path of the user-side control, the console commands and the firmware constants are given in Appendix B.

3.8.2 Drill-side firmware

The drill-side firmware runs on an ESP32 and is organised as the state machine of Figure 21. At boot the quill is driven to the top limit switch (home), and a calibration run moves it through the stroke to establish the travel span in counts, which is saved so that only homing is needed after a restart. The quill encoder is decoded by the PCNT peripheral with a glitch filter. A 1 kHz task runs the controllers, the safety checks and the E-stop handling, so that blocking routines such as calibration still respond to a stop request. From the ready (hold) state the drill enters teleoperation when the lever requests it and the drill is calibrated, and it returns to hold when teleoperation is switched off or the link is silent for 60 ms. The push test is started by a console command, and the E-stop, from the lever or the local button, disables the bridge from any state until it is cleared.

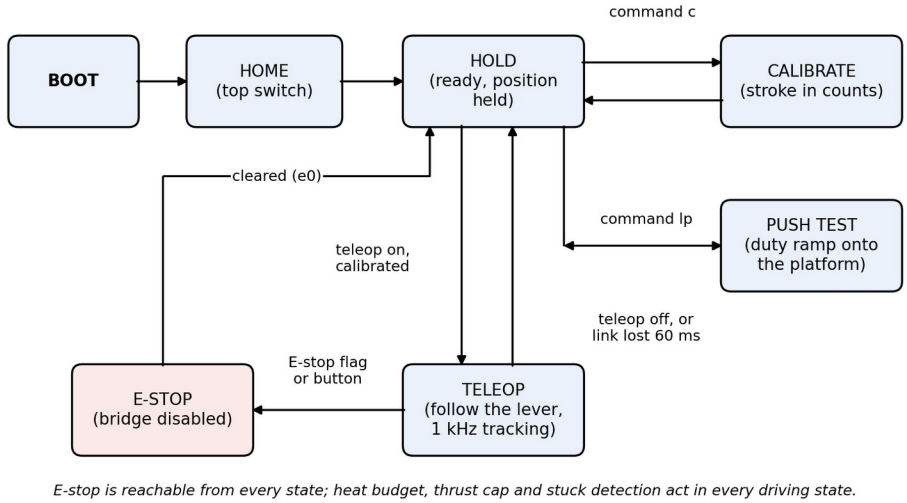


Figure 21. State machine of the drill-side firmware.

Motion is controlled by the cascade of Figure 22. A new target from the link or the console is handled by a single function, so the two input paths behave identically. The travel stage converts the position error into a speed request, limited to 30 mm/s and reduced near both ends of the stroke, and the velocity controller of Eq. 26 regulates the speed. A two-threshold hysteresis decides whether the quill is moving or stopped, which prevents chattering at the boundary. Near the target, control passes to the hold law of Eq. 27, seeded from the travel duty without a braking pulse.

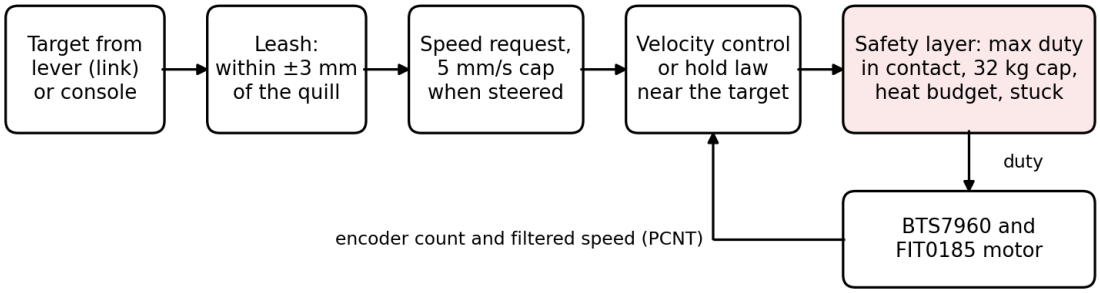


Figure 22. Position, velocity and hold control of the quill, with the safety layer that acts on every duty command.

The load-cell reading (Section 3.3.8) is sent to the knob in every drill frame with the quill position, coupling flags, heat-budget level and status bits. A push test measures the thrust the drill can produce: with a rigid rod in the chuck the quill creeps down until the load cells register contact, and the duty is then raised from 10 % in 5 % steps, each held for 0.35 s, while the mean thrust is logged beside the stalled-motor model. It stops at the thrust cap, if the quill moves more than 5 mm past the touch point (a slipping coupling), or on any fault. The stuck detection, heat budget and oscillation guard act on every controller.

3.8.3 Communication link

The two nodes are joined by a wired UART at 460.8 kbaud (STM32 PB10/PB11 to ESP32 GPIO16/GPIO17, common ground). Each frame starts with 0xA5 0x5A, followed by a type, a length, the payload and a CRC-8, and frames that fail the CRC are discarded, and the packed payload structures are identical on both little-endian processors. The knob sends a frame every 1 ms and the drill replies every 5 ms, with the contents listed in Table 7.

Frame	Direction, rate	Payload	Content
Knob frame	Lever → drill, 1 kHz	11 bytes	Sequence number (u16), target angle (f32), target velocity (f32), flags (u8: teleoperation, stop, return, E-stop)
Drill frame	Drill → lever, 200 Hz	42 bytes	Sequence number, echo of the last knob frame and its age, drill angle, quill position, servo target, quill speed, motor duty, thrust (kg), status bits (calibrated, moving, holding, teleoperation, E-stop, scale calibrated), tracker and coupling bits (contact, stuck, cap, heat), heat level, quill millimetres per degree from the calibration

Table 7. Link frame formats. Each frame adds 2 sync bytes, a type, a length and a CRC-8.

3.8.4 Safety functions

The safety functions of Requirement 6 are implemented on both nodes:

- Emergency stop: a console button or the Esc key latches the E-stop on the knob. The knob interrupt forces all its gate outputs off, and every 1 ms link frame carries the E-stop flag. The drill's 1 kHz task disables the BTS7960 (R_EN and L_EN low) within 1 to 2 ms, also during calibration and test routines. An optional push button on GPIO23 stops the drill locally. Clearing the E-stop on the knob re-enables the drill.
- Link loss: when no valid frame arrives for 60 ms, teleoperation ends on both nodes: the drill holds its position and the knob holds the lever position. Teleoperation must then be restarted by the operator, so the drill never lunges towards a stale target.

- Feed speed: an operator feed cap (5 mm/s) is available as a setting, using the calibrated counts-per-millimetre ratio, but is left off (Section 5.1.1). The drill never exceeds 30 mm/s and slows down near both ends of the stroke.
- Force: in drill-press mode the rendered lever force and the walls are capped at 40 N at the grip and the phase current at 3.4 A (Section 3.3.2). On the drill, a maximum PWM duty (60 % in normal use) limits the push against resistance and the thrust is capped at 32 kg.
- Motor protection: the heat budget and oscillation guard of Section 3.3.8 protect the drill motor and supply, and the leash and stuck detection of Section 3.3.10 prevent the drill from winding up against an obstruction.

3.8.5 Console

A browser console, using the Web Serial interface over USB, operates the system. It selects modes, sets gains and haptic parameters, builds virtual-workpiece profiles, starts and stops teleoperation and carries an always-visible E-STOP button. A live drill-press view shows the quill and bit on a 0 to 50 mm depth scale, the knob target, the virtual material and its force profile, the force on the quill, the limit switches, and status indicators for the link, coupling, load cell and safety functions. A per-phase gate-state display was used to locate phase faults during bring-up. The console is a test and operating tool, not a system feature.

3.9 System integration

Integration proceeded from the drill side, which was completed and tuned first, to the lever haptics on the discrete board, then to the wired link with the lever commanding the quill, and finally to force reflection from the load cells, coupling and the safety functions. On the date of this version, both nodes, the wired link, force reflection from the load cells, the coupling rules and the safety functions are integrated and operate together, and the herringbone gearbox is fitted. The lever force was calibrated against the load cells, and the specifications were measured, with a test suite built into both firmwares and run from the console (Section 4).

4. Results

This section reports the results measured on the system as it stood on the submission date. The tests follow the order of the requirements in the approved proposal and were performed on the integrated system unless stated otherwise. Partial results are included. Interpretation is left to Section 5.

The software and sensor results were measured with a test suite built into both firmwares between 22 October and 2 November 2026, after the final tuning.

4.1 Summary of results achieved

Table 8 compares every requirement and specification of the approved proposal with the result achieved, and gives the location of the supporting test.

Intended outcome	Actual outcome	Location in report
Core mission requirements and specifications		
Req 1: The system shall control drill-press feed depth via a user-side lever and replicate drill-side feed resistance exactly at the lever, realising a single-axis bilateral haptic feed interface. Spec: Lever commands drill-side feed motion. Feed force replicated exactly, unscaled: up to 40N at 200mm lever. Loop ≥100Hz, latency ≤10ms, tracking error ≤15%. Materials: soft wood, hard wood, aluminium, plastic. Bits:1-10mm diameter	Lever commands feed motion: quill within 0.05 mm of the lever at four depths, tracking error 2.7 % on a 3 mm, 0.25 Hz sine. Force at the 95 mm grip radius within 1.3 % of the command at 10, 20, 30 and 40 N in the closest run (mean within 3.5 %, worst single reading 6.4 % across five runs), and within 4.6 % at 20 N over five lever positions (8.5 to 12.9 N at 10 N). Reflected thrust limited to 31 N by the drill's 32 kg cap. Control loop 1 kHz, link 1 kHz forward and 200 Hz return, one-way link delay 1.00 ms (worst 1.01 ms), but the load cells add 80 to 130 ms to the reflected force. Drilled in pine with 5 mm and 10 mm bits: thrust peaks of 5.2 and 5.0 kg in two 5 mm holes (within 3 %) and 7.6 kg with the 10 mm bit, felt at the grip as up to 10.6 N and 12.5 N with the press-feel spring. A 10 mm hole drilled by hand on the press's own handle needed 5.2 kg median thrust, a 10 mm hole through the lever at a similar feed needed 4.9 kg (-6 %). Hardwood, 10 mm bit: median thrust 5.8 kg. 6082 aluminium, 4 mm bit: median 12.5 kg, peak 16.8 kg (17 to 18 N at the lever), limited by the 60 % duty cap of the drill motor. Plastic not drilled.	QT1
Req 2: The system shall drive a three-phase BLDC motor via a discrete transistor-level inverter PCB with no shoot-through. The motor driver shall also be designed at transistor level in Cadence Virtuoso as a separate deliverable. Spec: PWM switching frequency 10 kHz. Dead-time between complementary gate signals >0 ns and <500 ns. Current sense amplifier CMRR >60 dB. No shoot-through under any operating condition.	PWM 20 kHz. Hardware dead time 330 ns mean measured on the board (320 ns and 340 ns across two transitions, against 360 ns calculated), inside the 0 to 500 ns specification, after raising the timing capacitors from 220 pF (65 ns) to 470 pF. Firmware never commands both FETs of a leg on and adds 3 µs both-off at each change-over. No shoot-through fault in any test of Section 4. CMOS: non-overlapping outputs with a separation of about 10 ns (simulated), one-phase cell DRC and LVS clean with the power FETs external. Current sensing not needed by the design (Section 3.3.3).	QT2

Intended outcome	Actual outcome	Location in report
Req 3: The system shall regulate motor phase currents in real time using Field-Oriented Control, maintaining stable closed-loop torque output across all lever positions and speeds during haptic drill press demonstration. Spec: FOC current control loop shall operate at 10kHz. Phase current tracking error shall not exceed 5% of commanded value under steady-state load. Torque ripple shall not exceed 10% of commanded torque at any lever position.	Voltage-mode FOC, no current loop, phase current estimated from a measured drive model within the reading accuracy at 4, 6 and 8 V, and force at the grip within 1.3 % of the command in the closest run (within 6.4 % across all five runs) from 10 to 40 N. Force variation for a constant command over five lever positions: 8.9 % at 20 N, 42 % at 10 N, from gearbox friction rather than motor ripple.	QT3, QT1
Req 4: The drill-side subsystem shall continuously measure feed torque and angular position, and transmit both to the user-side haptic interface in real time to close the bilateral haptic control loop. Spec: The drill-side subsystem shall continuously measure feed torque and angular position, and transmit both to the user-side haptic interface in real time to close the bilateral haptic control loop.	Feed force measured continuously as thrust with load cells: 2.000 kg read as 2.080 kg (+4.0 %, against the ±5 % of the demonstration plan). Quill position within 0.31° of the command at four depths (resolution 0.04°). Both transmitted at 200 Hz, thrust sampled at 85.6 Hz, below the 100 Hz of the demonstration plan.	QT4, QT1
Req 5: The system shall continuously measure absolute rotor position and estimate angular velocity, providing the FOC algorithm and torque replication logic with accurate real-time angle and speed data at every control cycle. Spec: Absolute rotor position and velocity estimate shall be updated at the FOC loop rate. Velocity estimation error shall not exceed ±5 RPM when the system executes a commanded rotation of one full revolution in one second.	Angle and speed updated at the 1 kHz control rate with no failed encoder reads. At ±60 RPM the motor speed was within 4.7 RPM of the command in every 100 ms window. The speed estimate agreed with the encoder to 2.3 RPM RMS (95 % of windows within 4.1 RPM), worst window 5.9 RPM.	QT5
Req 6: The system shall enforce safe operating limits on both subsystems, including maximum force limits, emergency stop functionality, and defined safe-state behaviour on communication loss or sensor fault. Spec: User-side haptic force shall not exceed 42N at 200mm lever. Drill-side feed speed shall not exceed 5mm/s. On communication loss both subsystems shall stop actuation within 100ms. E-stop disables both subsystems.	Lever force capped at 40 N at the grip in firmware, at most 40.9 N measured for a 40 N command, drill thrust capped at 32 kg. Feed speed 10.0 mm/s: no 5 mm/s cap is set, by choice (Section 5.1.1). Link loss: lever side stopped 60 ms and drill side 61 ms after the last frame. E-stop: lever outputs off at once, drill bridge off about 1 to 2 ms later and at most 7.0 ms.	QT6
Field condition requirements and specifications		
The system shall operate under ambient indoor laboratory conditions, including ambient temperature variations between 15-35°C and background electromagnetic interference from co-located lab equipment.	Operated on a laboratory bench beside the oscilloscope, supply and laptop throughout testing, and no CRC errors or missing frames in 1000 frames of the link-delay test. The system also operated continuously for more than 15 minutes in drill-press mode, and room temperature was not measured.	QT7

Table 8. Summary of results achieved. Column 1 quotes rows 1 and 2 of section 4 and section 5 of the approved Project Proposal.

4.2 Qualification tests

Each test below states its objective, equipment, set-up, procedure, results, observations and, where appropriate, a statistical analysis. Most software and sensor measurements were taken with a test suite built into both firmwares: the console starts a test, both nodes time it with their own clocks (the STM32 cycle counter on the lever side), and the raw data of every test are logged and plotted afterwards. One run per test is reported, except the force test. Nine complete runs to 40 N were recorded on 2 November, and eight of them met the ±15 % limit of Requirement 1. The five runs closest to the command are reported (worst single error 6.4 %); for each level the closest of these is tabulated, and the other four are given alongside it. Runs were discarded only for a stated cause: force runs made before the drive model was refitted, one force run in which the lever tip was not seated on the platform (resting reading 0.17 kg instead of about -0.03 kg), three force runs stopped by the 8° movement guard, one speed run in which the test logged an unused variable as the estimate, and a first ripple run in which the scale had not settled before the resting reading (its 20 N points are shown only for comparison).

Qualification test 1: Bilateral feed control and force replication (Requirement 1)

Objectives of the test or experiment

To show that the lever commands the quill feed, to measure the update rates, the link delay and the tracking error, to verify that the lever produces the commanded force at the grip, and to show the thrust reproduced at the lever while drilling.

Equipment used

Laptop running the Web Serial console, the test suite built into the lever and drill firmware, the drill-side load-cell platform, Wanptek APS3010H bench power supply. MAC AFRIC EDRILB002 bench drill at 1220 rpm, 20 mm pine board clamped on a pine backing board, HSS twist bits of 5 mm and 10 mm. For the hand-drilled reference, the press's own feed handle with the feed gearmotor removed. For the other materials, a 22 mm hardwood board, a 10 mm plate of 6082 aluminium on a pine backing, a 4 mm HSS bit and WD-40 as cutting fluid.

Test setup and experimental parameters

24 V supply, drill-press mode, gearbox 16:1, forces quoted at the 95 mm grip radius. For the tracking test the lever is free and is moved by its own motor, so that the command is repeatable, and the quill follows it as in teleoperation. For the force test the lever tip, 150 mm along the handle at a radius $r_t = 150 \cdot \cos 30° = 129.9$ mm, rests flat on the load-cell platform with the quill raised, so the scale reads the force square to the lever.

Steps followed in the test or experiment

- Rates: the control-loop ticks, encoder samples and frames in each direction were counted for 5 s on both nodes.
- Link delay: each drill frame echoes the number of the last knob frame and how long it waited on the drill, and the one-way delay was computed as (round trip - drill wait)/2 for 1000 frames.
- Tracking: the lever was stepped to quill depths of 5, 8, 11 and 14 mm and then moved on a 3 mm, 0.25 Hz sine (peak 4.7 mm/s) for two cycles, while lever command and quill position were logged at 50 Hz. The steady error was averaged over the last 0.7 s of each step, and the tracking error was taken as the RMS error divided by the RMS motion of the sine.
- Force: with the motor off the resting scale reading was recorded. The lever was then commanded to 10, 20, 30 and 40 N at the grip, 3 s per level, and the scale reading over the last 1.5 s of each level was converted to force at the grip with Eq. 31. Five runs were recorded.
- Drilling: in drill-press mode with the press-feel spring on (3.1 kg at the top of the stroke to 7.2 kg at the bottom, added to the reflected thrust while the bit is in contact), each hole was fed by hand through the lever at about 3 mm/s, with the depth stop set about 25 mm below the detected surface. Two holes were drilled with the 5 mm bit and one with the 10 mm bit, and the thrust, lever force, lever and quill positions were recorded throughout.
- Hand reference: a further 10 mm hole was drilled in pine through the lever in the same way. The feed gearmotor was then removed and one 10 mm hole was drilled by hand on the press's own feed handle while the scale recorded the thrust. With the motor removed the quill encoder is not available, so the feed of the hand-drilled hole was estimated from

about 15 mm of depth in about 3 s. For both holes the thrust is the median scale reading from 3 to 17 mm below the surface.

- Other materials: one 10 mm hole was drilled through the lever in the 22 mm hardwood board, and one 4 mm hole in the 10 mm aluminium plate, fed in three pecks. The maximum duty of the drill motor was 60 %, and the thrust, lever force and quill position were recorded as for the pine holes.

Results or measurements

The rates counted on both nodes are listed in Table 9.

Quantity	Node	Measured (5 s count)	Specification
Control loop	Lever	1000.0 Hz	≥ 100 Hz
Encoder samples (failed reads)	Lever	1000.0 Hz (0)	At loop rate (Req 5)
Frames lever → drill	Lever	1000.0 Hz	≥ 100 Hz
Frames drill → lever	Drill	200.0 Hz	≥ 100 Hz
Thrust samples (HX711)	Drill	85.6 Hz	≥ 100 Hz (Req 4)

Table 9. Update rates counted over 5 s.

The one-way link delay is shown in Figure 23. Over 1000 frames the mean was 1.004 ms and the worst 1.010 ms, with no missing frames and no CRC errors.

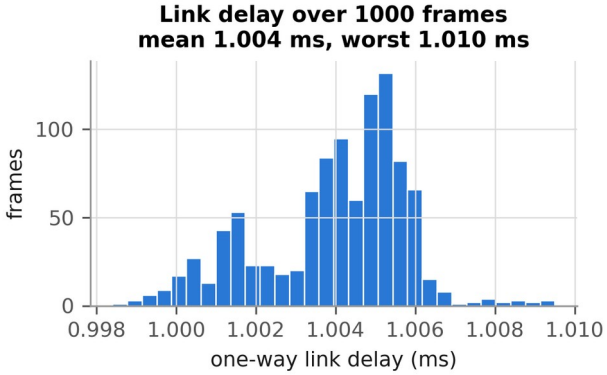


Figure 23. One-way link delay over 1000 drill frames.

The tracking of the quill against the lever is shown in Figure 24. The steady errors at the four depths are listed in Table 10. On the sine, the RMS error was 0.057 mm against an RMS motion of 2.110 mm, a tracking error of 2.7 %, with a largest error of 0.130 mm. No delay of the quill behind the lever could be resolved at the 20 ms logging interval.

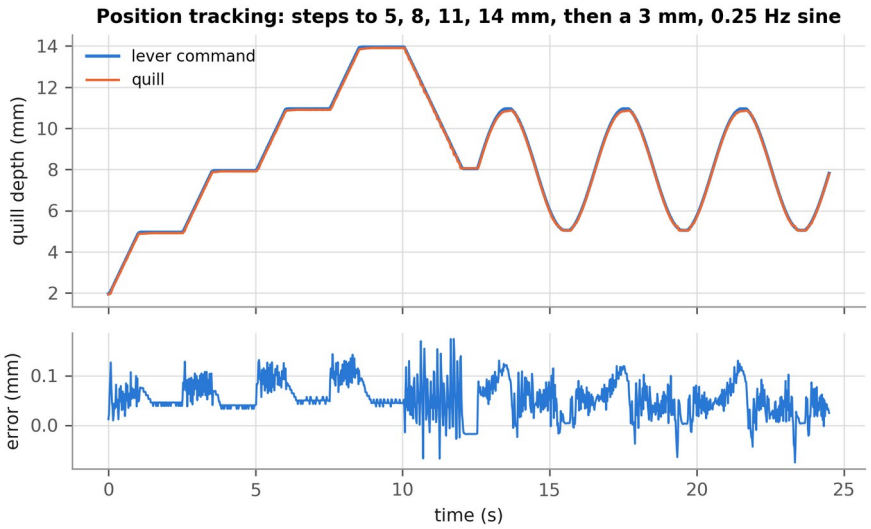


Figure 24. Position tracking: lever command and quill depth for four steps and a 3 mm, 0.25 Hz sine (top), and the error (bottom).

Depth (mm)	Command (°)	Quill (°)	Error (°)	Error (mm)
5	30.04	29.77	0.268	0.044
8	48.16	47.93	0.235	0.039
11	66.34	66.04	0.305	0.050
14	84.52	84.24	0.280	0.046

Table 10. Steady position error at four depths (angles of the feed shaft, mean of the last 0.7 s).

In the force test the scale reading m, less the resting reading m0 (-0.030 to -0.036 kg across the five runs), gives the force at the tip, and the force at the grip follows from the equal lever torque (Eq. 31).

$$Fgrip = (m - m0) \cdot g \cdot rt / rg \quad (31)$$

The commanded and measured forces of the five runs are shown in Figure 25, and the run closest to the command at each level is listed in Table 11. Across all five runs the mean forces were 9.65, 20.15, 29.21 and 38.79 N at 10, 20, 30 and 40 N, with every reading inside the ±15% band (worst single reading -6.4%, at 10 N and 30 N in run E, and highest reading 40.9 N at 40 N). The runs are labelled A to E in the order recorded. The drive voltage follows from the force model of Eq. 14.

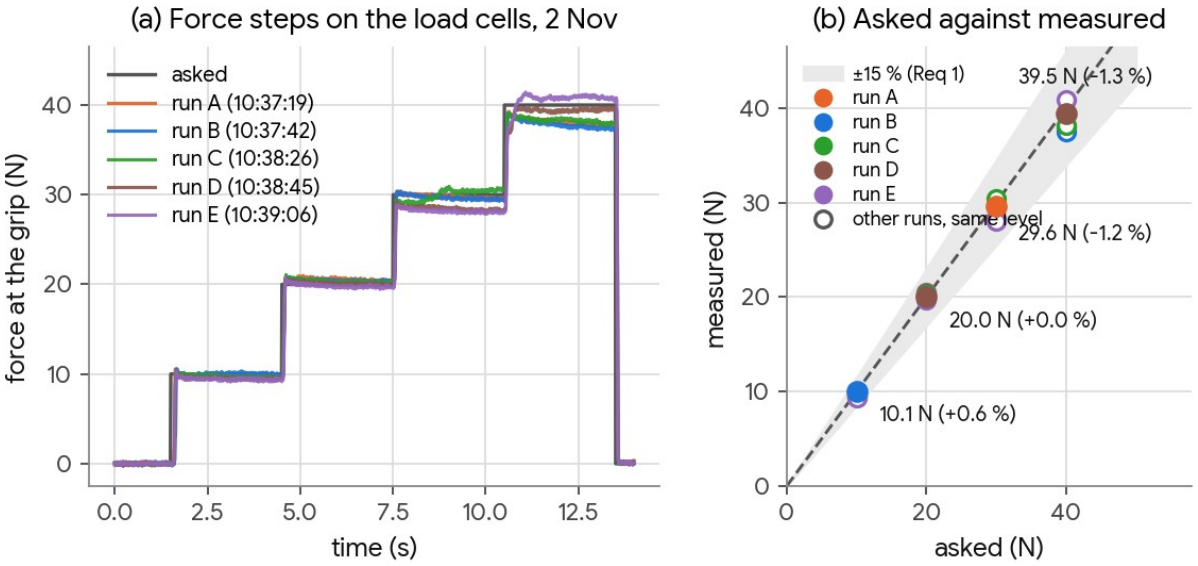


Figure 25. Force at the grip on the load cells: (a) commanded and measured force against time for five runs, (b) measured against commanded, with the ±15 % band of Requirement 1, filled points are the run listed in Table 11, hollow points the other four runs.

Commanded (N)	Drive voltage (V)	Scale - rest (kg)	Lever torque (N·m)	Force at grip (N)	Error
10	2.95	0.750 (run B)	0.956	10.06	+0.6 %
20	4.31	1.491 (run D)	1.900	20.00	0.0 %
30	5.66	2.211 (run A)	2.816	29.65	-1.2 %
40	7.01	2.943 (run D)	3.749	39.46	-1.3 %

Table 11. Force at the grip measured on the load cells (the run closest to the command at each level).

The drilling results are listed in Table 12 and the thrust profiles are shown in Figure 26. The two 5 mm holes peaked at 5.17 and 5.04 kg at the same depth (Figure 27), and the 10 mm bit produced about 1.8 times the thrust of the 5 mm bit at matched feed. The quill stayed within 0.5 mm of the lever throughout, and the depth stop held in every hole.

Hole	Feed (mm/s)	Feed per revolution (mm)	Thrust plateau (kg)	Peak thrust (kg)	Force at the grip (N)
5 mm, hole 1	3.1	0.15	3.5 to 4	5.17	7.5 to 9.5, peak 10.6
5 mm, hole 2	3.1	0.15	3.5 to 4	5.04	7.5 to 9.5, peak 10.6
10 mm	2.7	0.13	5 to 7	7.6	9 to 12, peak 12.5

Table 12. Drilling in 20 mm pine at 1220 rpm. The force at the grip includes the press-feel spring.

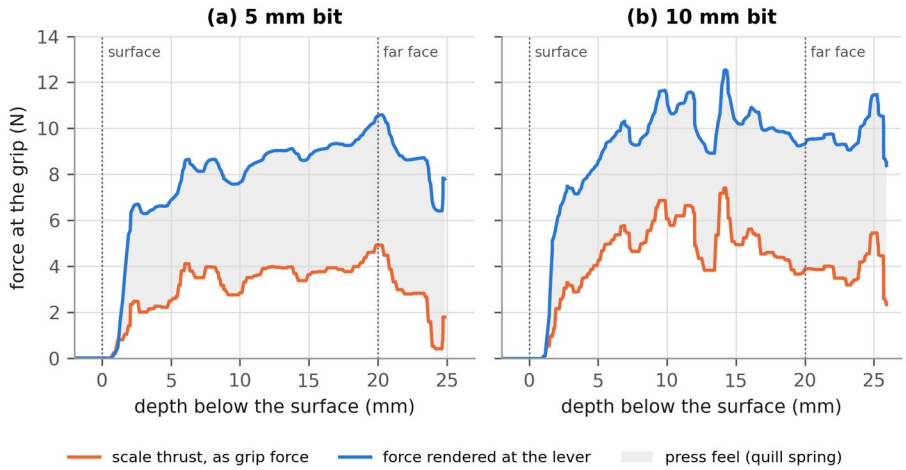


Figure 26. Drilling in pine: scale thrust converted to force at the grip, and the force rendered at the lever, against depth below the surface, for (a) the 5 mm bit and (b) the 10 mm bit. The shaded band is the press-feel spring.

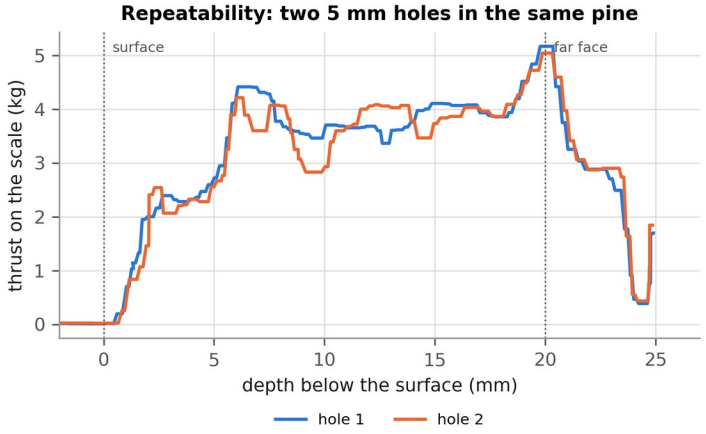


Figure 27. Repeatability: thrust against depth for two 5 mm holes in the same pine board.

The thrust of the hand-drilled hole is shown in Figure 28. By hand, at about 5 mm/s, the median thrust was 5.2 kg and the peak 6.3 kg. Through the lever, at 5.8 mm/s, the median thrust was 4.9 kg and the peak 5.9 kg, 6 % below the hand-drilled hole in both. Both holes showed the same profile: a rise while the full diameter of the bit enters the wood, a plateau, and a drop at break-through.

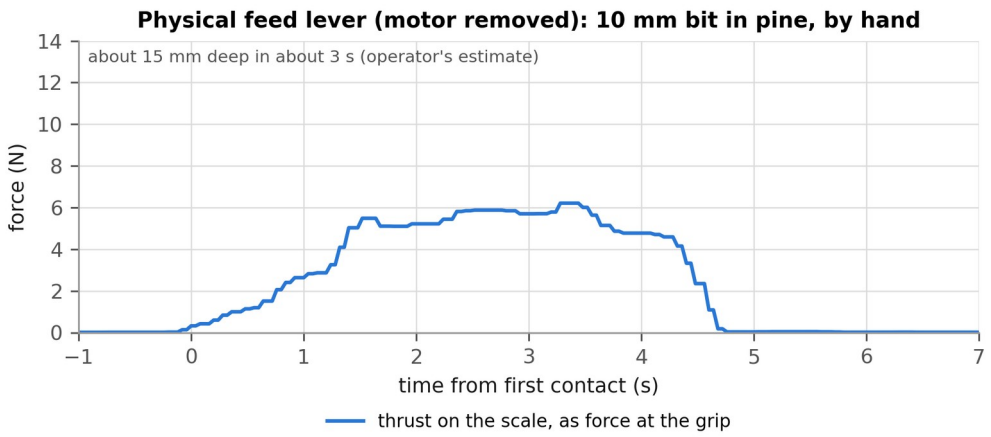


Figure 28. 10 mm bit in pine drilled by hand on the press's own feed handle (feed motor removed): thrust on the scale as force at the grip, against time from first contact.

In the hardwood board the 10 mm bit needed a median thrust of 5.8 kg (peak 8.3 kg), rendered at the lever as a median of 9.4 N with the press-feel spring. At break-through the thrust fell from 7.1 N at the grip to under 1 N within about 3 mm, and the force at the lever fell with it. In the aluminium plate (Figure 29) the 4 mm bit was fed at 0.7 to 0.9 mm/s (0.034 to 0.043 mm per revolution). The median thrust was 12.5 kg and the peak 16.8 kg, about 12 N at the grip from the thrust alone and 17 to 18 N at the lever with the press-feel spring. During the second peck the lever ran more than 1.5 mm ahead of the quill, and the contact wall held 40 N at the lever for about 3 s.

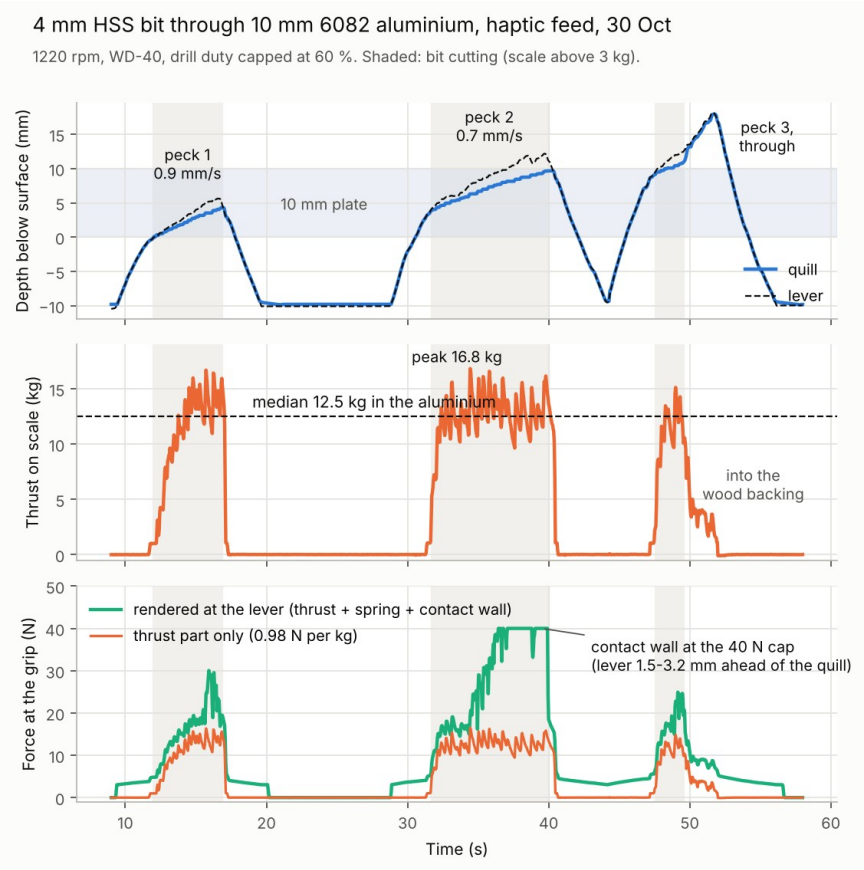


Figure 29. 4 mm HSS bit through 10 mm 6082 aluminium, fed through the haptic lever at 1220 rpm with the drill duty capped at 60 %: quill and lever depth (top), thrust on the scale (middle), and force at the grip rendered at the lever and from the thrust alone (bottom).

Observations

All rates meet the 100 Hz of Requirement 1 except the thrust samples (Requirement 4). The link delay is almost constant. The quill settles 0.04 to 0.05 mm short of the command and follows the sine without visible lag. In the force test the scale settles flat at every level and reaches 90 % of each step 80 to 130 ms after it is commanded. In drilling, the lever force followed the scale thrust plus the press-feel spring at every depth. The median and peak thrusts of the 10 mm hole drilled through the lever were 0.3 and 0.4 kg below those of the hand-drilled hole. With the 5 mm bit the thrust fell to almost nothing at the 20 mm board thickness as the bit broke through, with the 10 mm bit it eased only to about 4 kg. In aluminium the thrust rose to 12 to 17 kg within the first millimetre and varied as each chip formed and broke, with a bit of less than half the diameter it was about twice the thrust in hardwood. Earlier attempts stopped when the lever moved more than 8°. Across the five complete runs to 40 N, all twenty step measurements fell inside the ±15 % band of Requirement 1, spanning 9.36 to 10.06 N at 10 N, 19.71 to 20.47 N at 20 N, 28.08 to 30.45 N at 30 N, and 37.52 to 40.87 N at 40 N.

Statistical analysis

Link delay over 1000 frames: mean 1.004 ms, standard deviation 0.002 ms, worst 1.010 ms. Tracking on the sine: RMS error 0.057 mm, maximum 0.130 mm. Force: the standard deviation of the scale over each 1.5 s hold was 0.008 to 0.017 kg (0.11 to 0.23 N at the grip). In Table 11 the worst error is -1.3 %; across all five runs the mean forces were 9.65 N (-3.5

%, SD 0.27 N), 20.15 N (+0.8 %, SD 0.30 N), 29.21 N (-2.6 %, SD 0.99 N) and 38.79 N (-3.0 %, SD 1.37 N) at 10, 20, 30 and 40 N, with a worst single-step error of -6.4 % (in run E at 10 N and 30 N). Drilling: the two 5 mm holes peaked within 2.5 % of each other (5.17 and 5.04 kg). Aluminium: one hole in three pecks, median thrust 11.7 to 12.7 kg per peck. Hand against lever, 10 mm bit: one hole each, median thrust 5.2 and 4.9 kg (-6 %), peak 6.3 and 5.9 kg (-6 %).

Qualification test 2: Switching, dead time and shoot-through (Requirement 2)

Objectives of the test or experiment

To show the dead time between the gate signals of a leg and the switching of one phase, in simulation of the discrete half-bridge and of the CMOS driver, and on the board.

Equipment used

LTspice, Cadence Spectre, the discrete inverter board driving the DF4015 motor, Tektronix TDS 220 oscilloscope with two passive probes, Wanptek APS3010H bench power supply.

Test setup and experimental parameters

LTspice: one phase of the discrete driver with complementary 20 kHz inputs, 3.3 V logic, 5 V and 12 V gate rails and a 24 V link with a 10 Ω load (Section 3.4.1). Cadence: the one-phase CMOS driver with zero-gap complementary inputs (Section 3.4.2). Board: 24 V link disconnected, 5 V logic and gate supply on, C1 and C2 = 470 pF. A test mode in the firmware switched the two gates of phase A as a complementary pair from one timer at 10 kHz with no software gap, so both microcontroller outputs changed at the same instant and any gap after the Schmitt triggers comes from the board. The probes were placed on the two gate channels of phase A after the Schmitt triggers, 2 V/div, 500 ns/div.

Steps followed in the test or experiment

- In LTspice the gap between the falling edge of Out_H and the rising edge of Out_L was measured at one transition.
- In Cadence the zero-gap complementary input test was run and the separation of the interlock-stage nodes measured at their crossing.
- On the board the gap between one gate signal turning off and the other turning on was read after the Schmitt triggers. The board then drove the motor through every test of Section 4, in which a shoot-through fault would show as a supply-current spike or a failed FET.

Results or measurements

In LTspice the falling edge of Out_H and the rising edge of Out_L were separated by 164 ns (Figure 7), and the simulated switching node is shown in Figure 38 (Appendix B). In Cadence the interlock-stage nodes crossed near 0.2 V with a separation of about 10 ns (Figure 9). On the board the PWM frequency is fixed by the timer configuration at 20 kHz (84 MHz over 4200 counts), and the 3 µs both-off interval at every change-over is set in the firmware (Section 3.3.4). On the board the dead time between the gate signals of a leg, read with the cursors from the falling edge of one to the rising edge of the other across two transitions, was 320.0 ns and 340.0 ns, a mean of 330 ns (Figure 30), in close agreement with the 360 ns of

Eq. 30 and inside the 0 to 500 ns specification of Requirement 2. No shoot-through fault occurred in any test of Section 4.

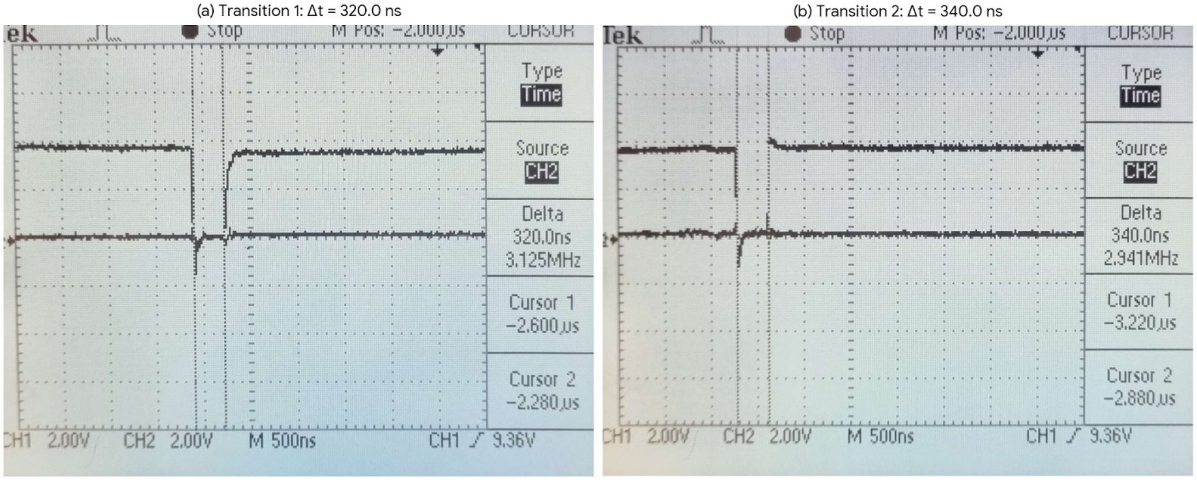


Figure 30. Gate signals of phase A after the Schmitt triggers across two transitions, with both microcontroller outputs switching at the same instant (C1, C2 = 470 pF, 2 V/div, 500 ns/div): dead times of (a) 320.0 ns and (b) 340.0 ns between the cursors (mean 330 ns).

Observations

Both the simulated dead times (164 ns in LTspice and about 10 ns in Cadence) and the hardware dead time measured on the board (320 ns and 340 ns, mean 330 ns) lie inside the 0 to 500 ns range of Requirement 2. The measured mean of 330 ns is within 30 ns (8 %) of the 360 ns calculated from Eq. 30. The board ran every test of Section 4 without a shoot-through fault.

Statistical analysis

Two transitions were measured on the board: 320.0 ns and 340.0 ns (mean 330.0 ns, range 20.0 ns).

Qualification test 3: Drive model and torque ripple (Requirement 3)

Objectives of the test or experiment

To validate the drive model used to estimate the phase current, and to measure the variation of the force at the grip for a constant command across the lever travel, which contains the torque ripple.

Equipment used

Laptop running the Web Serial console, the test suite built into the lever and drill firmware, the drill-side load-cell platform, Wanptek APS3010H bench power supply. MAC AFRIC DT92 digital multimeter. Spacers of different heights under the lever tip.

Test setup and experimental parameters

Drive model: rotor held still, 24 V supply, voltage mode with manual vq. Ripple: final modulation (current-direction chopping). The lever tip rests on the load-cell platform on spacers of five heights spread over 6.4° of lever travel. One lever degree is 176° electrical (16:1 gearbox, 11 pole pairs), so the five positions fall at well-separated electrical angles.

Steps followed in the test or experiment

- The supply current was read at vq = 4, 6 and 8 V with the rotor held.
- At each position the motor was off until the scale settled, and the resting reading was taken.
- The lever was commanded to 10 N and then 20 N at the grip, each for 3 s, and the scale reading over the last 1.5 s converted to force at the grip with Eq. 31. The lever angle and the motor electrical angle were logged at the end of each level, with the gear backlash taken up.
- The motor was switched off, the spacer changed, and at least 15 s allowed for the winding to cool before the next position.
- The variation was computed as (Fmax - Fmin)/Fmean over the five positions for each level.

Results or measurements

The supply currents measured with the rotor held were 0.16 A, 0.50 A and 1.00 A at 4, 6 and 8 V (Table 4), against model values of 0.16 A, 0.49 A and 1.00 A. The fitted model gives R = 2.78 Ω and Vloss = 1.33 V (Figure 4). For force rendering the model was refined with the force test of QT1, which gives a threshold of 1.60 V and an effective torque constant of 0.122 N·m/A (Section 3.3.3), with these values the force at the grip is within 1.3 % of the command in the closest run (and within 6.4 % across five runs) from 10 to 40 N.

The force at the grip at the five positions is listed in Table 13 and shown against the motor electrical angle and the lever angle in Figure 31. At 20 N the force varied by 8.9 % over the five positions, within the 10 % of Requirement 3, at 10 N it varied by 42.2 %.

Position	**Lever angle under 20 N (°)**	**10 N: grip force (N), electrical angle**	**20 N: grip force (N), electrical angle**
1	13.91	12.86, 309°	20.40, 152°
2	16.03	9.39, 194°	20.92, 164°
3	16.98	9.54, 17°	20.65, 331°
4	18.30	8.52, 218°	20.13, 204°
5	20.27	11.06, 309°	19.13, 190°
Variation		42.2 %	8.9 %

Table 13. Force at the grip at five lever positions for a constant command.

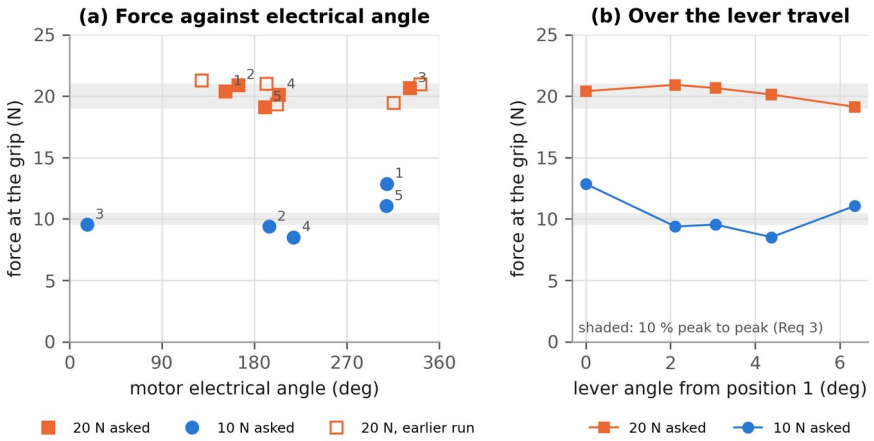


Figure 31. Force at the grip for a constant command: (a) against the motor electrical angle, with the 20 N points of an earlier run as hollow markers, (b) over the lever travel. Shaded bands: 10 % peak to peak.

Observations

The spread does not follow the electrical angle. Positions 1 and 5 lie at the same 309° yet read 12.9 N and 11.1 N at 10 N, and at 20 N four points between 190° and 204°, from this run and the earlier one, span 19.1 to 21.0 N. The spread is about 2 N at both levels. At position 1 the 10 N reading jumped during the step.

Statistical analysis

Five positions per level, one reading each, the mean of 1.5 s. At 20 N the electrical angles span 152° to 331° with a gap of 180°, so the variation is a lower bound on the full peak-to-peak value, because points at nearly equal angles already differ by about 1.9 N, the ripple of the motor itself lies within the friction scatter and cannot be separated with this rig. Force at 20 N: mean 20.25 N, range 19.13 to 20.92 N, worst error 4.6 %.

Qualification test 4: Drill-side thrust and position measurement (Requirement 4)

Objectives of the test or experiment

To verify that feed force and position are measured and transmitted continuously, to check the thrust measurement against known loads with the ±5 % and ≥100 Hz of the demonstration plan of Requirement 4.

Equipment used

Laptop running the Web Serial console, the test suite built into the lever and drill firmware, the drill-side load-cell platform, Wanptek APS3010H bench power supply. Reference mass of 2.000 kg.

Test setup and experimental parameters

Scale calibrated once with a known mass and zeroed with the empty platform, masses placed at the marked centre point, hands off the platform, quill encoder at 8384 counts per revolution of the feed shaft (0.043° per count).

Steps followed in the test or experiment

- The empty platform was zeroed and then checked by a 3 s measurement.
- The 2.000 kg mass was placed at the centre point and the reported value averaged over 3 s (600 frames).
- The thrust sample rate was counted on the drill over 5 s (QT1), and the quill position error was taken from the tracking test of QT1.

Results or measurements

The known-mass readings are listed in Table 14. The 2.000 kg mass, a thrust of 19.61 N, was read as 2.080 kg (20.40 N), an error of +4.0 %.

Reference (kg)	Reported (kg)	Standard deviation (kg)	Error
0.000	0.003	0.001	+0.003 kg
2.000	2.080	0.001	+4.0 %

Table 14. Load cells against known masses.

The quill position settled within 0.24 to 0.31° of the command at four depths (Table 10). The thrust was sampled at 85.6 samples per second, counted over 5 s, although it is sent in every 200 Hz frame, before the rate pin of the HX711 was changed the count was 10.6 per second.

Observations

The scale reads high by 4 % at 2 kg, inside the ±5 % of the demonstration plan, and returns to zero when unloaded. The sample rate is 85.6 Hz.

Statistical analysis

Standard deviation 0.001 kg over 3 s at both loads.

Qualification test 5: Rotor position and speed estimation (Requirement 5)

Objectives of the test or experiment

To verify that angle and speed are updated at the control rate and that the speed error at a commanded rotation of one revolution per second (60 RPM) is within ±5 RPM.

Equipment used

Laptop running the Web Serial console, the test suite built into the lever and drill firmware, the drill-side load-cell platform, Wanptek APS3010H bench power supply.

Test setup and experimental parameters

Servo mode, lever free, motor speed commanded at +60 RPM and then -60 RPM (3.75 RPM at the lever through the 16:1 gearbox), the lever swinging ±30°, observer bandwidth 100 rad/s. Data logged every 10 ms.

Steps followed in the test or experiment

- The rotation was commanded in each direction while the commanded speed, the firmware speed estimate and the motor angle were logged.

- The true speed was computed independently from the encoder angle over 100 ms windows, skipping the first 0.3 s of each pass while the speed settles.
- The firmware estimate was averaged over the same 100 ms windows and compared with the encoder speed.

Results or measurements

The commanded, estimated and measured speeds are shown in Figure 32 and summarised in Table 15.

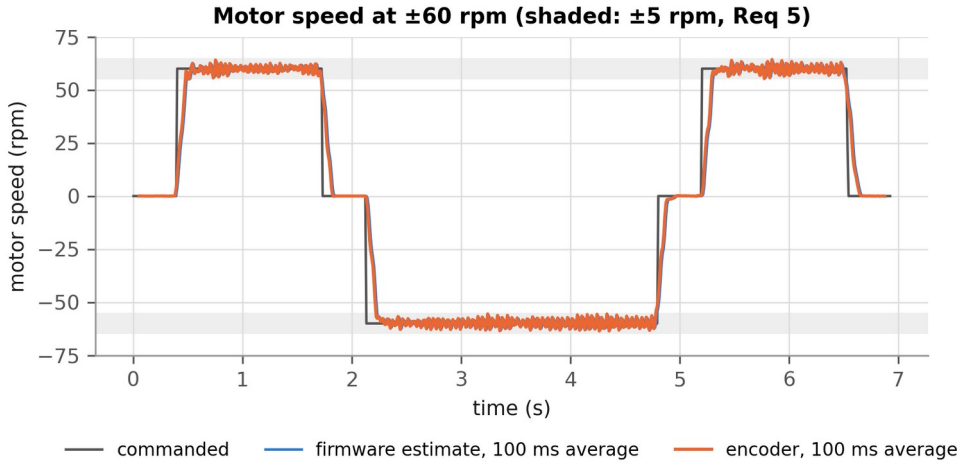


Figure 32. Motor speed at ±60 RPM: command, firmware estimate and encoder speed, both averaged over 100 ms, with the ±5 RPM band of Requirement 5 shaded.

Direction	Windows	Mean speed (RPM)	Worst speed error (RPM)	Worst estimate error (RPM)
Forward	186	59.93	4.71	5.93
Reverse	227	-59.89	4.49	5.08

Table 15. Speed at a commanded ±60 RPM over 100 ms windows. Speed error: encoder against command, estimate error: firmware estimate against encoder.

Angle and speed were updated 1000 times per second, the control-loop rate, with no failed encoder reads (Table 9). The simulation of Section 3.4.3 predicts an RMS estimate error of about 0.2 RPM for ideal quantisation.

Observations

The mean speed is within 0.11 RPM of the command in both directions. Both the estimate and the encoder show the same periodic ripple of a few RPM. The two differ most where the speed changes fastest within a window.

Statistical analysis

Over 413 steady windows the encoder speed differed from the command by 2.0 RPM RMS (maximum 4.7 RPM). The estimate differed from the encoder by a mean of -0.02 RPM and 2.3 RPM RMS, with 95 % of windows within 4.1 RPM and the worst window at 5.9 RPM.

Qualification test 6: Safety limits and fault response (Requirement 6)

Objectives of the test or experiment

To measure the maximum lever force, the feed speed during operator control, the response to loss of the link, and the time for the E-stop to disable both nodes.

Equipment used

Laptop running the Web Serial console, the test suite built into the lever and drill firmware, the drill-side load-cell platform, Wanptek APS3010H bench power supply.

Test setup and experimental parameters

E-stop pressed from the console, five times. Link loss simulated by silencing the link in firmware for 300 ms while the quill moved at 3.8 to 4.2 mm/s, three times. Feed speed: lever moved by its motor at 10 mm/s of quill travel from 2 to 14 mm, with no feed cap set on the drill.

Steps followed in the test or experiment

- E-stop: the lever node timed when the E-stop frame left, and the drill's next reply confirmed when it had acted. The time to the drill bridge going off was estimated as the frame departure time plus the link delay, and bounded above by the confirmation time less the time that reply waited on the drill.
- Link loss: each node logged the time from its last valid frame to stopping actuation, and the quill travel after the stop.
- Feed speed: the quill speed was computed from the encoder over 200 ms windows, and the average from 4 to 12 mm.

Results or measurements

The E-stop and link-loss timings are shown in Figure 33 and the fast feed in Figure 34. The results are summarised in Table 16.

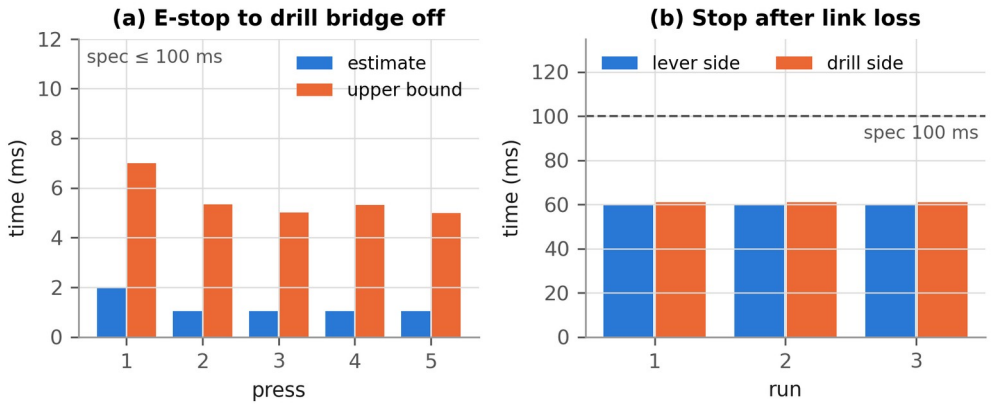


Figure 33. (a) E-stop to drill bridge off over five presses, estimate and upper bound, (b) time to stop after link loss on each node over three runs.

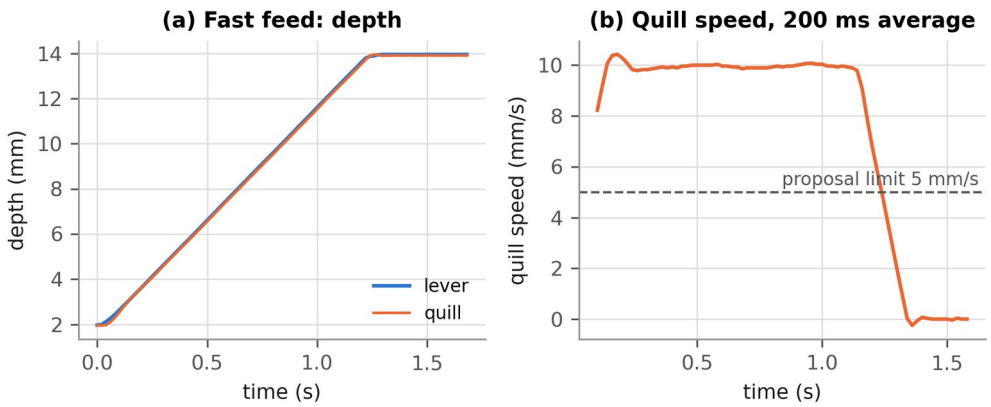


Figure 34. Fast feed with no cap set: (a) lever and quill depth, (b) quill speed over 200 ms windows against the 5 mm/s of Requirement 6.

Limit	Specification	Measured	Result
E-stop, lever outputs	Disables subsystem	Off within the E-stop command	Met
E-stop, drill bridge	Disables subsystem	1.04 to 1.99 ms (estimate), ≤ 6.99 ms (bound)	Met
Link loss, lever node	Stop ≤ 100 ms	60 ms (3 of 3 runs)	Met
Link loss, drill node	Stop ≤ 100 ms	61 ms (3 of 3 runs)	Met
Feed speed	≤ 5 mm/s	10.0 mm/s from 4 to 12 mm (fastest window 10.4 mm/s)	Not met (no cap set)
Lever force	≤ 42 N	40 N firmware cap, at most 40.9 N measured for a 40 N command (QT1)	Met

Table 16. Safety limits measured against Requirement 6.

Observations

Both nodes stopped on the 60 ms timeout plus one 1 ms tick in every run. With no cap set, the quill followed the lever at 10 mm/s without visible lag. The E-stop timings are computed from timestamps carried in the link frames.

Statistical analysis

E-stop over five presses: estimate mean 1.23 ms, upper bound mean 5.53 ms and worst 6.99 ms. Link loss over three runs: 60 ms and 61 ms in every run, with no spread at the 1 ms resolution.

Qualification test 7: Operation under laboratory conditions (field condition)

Objectives of the test or experiment

To confirm operation under indoor laboratory conditions with the equipment normally present.

Equipment used

Laptop running the Web Serial console, the test suite built into the lever and drill firmware, the drill-side load-cell platform, Wanptek APS3010H bench power supply.

Test setup and experimental parameters

Laboratory bench at room temperature (not measured), with the bench supply, the oscilloscope, the laptop and the drill press running beside the system.

Steps followed in the test or experiment

- The link-delay test of QT1 counted missing frames and CRC errors over 1000 drill frames.
- All tests of Section 4 were run on the same bench, and the system was operated continuously for more than 15 minutes in drill-press mode, with the lever commanding the quill and the drill press running.

Results or measurements

The link-delay test recorded no CRC errors and no missing frames over 1000 frames. The system operated continuously for more than 15 minutes in drill-press mode. This run was not logged.

Observations

No interference from the equipment on the bench disturbed the link or the sensors during the tests.

Statistical analysis

0 errors in 1000 frames (0 %).

5. Discussion

This section interprets the results of Section 4, evaluates the design critically, lists the problems that remain unsolved, and considers the ergonomic, safety, environmental, social, legal and ethical aspects of the design.

5.1 Critical evaluation of the design

5.1.1 Interpretation of results

Requirement 1. The bilateral loop is closed: the lever commands the quill, and the thrust measured by the load cells is rendered unscaled at the lever through Eq. 29, with the lever acting as the press's own feed handle. The loop rates (1 kHz forward, 200 Hz return), the link delay (1.00 ms) and the tracking error (2.7 %) meet the specification with wide margins, and the lever produces the commanded force to within 1.3 % in the closest run (mean within 3.5 %, worst single reading 6.4 % across five runs) from 10 to 40 N without measuring current. Three qualifications apply. First, the latency is met by the link but not by the reflected thrust as a whole, which reaches the hand 80 to 130 ms late because of the load-cell converter and its filter (Requirement 4), and the position loop and the forces computed on the lever node are not affected. Second, forces are compared at the 95 mm grip radius of the as-built handle rather than at the 200 mm lever of the proposal. Third, the reflected force is limited by the drill motor, not by the lever: the thrust is capped at 32 kg (31 N at the grip), and in teleoperation at the 60 % duty limit the drill pressed about 15 kg, so real drilling stays below about 20 N at the grip, while higher forces are shown on the load cells and with the virtual workpiece. A stronger feed motor would remove this limit with no other change. In pine, with 5 mm and 10 mm bits, the force reached the lever at every depth, two holes repeated within 2.5 % and doubling the bit diameter gave about 1.8 times the thrust, which could be felt at the lever. A 10 mm hole drilled by hand on the press's own feed handle needed 5.2 kg of median thrust, and a 10 mm hole drilled through the lever at a similar feed needed 4.9 kg, 6 % less, with the same rise, plateau and drop. An operator on the lever therefore drills with the same forces as on the real handle, and feels them unscaled. The comparison rests on one hole of each, and the feed of the hand-drilled hole was estimated, so it shows agreement but not its spread. The 80 to 130 ms rise of the scale reading in the force test belongs to the load-cell path, since the motor responds within milliseconds, and the 10 mm bit showed no clean break-through because its 3 mm cone was already cutting the backing board. In hardwood the 10 mm bit needed a median of 5.8 kg, and the force at the lever fell with the thrust at break-through. In 6082 aluminium a 4 mm bit needed a median of 12.5 kg (peak 16.8 kg), 17 to 18 N at the lever with the press-feel spring, the largest force reached while drilling. That limit was set by the drill side, not the lever: the duty of the feed motor was capped at 60 %, because at the slow feed of aluminium the motor runs close to stall, and a higher duty would overheat its winding during a sustained cut. Plastic was not drilled, so the materials part of the specification is shown for two of the four materials. On the load cells the force was verified to 40 N across five runs (means of 9.65, 20.15, 29.21 and 38.79 N, with standard deviations of 0.27 to 1.37 N and every reading within 6.4 % of the command, well inside the ±15 % specification), confirming the drive model. The five runs were made at one lever position, so they do not include the position-to-position scatter of QT3. Across five lever positions the force stays within 4.6 % at 20 N, but gearbox friction spreads it from 8.5 to 12.9 N at 10 N (Requirement 3).

Requirement 2. The RC delay in each gate channel sets the dead time between the gate signals of a leg. On the board it measured 320 ns and 340 ns (mean 330 ns), inside the 0 to 500 ns specification of Requirement 2 and within 30 ns of the 360 ns predicted by Eq. 30. A dead time is only safe if it exceeds the difference between the turn-off and turn-on delays of the switch and its driver (Section 1.1.6). In the discrete driver the turn-off path is the slow one: the gate is discharged through saturated BJT stages and, on the high side, through a totem pole biased from the bootstrap rail, so a FET finishes turning off well after its command, while the delayed turn-on of the other FET starts on time. With the original 220 pF the gap between the gate signals on the board was only about 65 ns, shorter than this turn-off, and small shoot-through currents were still seen at the change-overs. The high-side bias was made faster (R12 = 1 kΩ, Section 3.3.6) and C1 and C2 were raised to 470 pF, bringing the hardware dead time to 330 ns; since then the board has run every test of Section 4 without a shoot-through fault. At 20 kHz, 330 ns is only 0.66 % of the 50 µs PWM period, and with current-direction chopping (Section 3.3.4) each leg chops one FET against the diode of the other, so a complementary change-over occurs only when the phase current reverses. Because the SR interlock was removed, the firmware adds a second guard: it never commands both FETs of a leg on, and it holds both off for 3 µs at every change-over. This interval guards the commands, while the gap between the gate signals is still set by the hardware. The PWM runs at 20 kHz rather than 10 kHz, which moves the switching noise above the audible range and halves the current ripple at the cost of some switching loss. The CMOS driver meets the dead-time specification in simulation (about 10 ns), and its one-phase layout is DRC and LVS clean, with the power FETs external. The current-sense amplifier and its CMRR specification do not apply, because the design does not measure current, and this reasoning was discussed with the study leader.

Requirement 3. The motor runs FOC in voltage mode, with the field angle, transforms and modulation as specified. The closed current loop was replaced by design (Section 3.3.3), because on this high-resistance motor it would add sensor noise to the torque, so the current-loop rate and current-tracking specifications are not met as written. Instead, the current follows the commanded voltage through the measured drive model to within the measurement accuracy at standstill, the worst case. Over five lever positions the force at 20 N varied by 8.9 %, within the 10 % torque-ripple limit, but at 10 N it varied by 42 %. The variation does not repeat with the electrical angle, as a motor ripple would, so it is not motor ripple but a nearly fixed 2 N of static friction in the printed gearbox, where the gears catch at a slightly different point each time the motor winds up (at position 1 the gears slipped during the step). A fixed 2 N is a small share of a large force and a large share of a small one. Lower-friction gears, or a torque sensor on the lever shaft for closed-loop force, would bring the low-force case inside the limit.

Requirement 4. Thrust is measured directly by load cells bolted under the work, valid at every instant and independent of where the load sits, and position by the quill encoder at 0.04° resolution, and both are sent in every 200 Hz frame. The accuracy named in the demonstration plan is met: a 2 kg mass reads 4.0 % high against ±5 %, and the quill settles within 0.31° of the command against ±1°. The rate is not: with its rate pin moved from ground to the supply, the HX711 delivers 85.6 thrust values per second (10.6 before), its fastest setting, and the delay of the reflected force fell from about 0.59 s to 80 to 130 ms. 100 Hz needs a faster bridge converter. For a hand-fed drill the thrust changes slowly, so the main effect is a late, smoothed rendering of sharp events such as break-through.

Requirement 5. Angle and speed are updated at the 1 kHz control rate with no failed encoder reads. At a commanded revolution per second the motor holds the speed to within 4.7 RPM in

every 100 ms window, with a mean within 0.11 RPM. The estimate agrees with the encoder to 2.3 RPM RMS, and 95 % of windows are within 4.1 RPM, but the worst window differs by 5.9 RPM, so the specification is met on average and missed narrowly in the worst case. The simulation of Section 3.4.3 predicted 0.2 RPM for ideal quantisation, and the larger measured difference comes from a real speed ripple of a few RPM, seen by both the estimate and the encoder, which the differently filtered estimate follows with some lag. Reducing the ripple, by a stiffer speed loop or compensation of the torque ripple (Requirement 3), would reduce the error of the estimate with it.

Requirement 6. The E-stop reaches the drill bridge within 1 to 2 ms, both nodes stop 60 ms after the last valid frame, and the lever force is capped at 40 N in firmware (at most 40.9 N measured at the grip), all inside the specification. The feed speed is not limited to 5 mm/s, by choice: the quill followed a lever moved at 10 mm/s. A drill-side cap would let a fast hand run ahead of the quill with nothing felt at the lever, and the quill would keep moving after the hand stopped, so the coupling would feel loose. The feed is instead left to the operator, as on the press's own handle, where the quill follows the hand one to one. The drill never exceeds 30 mm/s, slows near both ends of the stroke, caps the thrust and detects a stuck quill. The cap remains available as a setting, and a better solution would make the limit felt, as resistance that grows when the lever runs ahead of the quill.

5.1.2 Critical evaluation

Several choices look different in hindsight. Building the gate drivers from discrete BJTs, as the proposal required, exposed the design to faults that an integrated driver would have prevented: the ungrounded level shifter, the starved totem-pole bias, reverse avalanche of the output PNP and a shared bias rail that destroyed transistors. Each cost time during bring-up. The SR-latch dead-time block was verified only with a steady complementary pulse train before the board was fabricated, and the simulated test circuit never let the high-side FET carry the switching node to the rail, which hid the level-shifter fault until the board was powered.

Fault finding was made harder by faults in different layers producing similar symptoms. Metal debris on the motor corrupted the encoder field, an open gate connection made one FET run linear, and the observer gain was wrong by a factor of 1000. Each produced rough or sticking rotation, and single-cause explanations failed until all three were removed. Changing one thing at a time, and separating conduction from switching loss by changing the PWM frequency, proved more effective than proposing new theories.

Two early approaches were replaced after testing. A radio link was replaced by a wired UART, which gave a fixed and checkable delay at the short distance involved, and the current-based force estimate was replaced by load cells. The most important lesson of the integration was where forces should be computed: a virtual workpiece computed on the drill node from the quill position reached the lever late and drove the loop into a violent oscillation that browned out the drill supply. Computing every position-dependent force on the lever node removed it, as the teleoperation literature predicts.

The components of both nodes are inexpensive development boards and modules. The discrete driver is cheap but labour-intensive to assemble and fragile. A production version would use an integrated half-bridge driver or the CMOS design of Section 3.6, and a feed motor sized for the full thrust range.

5.1.3 Unsolved problems

The following problems remain unsolved on the submission date:

- The drill gearmotor cannot sustain the thrust that corresponds to 40 N at the grip, reflected force is exact only up to the 32 kg cap (31 N).
- At 10 N the force at the grip varies by 42 % over the lever travel, because of static friction in the printed gearbox, at 20 N the variation is 8.9 %.
- The thrust is sampled at 85.6 Hz, the fastest setting of the HX711 and below the 100 Hz named in the demonstration plan of Requirement 4, and the reflected thrust reaches the hand 80 to 130 ms late.
- The hardware dead time (330 ns mean on phase A) has not been characterised over temperature or across all three legs.
- Plastic has not been drilled, and aluminium only with one 4 mm hole, limited by the 60 % duty cap of the drill motor.
- The feed speed is not capped at 5 mm/s, by choice (Section 5.1.1).
- In the worst 100 ms window the speed estimate differs from the encoder by 5.9 RPM, against ±5 RPM.
- The 2N2907 output transistors of the gate drivers operate close to their current rating, and the gate channels are no longer interlocked in hardware, so shoot-through protection relies on the firmware never commanding both FETs of a leg on.

5.1.4 Strong points of the design

The bilateral loop is stable because of where each force is computed: position-dependent forces on the lever node, only the measured thrust across the link, smoothed and rate-limited, and coupling rules (leash, stuck detection and walls against a still quill) that keep the two sides consistent when the quill cannot follow. Safety is layered and independent of the control code: a latched E-stop carried in every 1 ms frame, link-loss hold, force and thrust caps and a heat budget. The drill hold controller achieves sub-0.1 mm holding on a plant dominated by stiction. The measured drive model removed the need for current sensors with evidence rather than assumption. The modulation never switches the two FETs of a leg as a complementary pair, every change-over is covered by an explicit both-off interval, and the hardware delay keeps the gate signals apart at the board. Designing the driver both in CMOS and in discrete form allowed the same topology to be compared in simulation and in hardware.

5.1.5 Expected failure conditions

The design is expected to fail, or to degrade, under the following conditions:

- Link cable unplugged or damaged: after the timeout both nodes hold position (fails safe), and corrupted frames are rejected by the CRC.
- Drill binding beyond the gearmotor's stall torque: the stuck detection drops the duty to 20 % and the lever presents a wall, sustained stall empties the heat budget and limits the duty to 25 % (fails safe).
- Overload of the load cells: the 32 kg cap stops the drill far below the 200 kg combined rating, and the cells are bolted to the drill-press table so the platform cannot shift.
- Gear tooth or shaft failure, or a gear walking along its shaft: lever position no longer corresponds to motor angle. The gears are protected from overload because the unlocked motor turns before the teeth are highly stressed.

- Supply brown-out on the drill node during violent reversals: the oscillation guard limits the duty, and the drill reports the reset cause after restarting.

5.1.6 Comparison with the literature

The results can be compared with the literature in three respects.

First, the system is a direct force-reflecting teleoperator in the sense of Hokayem and Spong [6]. As Anderson and Spong [4] and Heck et al. [7] predict, position-dependent forces computed on the drill node reached the lever late and made the loop oscillate, computing them on the lever node removed the delay, so only the measured thrust crosses the link, smoothed and rate-limited. The rendered stiffness lies well inside the bound of Colgate and Brown [3] (Section 3.3.5).

Second, the choice between current-mode and voltage-mode FOC was made late. Current-controlled FOC on a general-purpose MCU, as in [16], is the usual approach and was planned here. Only while building and programming the drive did it become clear that, for a high-resistance gimbal motor at haptic speeds, the phase current is set by the applied voltage, and that a current loop mainly adds sensor noise to the torque (Section 3.3.3). A deeper understanding of the motor and of the feel required would have led to voltage mode from the start.

Third, the first, high-side-only chopping scheme introduced a current-dependent voltage error comparable to the dead-time distortion described by Murai et al. [22]: while a phase carried current back into its leg, the node stayed at the positive rail during the off-interval and the phase received the full VDC regardless of its duty. A cogging table measured on that drive learned this distortion rather than magnetic cogging, which is why it made the ripple worse. Choosing the chopped FET by current direction removes the error at its source, as dead-time compensation does in complementary inverters.

5.2 Considerations in the design

5.2.1 Ergonomics

A 150 mm lever, angled like the press handle and gripped in the fist, is a natural input for feed control and has more inertia and damping than a fingertip knob, which masks small torque ripple. The artificial return spring reproduces the feel of a drill-press feed lever, and the reflected thrust lets the operator feel contact, cutting and break-through. Because the firmware works in motor angle, spring spans and detent spacings are set in lever-referred units for a natural feel.

5.2.2 Health and safety

Teleoperation separates the operator from the rotating chuck, which is itself a safety benefit. The feed follows the operator's hand, limited to 30 mm/s and slowed near the ends of travel, the limit switches define the travel, and the E-stop disables both nodes within milliseconds. The workpiece must always be clamped, because unclamped wood can spin violently when the bit breaks through. The electronics operate at 24 V (safety extra-low voltage), and the mains wiring of the drill was not modified.

5.2.3 Environmental impact

The design reuses an existing drill press, and its electronics consume a few watts apart from the motors. 3D-printed parts and the transistors and FETs damaged during bring-up are waste that should be separated and recycled as plastic and electronic waste.

5.2.4 Social and legal impact

Remote feed control could make machine tools accessible to users who cannot safely stand at a machine, and could be extended to hazardous machining environments. Any such use of driven machinery falls under the Occupational Health and Safety Act 85 of 1993 and its Driven Machinery Regulations [30]. A production device would also need to comply with machine-safety standards for the electrical equipment and the emergency-stop function [31], [32].

5.2.5 Ethics clearance

No data were collected from human participants, so ethics clearance was not required.

6. Conclusion

This section summarises the work completed, the main findings, the contribution of the project and suggestions for future work.

6.1 Summary of the work completed

A single-axis bilateral haptic feed interface for a bench drill press was designed, built and integrated. The gate driver was designed at transistor level in the XH018 0.18 µm HV CMOS process, and one phase was laid out and verified as DRC and LVS clean, and the driver was also built as a discrete PCB that was brought up and reworked until it drove the motor reliably. The lever node, on an STM32F405, runs voltage-mode FOC with bottom-clamped, current-direction-chopped modulation, an α-β observer and a trajectory-based servo, estimates the phase current from a measured drive model, and renders spring, detent, return-spring, virtual-workpiece and reflected-thrust forces. The drill node positions the quill with a stiction-aware cascaded controller and measures the thrust with a four-cell load platform. A wired link at 1 kHz and 200 Hz closes the loop, with a latched E-stop, link-loss hold, force and thrust caps and a heat budget.

6.2 Summary of observations and findings

- A cross-coupled SR latch cannot be used as a dead-time generator in a PWM path, because its memory state locks under rapid toggling.
- In the CMOS design the non-overlap of the outputs comes mainly from the saturation storage time of the BJT interlock stage, not from the current-starved delay alone.
- A high-side level shifter must be referenced to ground, with its emitter on the switching node it cannot conduct once the node rises, and this fault stays hidden in any simulation where the high-side FET never pulls the node up to the rail.
- Totem-pole base drive sets the gate charge time: 10 kΩ gave transitions of about 1 µs and linear-region heating, and 1 kΩ reduced them to about 0.1 µs.
- Chopping only the high-side FET gives the wrong phase voltage whenever the phase current flows back into the leg, choosing the chopped FET by current direction removes this source of torque ripple, which a cogging table had wrongly learned.
- At haptic speeds the phase current of the drive is predictable from the commanded voltage ($R \approx 2.78\ \Omega$, $V_{loss} \approx 1.33$ V with the rotor held, and a 1.60 V threshold for force), so current sensors are not needed for the torque the lever requires: the force at the grip was within 1.3 % of the command in the closest run (and within 6.4 % across five runs) from 10 to 40 N.
- Position-dependent haptic forces must be computed at the master, computing them at the slave from a delayed position made the loop oscillate.
- Feed thrust measured with load cells is valid in transients where current-based inference is not, at the cost of a low sample rate (85.6 Hz with the HX711 at its fastest setting), which delays the reflected force by 80 to 130 ms.
- Velocity from a 12-bit encoder at 1 kHz must be observed rather than differentiated to meet a ±5 RPM specification.

6.3 Contribution

The following were new to the author: transistor-level design and layout in Cadence Virtuoso with a commercial HV PDK, field-oriented control and discontinuous modulation, bootstrap

and level-shifted gate driving, interrupt-driven motor-control firmware on the STM32, load-cell instrumentation, observer design, friction-aware position control, and the theory and practice of bilateral teleoperation. The study leader set the scope of the CMOS deliverable (layout to pass DRC and LVS), advised loosening the drill return spring, and discussed the authors reasoning that the design does not need current sensing. The course coordinator's feedback on the first revision of the proposal led to exact force replication and the 40 N lever specification. Generative AI was used as declared in item 5 of the Preamble.

6.4 Suggestions for future work

- Fit a feed motor, or a drill-side reduction, that can sustain the thrust corresponding to the full 40 N at the grip.
- Add a faster bridge converter, and add a passivity layer to the force reflection as in [7].
- Make the feed-speed limit felt at the lever, as resistance that grows when the lever runs ahead of the quill, instead of a cap on the drill.
- Replace the discrete gate drivers with stronger output transistors, and add a hardware interlock to the dead-time block that does not latch under PWM.
- Assemble the three-phase layout and consider fabrication.

7. References

[1] V. Hayward, O. R. Astley, M. Cruz-Hernandez, D. Grant, and G. Robles-De-La-Torre, "Haptic interfaces and devices," *Sensor Review*, vol. 24, no. 1, pp. 16-29, 2004.

[2] F. Gosselin, F. Ferlay, and A. Janot, "Development of a new backdrivable actuator for haptic interfaces and collaborative robots," *Actuators*, vol. 5, no. 2, art. 17, 2016.

[3] J. E. Colgate and J. M. Brown, "Factors affecting the Z-width of a haptic display," in *Proc. IEEE Int. Conf. Robotics and Automation*, San Diego, CA, USA, 1994, pp. 3205-3210.

[4] R. J. Anderson and M. W. Spong, "Bilateral control of teleoperators with time delay," *IEEE Trans. Automatic Control*, vol. 34, no. 5, pp. 494-501, 1989.

[5] D. A. Lawrence, "Stability and transparency in bilateral teleoperation," *IEEE Trans. Robotics and Automation*, vol. 9, no. 5, pp. 624-637, 1993.

[6] P. F. Hokayem and M. W. Spong, "Bilateral teleoperation: An historical survey," *Automatica*, vol. 42, no. 12, pp. 2035-2057, 2006.

[7] D. Heck, A. Saccon, R. Beerens, and H. Nijmeijer, "Direct force-reflecting two-layer approach for passive bilateral teleoperation with time delays," *IEEE Trans. Robotics*, vol. 34, no. 1, pp. 194-206, 2018.

[8] M. C. Shaw and C. J. Oxford, "On the drilling of metals 2: The torque and thrust in drilling," *Trans. ASME*, vol. 79, pp. 139-148, 1957.

[9] P. Kishore Kumar, K. Kishore and P. Laxminarayana, "Prediction of thrust force and torque in drilling on aluminum 6061-T6 alloy," *Int. J. Eng. Res. Technol. (IJERT)*, vol. 2, no. 3, Mar. 2013, doi: 10.17577/IJERTV2IS3379.

[10] M. Uddin, A. Basak, A. Pramanik, S. Singh, G. M. Krolczyk and C. Prakash, "Evaluating hole quality in drilling of Al 6061 alloys," *Materials*, vol. 11, no. 12, art. 2443, 2018, doi: 10.3390/ma11122443.

[11] M. Álvarez Alcón, L. N. López de Lacalle and F. Fernández Zacarías, "Multiple sensor monitoring of CFRP drilling to define cutting parameters sensitivity on surface roughness, cylindricity and diameter," *Materials*, vol. 13, no. 12, art. 2796, 2020.

[12] B. Armstrong-Hélouvry, P. Dupont, and C. Canudas de Wit, "A survey of models, analysis tools and compensation methods for the control of machines with friction," *Automatica*, vol. 30, no. 7, pp. 1083-1138, 1994.

[13] Avia Semiconductor, "HX711 24-bit analog-to-digital converter for weigh scales," datasheet. Accessed: Oct. 2026.

[14] F. Blaschke, "The principle of field orientation as applied to the new transvector closed-loop control system for rotating-field machines," *Siemens Review*, vol. 34, pp. 217-220, 1972.

[15] D. G. Holmes and T. A. Lipo, *Pulse Width Modulation for Power Converters: Principles and Practice*. Hoboken, NJ, USA: IEEE Press/Wiley-Interscience, 2003.

[16] R. C. Prayogo, A. Triwiyatno, and M. A. Riyadi, "Field oriented control implementation on BLDC motor controller with PI and SVPWM using STM32F103C8T6," *J. Physics: Conference Series*, vol. 2622, no. 1, art. 012025, 2023.

[17] A. M. Hava, R. J. Kerkman, and T. A. Lipo, "Simple analytical and graphical methods for carrier-based PWM-VSI drives," *IEEE Trans. Power Electronics*, vol. 14, no. 1, pp. 49-61, 1999.

[18] R. D. Lorenz and K. W. Van Patten, "High-resolution velocity estimation for all-digital, AC servo drives," *IEEE Trans. Industry Applications*, vol. 27, no. 4, pp. 701-705, 1991.

[19] N. Bianchi and S. Bolognani, "Design techniques for reducing the cogging torque in surface-mounted PM motors," *IEEE Trans. Industry Applications*, vol. 38, no. 5, pp. 1259-1265, 2002.

[20] T. M. Jahns and W. L. Soong, "Pulsating torque minimization techniques for permanent magnet AC motor drives: A review," *IEEE Trans. Industrial Electronics*, vol. 43, no. 2, pp. 321-330, 1996.

[21] N. Mohan, T. M. Undeland, and W. P. Robbins, *Power Electronics: Converters, Applications, and Design*, 3rd ed. Hoboken, NJ, USA: Wiley, 2003.

[22] Y. Murai, T. Watanabe, and H. Iwasaki, "Waveform distortion and correction circuit for PWM inverters with switching lag-times," *IEEE Trans. Industry Applications*, vol. IA-23, no. 5, pp. 881-886, 1987.

[23] R. Grezaud, F. Ayel, N. Rouger, and J.-C. Crebier, "A gate driver with integrated deadtime controller," *IEEE Trans. Power Electronics*, vol. 31, no. 12, pp. 8409-8421, 2016.

[24] N. Ly, N. Aimaier, A. H. Alameh, Y. Blaquière, G. Cowan, and N. G. Constantin, "A high voltage multi-purpose on-the-fly reconfigurable half-bridge gate driver for GaN HEMTs in 0.18-µm HV SOI CMOS technology," in *Proc. 18th IEEE Int. New Circuits and Systems Conf. (NEWCAS)*, Montréal, Canada, 2020, pp. 178-181.

[25] B. Razavi, *Design of Analog CMOS Integrated Circuits*, 2nd ed. New York, NY, USA: McGraw-Hill, 2017.

[26] R. J. Baker, *CMOS: Circuit Design, Layout, and Simulation*, 3rd ed. Hoboken, NJ, USA: Wiley-IEEE Press, 2010.

[27] V. G. Nasre and G. M. Asutkar, "Design of current starved voltage control oscillator with bandgap reference in 0.18 µm CMOS process," in *Proc. Int. Conf. Recent Innovations in Signal Processing and Embedded Systems (RISE)*, Bhopal, India, 2017, pp. 375-380.

[28] International Rectifier (Infineon), "IRLZ44N HEXFET power MOSFET (logic level)," datasheet. Accessed: Oct. 2026.

[29] International Rectifier (Infineon), "IRFZ44N HEXFET power MOSFET," datasheet. Accessed: Oct. 2026.

[30] Republic of South Africa, "Driven Machinery Regulations, 2015," Government Notice R. 540 of 24 June 2015, issued under the Occupational Health and Safety Act 85 of 1993.

[31] IEC 60204-1:2016, *Safety of machinery - Electrical equipment of machines - Part 1: General requirements*. Geneva: International Electrotechnical Commission, 2016.

[32] ISO 13850:2015, *Safety of machinery - Emergency stop function - Principles for design*. Geneva: International Organization for Standardization, 2015.

Appendix

Appendix A. Additional results

This appendix contains measurements that support the design but do not bear directly on a specification.

A.1 Thrust available from the drill (push test)

With a rigid rod in the chuck, the push test of Section 3.8.2 was run at maximum PWM settings of 40 to 60 % in 5 % steps, with the thrust cap at 32 kg, and the measured thrust was recorded against duty beside the stalled-motor model. Preliminary runs gave 5.1 kg at 40 % duty (31 % of the stalled-motor model) and about 9 kg at 50 %, about 0.4 kg per percent of duty above a dead zone of about 27 %, which is the duty needed to overcome the friction of the gearbox, rack and quill. At 60 % the thrust was about 13 kg while the duty was rising and about 24 kg when pressing statically, with peaks of about 31 kg when the quill arrived quickly.

A.2 Further timing measurements

The test suite of Section 4 also recorded the quantities in Table 17. The commutation angle is extrapolated between control ticks at the PWM rate, about 11 000 of these updates ran per second rather than 20 000, because the encoder read inside the 1 ms control tick briefly holds them off. At 60 RPM this is still about 1000 updates per electrical revolution.

Quantity	Measured
Commutation updates (lever)	11 000 per second
Drill control task	1000.0 Hz
Knob frames acted on by the drill	985.4 per second
Link round trip	2.04 ms mean
Quill travel after a link-loss stop	0.04 mm
Quill settling after the 10 mm/s feed	within 0.04 mm of target in about 0.2 s

Table 17. Further timing measurements from the test suite.

Appendix B. Supplementary design material

This appendix holds design detail that supports Section 3 but is not needed to follow it.

B.1 Development path and console commands

The user-side control was developed through a sequence of schemes, each replacing the previous one for a specific technical reason (Table 18).

Scheme	Result	Reason for replacement
Six-step commutation	Rotation achieved	Torque ripple too high for haptic feel
Bit-banged sinusoidal PWM	Open-loop FOC working	About 50 duty steps, timing disturbed by blocking I²C reads, software dead time sometimes skipped
Complementary hardware PWM with dead time	Deterministic timing	Hard low-side edges raised dV/dt and caused I²C errors
Complementary PWM with current loop	Sense chain functional	Low-side shunts unable to measure chopping phases
Bottom-clamp DPWM, high-side chopping, voltage mode, observer-based servo	Smooth spring, servo and detent modes, ported to the STM32F405	Wrong phase voltage while the current flows back into a leg, torque ripple
Current-direction chopping (final)	Correct phase voltage for both current directions	Retained, current estimated from the drive model

Table 18. Development path of the user-side motor control.

The main console commands are listed in Table 19.

Command	Function	Command	Function
A, i	Alignment, direction check	5	Drill-press mode
1, v⟨V⟩	Manual vq	E1, E0	Teleoperation on, off
2, g⟨deg⟩	Servo mode, go to angle	G⟨x⟩, R±1	Drill degrees per lever degree, direction
3, 4	Spring, detent mode	B, S, K	Return force, return speed, stroke end
k, y, I	Kp, Kd, Ki	#⟨mm⟩,⟨N⟩	Virtual-workpiece profile point
w, o	Reference, observer bandwidth	$1, $0	E-stop latch, clear
x	Stop (all gates off)	q, P	Print configuration, save calibration
j, f	Detent strength, width	J	Grip radius
m1, m0	Chop by current direction, high side only	!pm, !pk, !lp	Drill maximum duty, thrust cap, push test

Table 19. Main console commands.

B.2 Firmware constants

Table 20 lists the principal firmware constants of both nodes.

Node	Constant	Value	Basis
Lever	Pole pairs p	11	DF4015 datasheet, confirmed by alignment
Lever	Control rate, PWM period	1 kHz, 50 µs (20 kHz)	Section 3.8.1
Lever	Kp, Kd, Ki, ωobs	20 V/rad, 0.25 V·s/rad, 0, 100 rad/s	Section 3.3.5
Lever	Drive model R, Vloss, force threshold, Kt,eff	2.78 Ω, 1.33 V, 1.60 V, 0.122 N·m/A	Eqs. 13, 14
Lever	Gear ratio N, grip radius rg, pinion radius r	16 (18:72 × 18:72), 95 mm, from the calibrated stroke (9.4 mm)	Sections 3.3.2, 3.3.10
Lever	Force and current limits	40 N at the grip (drill mode, walls), 3.4 A phase	Requirement 6
Lever	Back-EMF feed-forward	0.06 V per rad/s (motor)	Section 3.3.10
Lever	Leg change-over gap, minimum duty	3 µs, 1 %	Section 3.3.4
Lever	Spring, detent strength, width, snap point	3 V at 30°, 1.8 V, 1.5°, 52 % of spacing	Section 3.3.5

Node	Constant	Value	Basis
Lever	Return spring force, speed	1.6 V (about 4 N), 5 mm/s	Section 3.3.10
Lever	Reflected-force smoothing, rate limit	≈ 30 ms, 400 N/s	Section 3.3.10
Link	Baud rate, frame rates	460.8 kbaud, 1 kHz and 200 Hz	Section 3.3.9
Link	Timeout	60 ms on both nodes	Requirement 6
Drill	HX711 rate, filter	80 SPS (rate pin tied to the supply), median of 3 + 0.5 smoother	Section 3.3.8
Drill	Thrust cap, maximum duty	32 kg (31 N at the grip), 60 % in normal use	Protects motor, gearbox and coupling
Drill	Feed speed limits	Operator cap off (5 mm/s available), 30 mm/s maximum	Section 5.1.1
Drill	Leash, stuck test	±3 mm, 150 ms at ≥ 40 %, < 0.5 mm/s, > 0.3 mm	Section 3.3.10
Drill	Heat budget	6 s at 100 %, then 25 % cap	Eq. 28
Drill	Oscillation guard	6 reversals in 0.3 s → 30 % for 1 s	Section 3.3.8
Drill	Hold P cap, D, I clamp	100, 0.3 per count/s, ±150	Eq. 27

Table 20. Principal firmware constants.

B.3 Discrete inverter components and bring-up faults

Reference	Value or part	Function	Design basis
M1 to M6	IRLZ44N	Power switches	55 V, 47 A, logic level, 0.1 W conduction loss at 2 A
U1 to U3	74LS14	Input Schmitt inverters	Edge squaring, inversion: GPIO high = FET off
R5, R6, C1, C2, D2, D3	1 kΩ, 470 pF (was 220 pF), diode	RC turn-on delay (hardware dead time)	Eq. 30: 360 ns, 330 ns mean measured (320 ns and 340 ns)
(removed)	74HC02	Original SR interlock latch	Removed because the latch locks under PWM
Q7, R8, C6	2N2222, 4.7 kΩ, 220 pF	Low-side inverter and speed-up	IB = 0.55 mA, R8C6 = 1.0 µs
R9	1 kΩ	Low-side pull-up to 5 V	IC = 4.3 mA
Q5, Q6, R7	2N2222, 2N2907, 10 Ω	Low-side push-pull and gate resistor	Peak gate current ≈ 0.43 A (Section 3.3.6)
Q8, R10	2N2222, 470 Ω	Level shifter (emitter to ground)	IB = (3.3 - 0.7)/470 = 5.5 mA
R12	1 kΩ (was 10 kΩ)	Totem-pole bias from the bootstrap rail	IB 4.3 mA, gate charge time about 0.15 µs
Q9, Q10, R11	2N2222, 2N2907, 4.7 Ω	High-side push-pull and gate resistor	Peak gate current ≈ 0.43 A, set by the R12 base drive
D1, C7	1N5817, 10 µF	Bootstrap supply	Droop 0.5 V/ms at 5 mA
RGS × 6	10 kΩ	Gate-source hold-off	Removed six-step shoot-through
RSH × 2	10 mΩ	Low-side shunts (fitted, unused)	Section 3.5.5
D × 3	1N4148	Clamp across totem-pole PNP emitter-base junction	Prevents reverse avalanche of the 2N2907
C bulk	470 µF, 50 V	DC-link capacitor	Ripple ≈ I·D(1 - D)/(C·fsw) ≈ 0.05 V at 2 A, 20 kHz

Table 21. Components of one phase of the discrete inverter.

Fault observed	Root cause	Correction
Short circuit on first power-up	IRFZ44N fitted reversed on all phases	Refitted, damaged FETs and BJTs replaced
Short to the 24 V rail	Jumper at R28 bridged to 24 V	Jumper removed
Phase B erratic	Dead-time header pins shorted	Bridge removed
Weak drive on one channel	Resistor fitted as 47 Ω instead of 1 kΩ	Correct value fitted
One channel of phases B and C dead	One failed gate in each 74LS14	ICs replaced
Wrong phase sequence	High and low pin assignments swapped relative to the firmware	Pin map corrected
No duty below 100 %	NOR SR latch locks under PWM	Latch removed, Schmitt outputs bridged to the drivers

Fault observed	Root cause	Correction
Shoot-through at six-step transitions	Undriven gates floating	10 kΩ gate-source resistors on all FETs
Instant short under FOC with motor disconnected	Q8 emitter on the switching node: high-side FET could not turn off	Q8 emitter moved to ground
PNPs on all phases and several phase B FETs destroyed	Current-sense bias shared the 5 V gate rail, and a supply sag collapsed the gate drive	Bias circuit removed with current sensing
Phase A heating	R12 = 10 kΩ starved the totem-pole base	R12 reduced to 1 kΩ
Phase B high-side heating and repeated failures	Open connection in the gate path, FET operated in its linear region	Connection repaired
Sticking every 32.7° and I²C errors	Metal debris on the motor next to the encoder	Debris removed
I²C failures under complementary PWM	Hard low-side edges raised dV/dt, coupling into the encoder bus	Modulation changed to high-side chopping (DPWM)
Phase B PNP gain falling over minutes of use	Repeated reverse emitter-base avalanche	1N4148 clamp diodes on all three phases, Q8 ground reference restored on B
Lever slipping under load	3D-printed D-shaft coupler slipped at about 0.7 to 0.8 N·m	Aluminium couplers
Drill ESP32 resetting during force tests	Drill reversing at full duty dipped the supply (brown-out)	Virtual workpiece moved to the lever node, oscillation guard

Table 22. Faults found during bring-up, their causes and the corrections.

B.4 Additional simulation results

The remaining LTspice schematics and waveforms of the discrete half-bridge (Section 3.4.1) and Cadence waveforms of the CMOS driver (Section 3.4.2) are shown below.

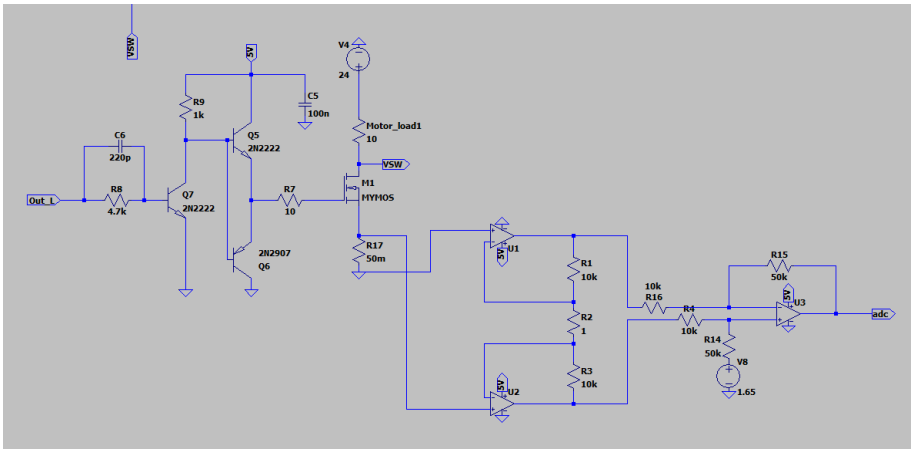


Figure 35. LTspice low-side driver and output stage, with the original current-sense amplifier.

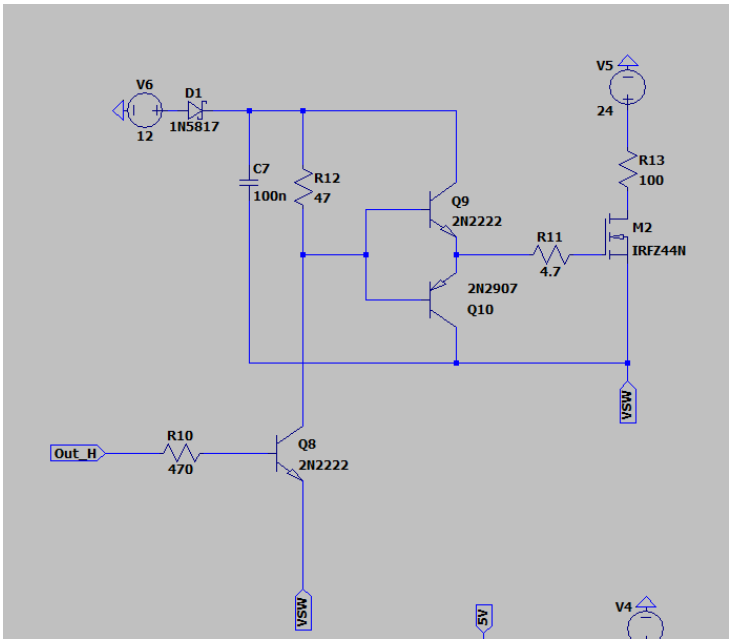


Figure 36. LTspice high-side driver with bootstrap supply and level shifter (design-stage values).

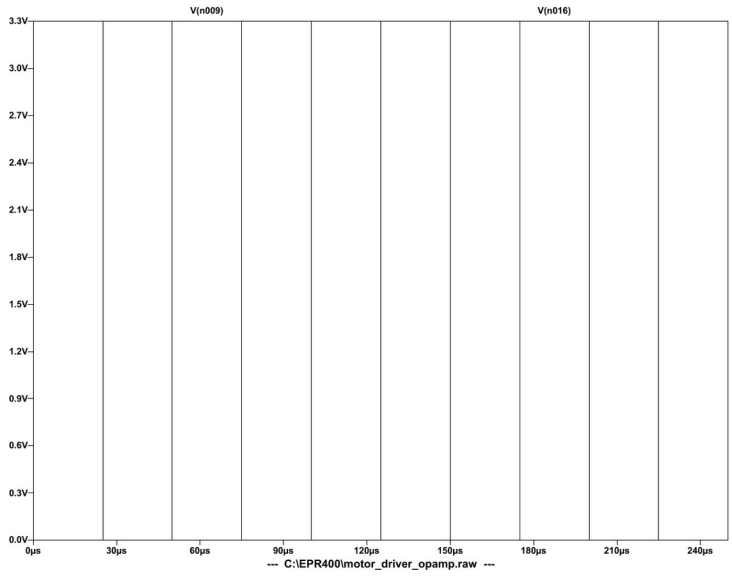


Figure 37. Simulated complementary inputs after the input Schmitt triggers (20 kHz).

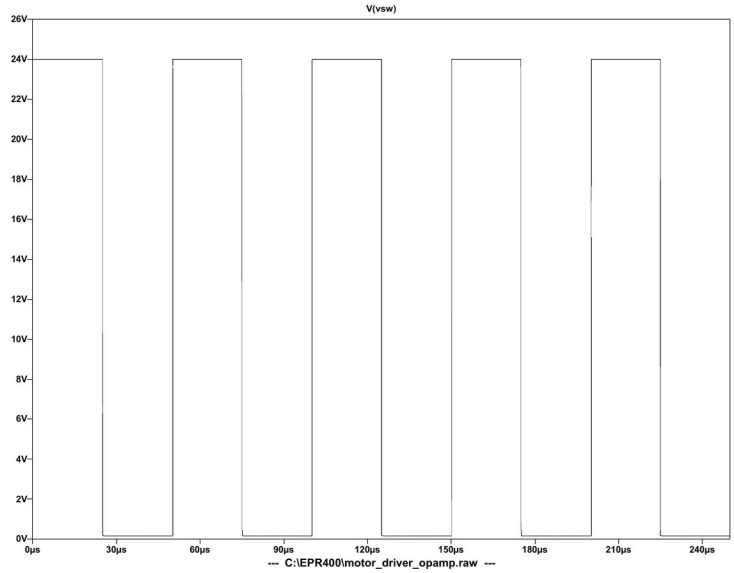


Figure 38. Simulated switching-node voltage VSW with a 10 Ω load to 24 V.

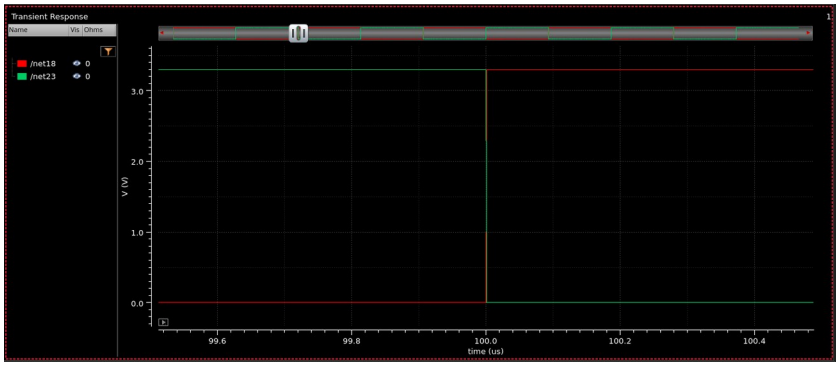


Figure 39. Detail of the channel outputs around the transition at 100 µs.

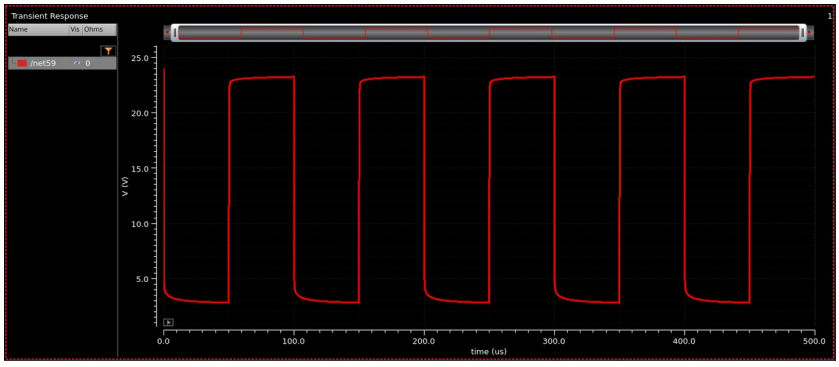


Figure 40. Simulated drain voltage of the low-side power FET (net59) with a resistive load to 24 V.

Appendix C. Physical Hardware Photographs

The completed hardware of both nodes is shown in Figure 41 and Figure 42. On the user side (Figure 41), the DF4015 motor, the AS5600 encoder, the first gear stage and the annular inverter board sit inside the 3D-printed drum, with a hex-vented back cover for cooling, while the second 18:72 herringbone stage drives the three-spoke handle (30° lean, 95 mm grip radius). Quick-grip clamps hold the base to the bench. On the drill side (Figure 42), the FIT0185 gearmotor sits on the feed-shaft hub in a printed bracket and is driven by the BTS7960 H-bridge on the column, while the work platform rests on the four 50 kg load cells read by the 80 SPS HX711 board.

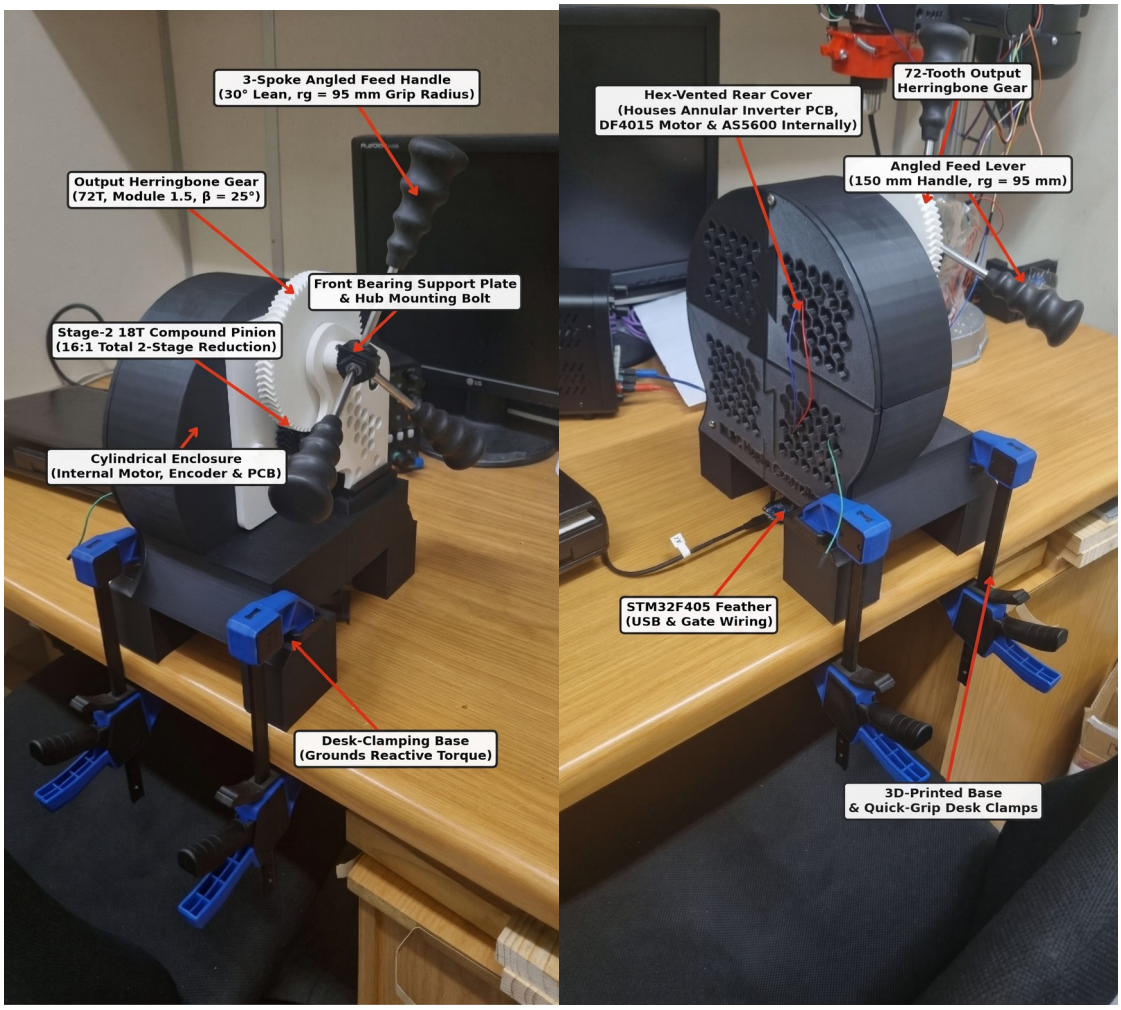


Figure 41. Hardware compilation of the manufactured prototype: (a) front perspective of the user-side haptic unit showing the 16:1 herringbone gear reduction and angled handle, (b) rear view showing the hex-vented annular enclosure and STM32F405 controller.

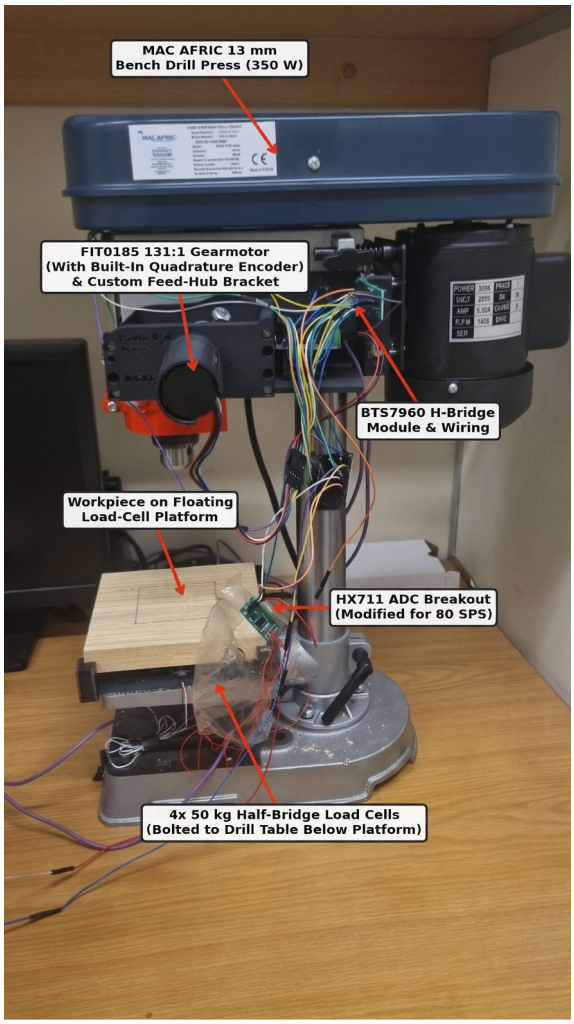


Figure 42. Drill-side actuator and floating load-cell platform installed on the bench drill press.